SFU

Department of
Earth Sciences

Aquifer Characterization, Recharge Modeling and Groundwater Flow Modeling for Well Capture Zone Analysis in the Oliver Area of the Southern Okanagan, BC

Final Report

Submitted by:

M.W. Toews and D.M. Allen

Department of Earth Sciences
Simon Fraser University
Burnaby, BC, V5A 1S6

Submitted to:

Vicki Carmichael and Mike Wei

Water Stewardship Division
Ministry of Environment
Victoria, BC

August 2007

EXECUTIVE SUMMARY

Aquifer characterization, recharge modeling and groundwater flow modeling are undertaken for the arid region of the south Okanagan Basin near Oliver, British Columbia. The primary objectives of the study are to map the distribution of geologic units in the study area with the aim of constructing a 3-dimensional architecture model of the aquifer(s); to quantify and map the spatial distribution of recharge to the aquifer(s) within the sub-region; to construct and calibrate a three-dimensional groundwater flow model that can be used to simulate groundwater conditions in the Oliver region; and to construct a local scale groundwater model for the Town of Oliver to obtain well capture zones for municipal wells.

The study region is located between Lake Vaseux and Lake Osoyoos; the Town of Oliver is in the center of the region. Okanagan River is the main surface water body in the region, which flows from Vaseux Lake, southward to Lake Osoyoos. The river is controlled near the outlet of Vaseux Lake by McIntyre Dam, which also diverts water into the SOLID irrigation channel. The majority of the streams entering the Oliver region are ephemeral, and do not extend far down into the valley. It is assumed that some of these small streams directly recharge to groundwater at the bedrock/valley-fill interface, since they disappear partway down the valley over unconsolidated material. There are also many small (~1 km) lakes along the valley bottom and valley sides. These water bodies do not have any major streams flowing in or out of their surface (with the exception of Tugulnuit Lake, which has a gravity-fed pipe down to Okanagan River), and are interpreted to be sustained through groundwater.

In the Oliver region, there is only a limited number of valley-bottom boreholes that reached bedrock through the valley fill. The spatial definition of the bedrock surface was approximated from a GIS analysis of borehole, digital elevation, slope, and orthophoto data. From the available data, the maximum depth of the bedrock surface ranges from approximately 0 to 100 m above sea level. There are no indications that the bedrock is eroded as deeply as in the northern Okanagan, where the bedrock contact is below sea level in many parts of the Valley. The valley fill within the Oliver area consists of Pleistocene-aged glaciolacustrine silt and clay overlain by glaciofluvial sand and gravel.

The main aquifer in the study region is the upper unconfined sand and gravel aquifer adjacent to Okanagan River. Deep confined sand and gravel aquifers are found along the valley margins, which are in alluvial deposits. Many of these alluvial fan deposits interfinger the glaciolacustrine deposits at depth, and likely extend less than several hundred metres toward the valley center.

Spatial recharge is modelled using available soil and climate data with the HELP hydrology model. Irrigation was added to precipitation in irrigation districts located in the Oliver region using proportions of crop types, and daily climate and evapotranspiration data generated from a stochastic weather generator (LARS-WG). Mean annual recharge rates have a median of 45 mm/yr, with first and third quartiles of 15 and 60 mm/yr, respectively. These values are approximately 20% of the annual precipitation. Recharge simulations using irrigation yield significant increases in net recharge in the irrigation districts, from 250 mm/yr to 1000 mm/yr.

A regional scale deterministic model is developed for the region extending from Vaseux Lake to Osoyoos Lake. Estimates of the hydraulic properties of the hydrostratigraphic units are obtained from available pumping tests or estimated from the literature. Model boundary conditions are established for existing rivers, streams, lakes and recharge (including irrigation return flow). Both a steady-state and transient model are run and calibrated to observed hydraulic head data. Model results suggest that groundwater in the Oliver region is regulated and maintained from Okanagan River and the bounding lakes. The water table is generally flat throughout the region, and ranges in elevation from 280 to 355 m.a.s.l. along the Vaseux Lake to Osoyoos Lake corridor. The water table rises up slightly in proximity to the benches. A large proportion of the water budget is sustained through recharge, and much of the recharge is from irrigation return flow.

A local scale stochastic model was developed for the Oliver area in which the aquifer properties in the upper two layers were generated stochastically using transition probabilities determined from the borehole data. This stochastic model was used to derive probabilistic capture zones for major production wells in the Oliver area. The stochastically-generated capture zones are similar to zones determined using the calculated fixed radius method (circular) where pumping rates are relatively low, and appear more elliptical where the groundwater flow rates are greatest, such as where there is a high hydraulic gradient and/or hydraulic conductivity.

TABLE OF CONTENTS

LIST OF FIGURES

LIST OF TABLES

1. INTRODUCTION

1.1. BACKGROUND

Groundwater is an important water supply in the Okanagan Basin and provides drinking water to communities as well as water for irrigation and industry. The Okanagan is one of the driest regions of Canada, and rapid development in the region due to both population and agricultural growth has significantly increased demands on both surface and groundwater resources. While exploitation of surface water is regulated, there is no current legislation governing the development and use of groundwater. This unregulated use of groundwater has the potential to have negative impacts on the sustainable development of the resource, and consequent negative impacts on long term social, economic, and agricultural activity in the watershed that rely on it.

In order to provide all levels of government with the tools needed to better understand and properly manage the groundwater resource in the watershed, a basic understanding of the current groundwater resource, its development, and vulnerability is required. Hydrogeologic mapping within the Okanagan region will provide important scientific information on the aquifers to support other Ministry and Provincial Government activities such as protection of drinking water sources (including groundwater supplies), implementation of drinking water and groundwater legislation, groundwater and surface water assessments, water allocation and planning (surface/groundwater interactions), regional land and resource planning, and groundwater quantity and quality monitoring through the Observation Well and the Ambient Water Monitoring Network.

Consequently, the Okanagan has been targeted for aquifer mapping and characterization through a joint effort between the BC Ministry of Environment (BC MoE) and the Geological Survey of Canada (GSC) under the auspices of the Groundwater Assessment of Okanagan Basin (GAOB) initiative. Specifically, there is a critical need for detailed information with respect to aquifer characteristics (e.g., location and extent of aquifer and aquitard units, groundwater flow directions, flow rates and sustainable capacities, inter-connection with surface water bodies, location of sensitive recharge areas, factors governing ambient groundwater quality, etc.). Hydrogeologic mapping and development of regional numerical groundwater models are two main tools that are being used to assess and characterize these aquifers.

The Department of Earth Sciences at Simon Fraser University (Dr. Diana Allen) is a co-collaborator for this research through her involvement as project leader for a Canadian Water Network funded research project entitled "*A Basin Approach to Groundwater Recharge in the Okanagan: Bridging the Gap Between Science and Policy".* The aim of that project was to contribute to science knowledge on groundwater recharge in the Okanagan Basin through hydrogeological modeling, geochemical sampling and analysis, and field-based studies of highland to valley bottom recharge processes, including contributions of surface water to groundwater recharge. One project sub-component addressed the direct recharge to Okanagan Basin aquifers through local and regional case studies. The local study was conducted in the Oliver region of the south Okanagan. The aquifer characterization and groundwater modeling for that study are documented in this report.

.

1.2. PURPOSE AND RESEARCH OBJECTIVES

The primary purpose of this research is to characterize the hydrogeology of the Oliver region of the south Okanagan, and construct a groundwater flow model for that aquifer. The Oliver region was selected in consultation with the BC MoE on the basis of available data and level of importance with respect to groundwater issues (e.g., contamination).

The original research objectives were:

1. To map the distribution of geologic units in the study area with the aim of constructing a 3-dimensional architecture model of the aquifer(s); and
2. To quantify and map the spatial distribution of recharge to the aquifer (s) within the sub-region;

Two additional objectives (added to provide a more complete study) were:

3. To construct and calibrate a three-dimensional groundwater flow model that can be used to simulate groundwater conditions in the Oliver region; and
4. To construct a local scale groundwater model for the Town of Oliver to obtain well capture zones for municipal wells.

1.3. METHODOLOGY AND APPROACH

The methodology builds on previous approaches for the Grand Forks aquifer (Allen 2000, 2001), by considering spatially-distributed recharge and the use of downscaled global climate model (GCM) data to generate stochastic weather series needed to drive the recharge model. This newer approach to recharge modeling was used in a follow-up study of the Grand Forks aquifer (Scibek and Allen, 2003, 2004; Scibek et al., 2004) and the Abbotsford aquifer (Scibek and Allen, 2005).

To meet with the research objectives, the following scope of work was undertaken:

1. Review Quaternary geology, borehole data and hydrogeologic data for the study area and Okanagan region;
2. Characterize and portray the 3-dimensional stratigraphic and hydrogeologic architecture of the aquifer(s) by constructing geologic cross-sections and maps from available water well information (WELLS and observation well databases), pump test data and geologic/hydrogeologic reports;
3. Identify major hydrostratigraphic units by considering the spatial variation in hydraulic properties and water table elevations (where available).
4. With the aid of a numerical model[1] and using the near surface distribution of soil and surficial materials and known climate data for the region, construct a distributed recharge map for the study area.
5. Build and calibrate a three-dimensional groundwater flow model for the south Okanagan region extending from Vaseux Lake to Osoyoos Lake.
6. Build and calibrate a local scale model for the Town of Oliver and conduct a well capture zone analysis for municipal wells.

1.4. OVERVIEW OF THE REPORT

This report consists of 5 sections. Section 1 provides a background to the study and states the objectives and scope of work. Section 2 describes the Oliver region physical setting and geology. Section 3 describes the hydrostratigraphy. Section 4 describes the recharge modeling

[1] The software HELP (US EPA) will be used for estimating recharge.

methodology and results. Section 5 describes the conceptual regional-scale model, the numerical model and its calibration, and presents the modeling results. Section 6 describes the local scale model and the generation of well capture zones.

2. OLIVER REGION PHYSICAL SETTING AND GEOLOGY

2.1. STUDY LOCATION

The Oliver study region is located between Lake Vaseux and Lake Osoyoos (Figure 2.1), in Okanagan Basin of the southern interior of British Columbia (BC). The Town of Oliver is in the center of the region, which has a population of about 4300. The rural region surrounding Oliver adds an additional 4500, which includes the Osoyoos Indian Band #1 Reserve on the Eastern side of the study region. Domestic water is obtained through several regional groundwater wells, and several hundred private domestic wells. The main industries of the region are agriculture (orchard and vineyards) and tourism, both of which have a strong dependence on fresh water resources. The region is popularly known as the "Wine Capital of Canada", and also hosts two world-class golf courses.

2.2. PHYSIOGRAPHY AND CLIMATOLOGY

Okanagan Valley is a narrow, north–south trending valley that is deeply incised in the Interior Plateau of the North American Cordillera. It has a topographic relief of ~1100 m from the valley bottom to the surrounding plateau level. Within the study region, the topography varies from 375 to 1862 m at Mt. Kobau, 7 km east of Oliver. The valley width ranges from less than 2 km at McIntyre Bluff at the north end of the Oliver study region, to 5 km near the Town of Oliver. The valley bottom is generally flat, with the exception of a few minor raised 'bars' along the valley center, and other small isolated topographic depressions. The sides of the valley have at least four terraces (also called benches).

The southern Okanagan is the only populated arid region in Canada, with typical 'wet' seasonal patterns occurring in the winter and summer periods. The annual precipitation in the valley bottom is about 300 mm, and nearly twice that amount at higher elevations, with a regional precipitation gradient decreasing toward the southwest. Winter precipitation is typically in the form of snowfall, derived from frontal systems, while rainfall from May to June is from cold lows, and from August to September from convective precipitation systems (B. Taylor, pers. comm. 2007; Environment Canada, 2006).

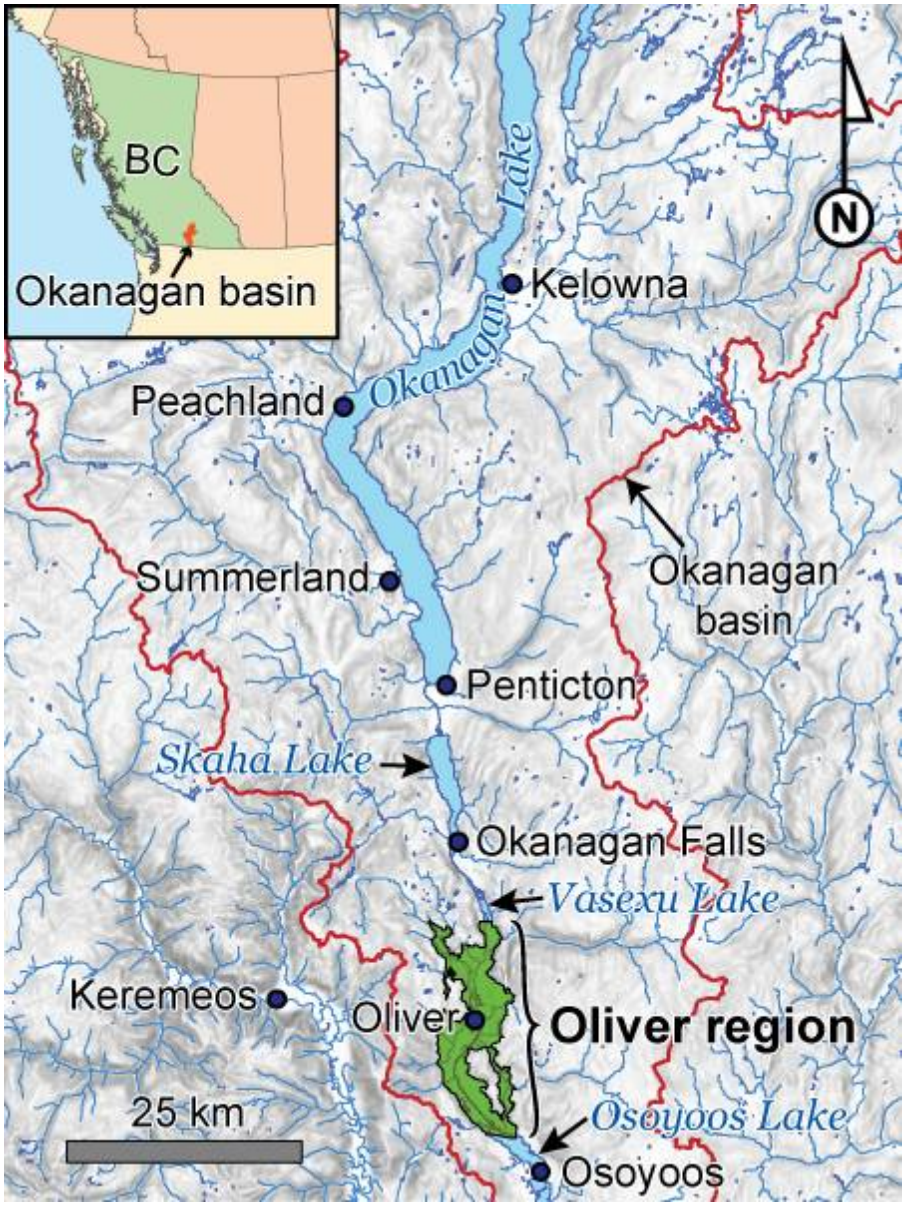

Figure 2.1: Map of southern Okanagan Basin, highlighting the Oliver study region, which is bounded by Vaseux Lake and Osoyoos Lake.

Natural climate variability in southern BC is influenced by the El Niño-Southern Oscillation (ENSO) (Trenberth, 1997), and the Pacific Decadal Oscillation (PDO) (Mantua and Hare, 2002). El Niño episodes generally result in decreased winter precipitation anomalies with warmer temperatures, while La Niña episodes result in increased winter precipitation with lower temperatures (Shabbar et al., 1997). During positive phases of the PDO, southern BC has higher temperature anomalies and slightly lower precipitation anomalies. The ENSO and PDO climate patterns have different time-scales, and can have coupled influences on the climatology.

2.3. SURFACE WATER

Okanagan River is the main surface water body in the region, which flows from Vaseux Lake, southward to Lake Osoyoos (Figure 2.2). The river is controlled near the outlet of Vaseux Lake by McIntyre Dam, which also diverts water into the SOLID[2] irrigation channel. While the upper reach of the river is natural (unaltered channels), the remaining 2/3 is channelized, from 1 km north of Oliver to Osoyoos Lake. The river was channelized in the 1950s to prevent flooding (Nichols, 1993), and has thirteen vertical drop structures to slow and control the river flow.

The majority of the streams entering the Oliver region are ephemeral, and do not extend far down into the valley. It is assumed that some of these small streams directly recharge to groundwater at the bedrock/valley-fill interface, since they disappear partway down the valley over unconsolidated material. The stream catchments to the bedrock interface are shown in Figure 2.2.

There are many small (≤1 km) lakes along the valley bottom and valley sides, such as Tugulnuit Lake,[3] Gallagher Lake, and Spotted Lake. These water bodies do not have any major streams flowing in or out of their surface (with the exception of Tugulnuit Lake, which has a gravity-fed pipe down to Okanagan River). It is interpreted that all of these lakes are sustained through groundwater.

2.4. ECOLOGY, AGRICULTURE, IRRIGATION AND LAND-USE

The valley-bottom of the Oliver region is in both *bunchgrass* and *ponderosa pine* biogeoclimatic zones (Pojar et al., 1987), which are indicative of hot, arid climates. The Oliver region has some of the most extensive irrigated agriculture in Okanagan Basin, which includes vineyards and fruit tree orchards (apple, plum, peach, etc.). Each crop generally has unique irrigation demands (see Neilsen et al., 2004), which is met from water abstracted during the growing season from Okanagan River (or connected irrigation channels), or from groundwater wells.

Other land uses and land coverages include gravel pits, golf courses, and natural riparian regions along reaches of Okanagan River. The upper valley sides are predominantly undeveloped, and consist of native bunchgrass, ponderosa pine and related vegetation. Natural

[2]South Okanagan Land Irrigation District
[3]This is the official geographic name, however, *Tuc-el-Nuit Lake* is also very common

vegetation is sparse, but is thicker and more prevalent on north-facing slopes (particularly in creek gullies), and at higher elevations.

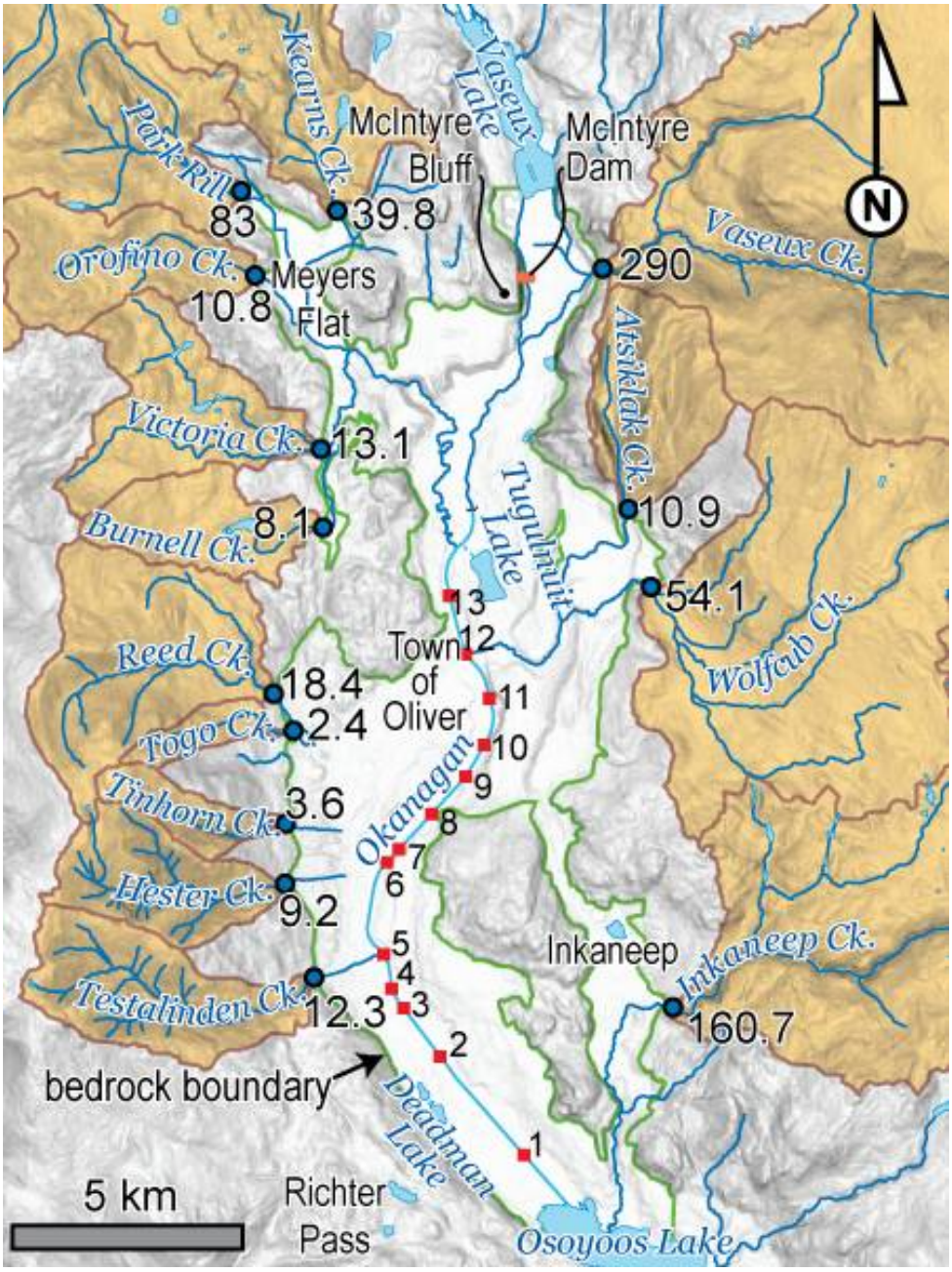

Figure 2.2: Surface hydrology, showing side catchment basins and areas to the bedrock-interface (catchment area in km² shown at blue dots). Okanagan River flows southward into Osoyoos Lake, and passes through 13 vertical drop structures (red squares) along the channelized portion.

2.5. QUATERNARY GEOLOGY

The Quaternary stratigraphy in the Okanagan Valley can be simplified as dominantly silt (by volume), with sand and gravel on the top and along sides of the valley. British Columbia has been glaciated multiple times throughout the past 1 Ma by the Cordilleran Ice Sheet (CIS), and the most recent glaciation ended about 11000 a (Clague, 1991). An extensive Glacial Lake Penticton (GLP) formed at the end of the last glaciation, into which fine-grained material was rapidly deposited. This fine-grained material comprises the characteristic silt bluffs, as found in many valleys in the Interior of BC (Fulton, 1965).

The Quaternary stratigraphy of Okanagan Basin was first documented in detail by Flint (1935), who described the character and distribution of the silt deposits, as well as the gradation of sands and gravels along the valley margins. Nasmith (1962) mapped and interpreted Quaternary deposits and landforms throughout the Okanagan, including the Oliver region (Figure 2.3). Nasmith identified several important depositional facies and landforms, including glaciofluvial deposits, kettled outwash, raised and present-day alluvial fans, and glaciolacustrine sediments. Fulton (1972) and Fulton and Smith (1978) constructed several stratigraphic sections across the BC Interior, and interpreted a record of multiple glaciations throughout the Cordilleran region, including in the valley-bottom of Okanagan Basin.

However, some of these initial interpretations for the Okanagan Valley have come into question; in particular: (1) the presence or absence of large volumes of glacial till and pre-glacial sediments in the valley bottom; and (2) the timing and sequence of deglaciation, and distribution of deglacial ice and GLP. These interpretations influence the interpretation of further data, the theory behind depositional conceptual models, and interpolation of stratigraphy where there is limited or no available data.

Several stratigraphic conceptual models have been published that relate geologic evidence to possible modes of valley erosion and/or the stratification, and the distribution of the valley fill. These conceptual models are largely incompatible with each other, but nonetheless are supported (or denied) by geologic evidence. Much of the newer supporting evidence is from seismic surveys, listed in Table 2.1.

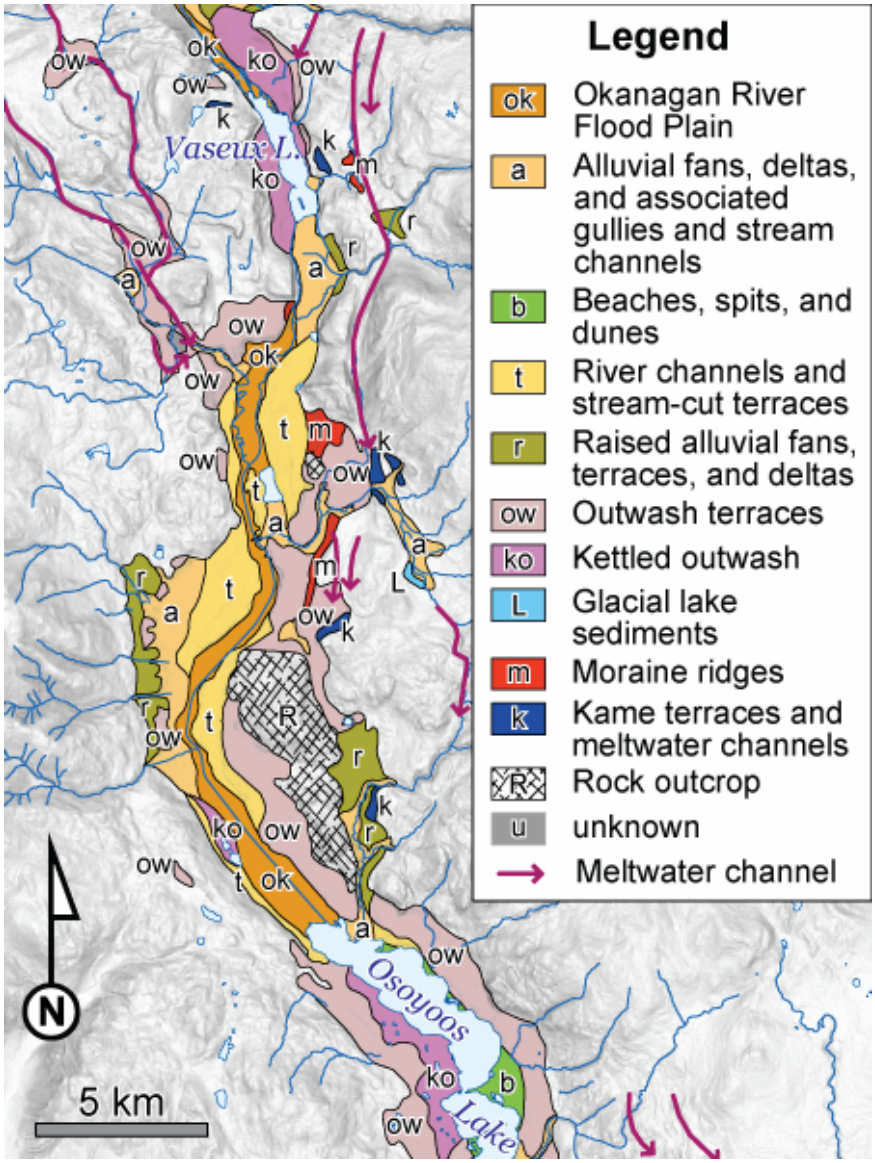

Figure 2.3: Surficial deposits of the Oliver region, as mapped and interpreted by Nasmith (1962). The legend order is from most recent to oldest.

Table 2.1: Seismic surveys in Okanagan Basin.

Reference	Location	Type	Source
MacAulay and Hobson 1972	north Okanagan	refraction	dynamite
Mullins et al. 1990	Kalamalka Lake	reflection	air gun
Eyles et al. 1990	Okanagan Lake	reflection	air gun
Vanderburgh 1993	north Okanagan	reflection	buffalo gun

The traditional conceptual model of glaciation in the Okanagan Valley is of alpine valley glaciation, where a large tongue of ice occupies the valley, producing complex stratigraphy and preserving previous glacial and non-glacial deposits. This conceptual model is supported by earlier interpretations by Nasmith (1962), Fulton (1965, 1972, 1991), and Fulton and Smith (1978), and it is an analogue of present-day alpine glacial environments. However, few till deposits have been confirmed in the valley bottom (many of these diamicton deposits have alternate diageneses), and the stratigraphy, as interpreted in seismic profiles, is relatively simple (Eyles et al., 1990; Eyles and Mullins, 1991).

Eyles and Mullins (1991) proposed a supraglacial lake hypothesis, in attempt to produce both simple stratigraphy and the silt bluffs. In this conceptual model, coarse material is deposited near the base of an active glacier from high-velocity subglacial drainage. Once the tongue of ice in the valley bottom is stagnant, fine lacustrine materials are rapidly deposited over the ice. The ice slowly melts, which lowers the lake bottom to produce silt bluffs.

Vanderburgh and Roberts (1996) developed a depositional systems framework, which is based on seismic profiles, borehole and sediment core lithologies. This empirically based conceptual model attempts to explain the seemingly complex stratigraphy as a result of the interactions of a few geologic processes, or depositional systems: (1) subglacial fluvial, (2) glaciolacustrine, (3) alluvial fan, and (4) channel systems (Figure 2.4).

Shaw et al. (1999) and Lesemann et al. (2005) proposed a revised depositional conceptual model, which is an extension of the work by Vanderburgh and Roberts (1996). They found lacustrine and related deposits at a higher elevation, which is evidence that the surface elevation and spatial extent of GLP was much greater than previously mapped by Fulton (1969). This glacial lake is interpreted to have a maximum elevation of at least 900 m (J.-E. Lesemann, pers. comm. 2006), which would have extended over many of the upper side valleys along the main valley and covered a vast region from northern Okanagan Basin to Okanogan Valley in Washington. Furthermore, Lesemann et al. (2005) suspect that this lake would have been beneath a thin cover of the Cordilleran Ice Sheet (as a subglacial lake), and would have had minimal ice-contact with the bedrock bottom of the valley. Other evidence suggests that this subglacial lake may have periodically and catastrophically drained, eroding smaller marginal valleys into bedrock, and over-deepening Okanagan Valley itself.

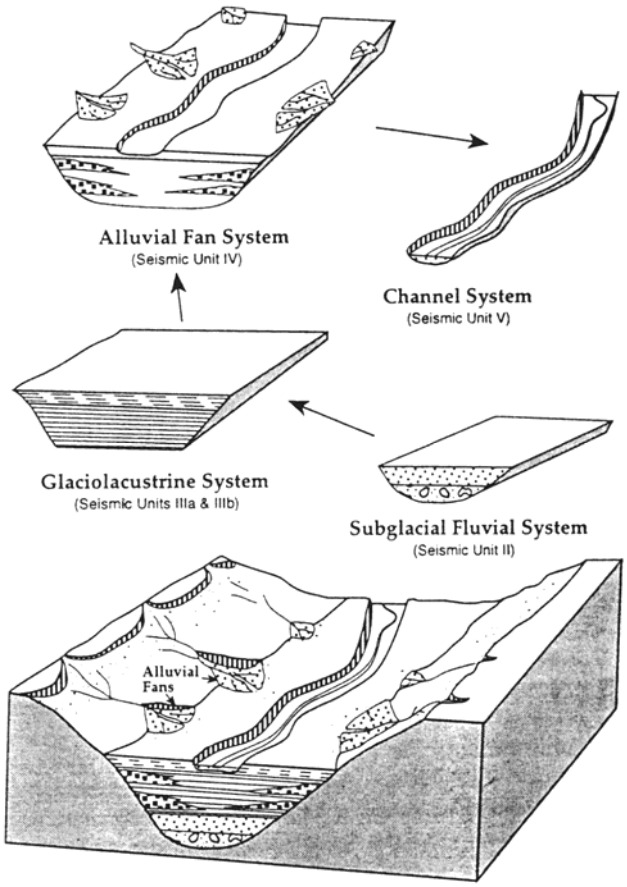

Figure 2.4: Depositional systems framework for the north Okanagan basin (Vanderburgh and Roberts, 1996).

From the review of Quaternary geology literature, it is apparent that more work is required to understand the geologic history and timing of the CIS. However, the general distribution and character of the unconsolidated sediments in Okanagan Valley are, for the most part, well understood.

2.6. BEDROCK GEOLOGY

2.6.1. BEDROCK COMPOSITION AND TECTONICS

The bedrock in the Oliver region consists primarily of metamorphic and intrusive igneous rocks (Figure 2.5), ranging in age from Proterozoic to Middle Jurassic (Massey et al., 2005). The Okanagan Valley fault system, which is a west-dipping crustal shear with 90 km of offset, strikes southward through the valley and was active during the Middle Eocene (Tempelman-Kluit and

Parkinson, 1986). The shear zone is approximately 1 to 2 km wide, and is characterized by mylonite and microbreccia.

2.6.2. BEDROCK SURFACE AND MODES OF EROSION

The bedrock surface in Okanagan Basin is highly variable, and has a similar spatial variability below the unconsolidated fill to where it is exposed—that is, the bedrock surface is very irregular, with many cliff-like drops. This is confirmed from large differences found in the elevations of the bedrock contacts between two closely-spaced boreholes throughout many regions of Okanagan Basin.

The bedrock surface beneath the unconsolidated deposits, as revealed using seismic techniques (see Table 2.1), is very deep and irregular. MacAulay and Hobson (1972) remark the "extreme changes in bedrock slope" from their seismic survey. The deepest bedrock erosion is in Okanagan Lake at 650 m *below* sea level (Eyles et al., 1990), which makes Okanagan Valley possibly one of the deepest known erosional features within a continental landmass. The down-axial bedrock elevation profile ranges upwards to 115 m above sea level (WTN[4] 82362, near Okanagan Falls), which indicates that the base of the bedrock surface along the valley can vary within an elevation range of 765 m.

The placement of the Okanagan Valley is along the fault system, as it provided a zone of weakness for erosion; however, there is no clear consensus regarding the erosional process(es) that created the present Okanagan Valley physiography (Tribe, 2005). Possible methods and processes are: (1) tectonic down-dropping during the Eocene; (2) river erosion; (3) glacier basal erosion; (4) subglacial fluvial erosion; and (5) erosional scouring from cataclysmic outburst flooding.

Erosion from rivers would have had to have been early in the history, and limited to the sea level elevation at that time (which would have been relatively higher than today); however, much of the bedrock valley is below present sea level (Fulton, 1972). Glacial erosion can potentially erode below sea level—Nasmith (1962) termed the Valley a "fiord-lake" to describe this phenomena found in Okanagan Basin. However, the down-valley bedrock profile is highly variable and is not graded.[5] Furthermore, the cross-valley widths and profiles are dramatically different along the valley (not a typical U-shape). A map-view of the main valleys reveals an

[4](WTN) Well Tag Numbers are unique well identifiers for the WELLS database
[5]A graded profile exponentially levels off to an vertical datum; an example is a river elevation profile

anastomosing pattern, whereby the main valleys diverge and converge from north to south. These clues fail to impress that classic valley glacier erosion was solely responsible for the over-deepening of the valley, as is thought by many.

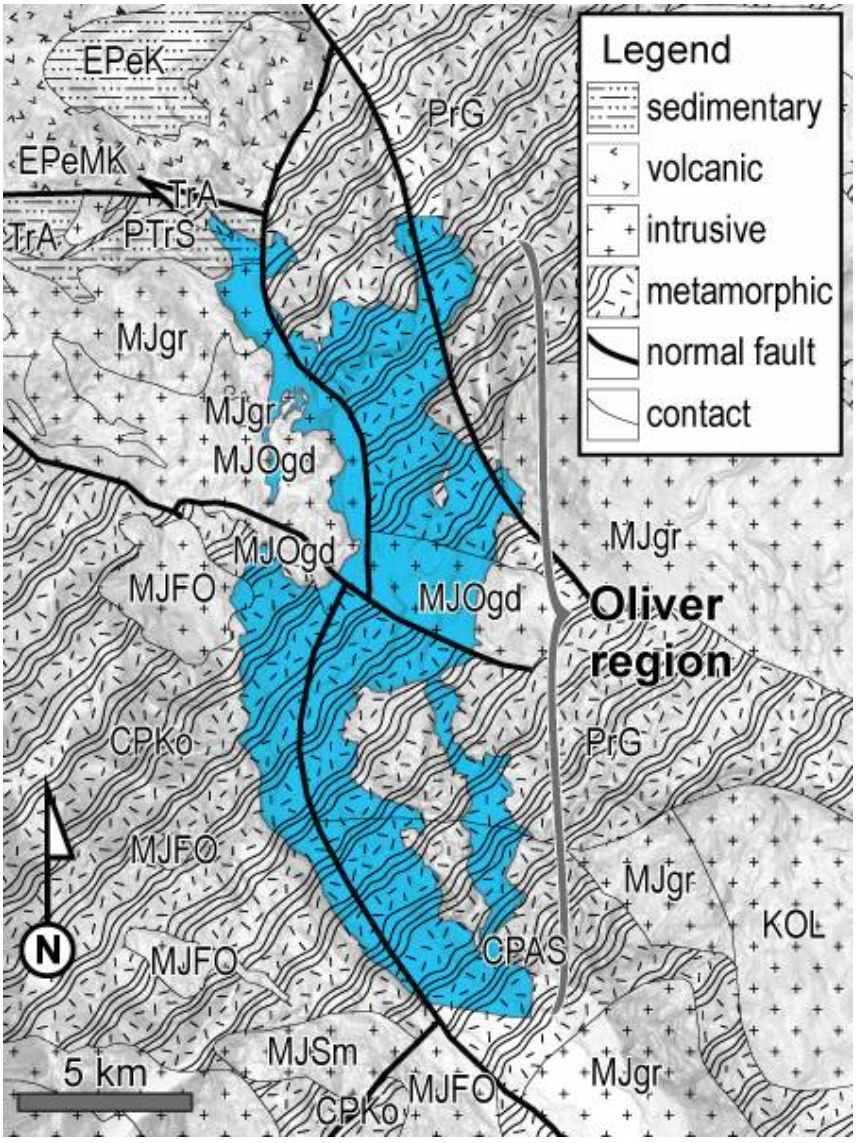

Figure 2.5: Bedrock geology and approximate locations of faults (Massey et al., 2005). The north–south trending Okanagan Valley fault system, which underlies the Oliver region (highlighted in the center), is beneath hundreds of metres of unconsolidated Quaternary sediment.

Eyles and Mullins (1991) and Vanderburgh and Roberts (1996) suggest that subglacial drainage systems were actively flowing beneath the CIS. In addition, Shaw et al. (1999) and Lesemann et al. (2005) speculate that the subglacial drainage might have been periodically cataclysmic

and responsible for the over-deepening of the valley. Subglacial fluvial systems are closed channel hydraulic systems, and have the ability to flow and potentially erode in any direction (including up and down). Tunnel valleys along the sides of the main valley (some of which "flow uphill") support an erosional mechanism. The deep and irregular bedrock profile of the main valley is also supported by this mechanism.

2.7. GEOLOGIC MODEL OF THE OLIVER AREA

2.7.1. DATA AND METHODS

Lithology data were obtained from the WELLS database,[6] which has been corrected, standardized and modified by Simon Fraser University under contract with the BC Ministry of Environment. A custom Microsoft Access database (Figure 2.6) was developed from the WELLS data[7] for use and interpretation as a standalone program, and within ArcGIS (ESRI, 2005). This database allows rapid correction and classification of the borehole data in a GIS. Additional routines, written in the Python programming language, translate the lithology data for GMS version 6.0 (Owen et al., 1996; EMRL, 2005) for 3D interpretation and surface interpolation.

Within the study region, the well database contains records from ~600 wells. The quality and detail vary from well to well, depending on the driller and depth of well. GMS can display borehole lithology data using two levels of interpretation: soil and hydrogeologic units. The former was used to classify the lithologic materials, while the later was used to group units into possible depositional facies.

The lithologic descriptions were manually classified into 10 material types: (1) bedrock, (2) diamicton (clay mixed with gravel, cobbles or boulders), (3) boulder and gravel, (4) gravel, (5) sand and gravel, (6) sand, (7) fine sand, (8) silt, (9) clay, and (10) organic materials.

The depositional facies (described later) are: (1) bedrock, (2) glacial till, (3) glaciolacustrine, (4) glaciofluvial, (5) boulder, (6) alluvial, and (7) recent fluvial channel.

[6]Accessed at `http://srmapps.gov.bc.ca/apps/wells/jsp/common/wellsreport7.jsp`
[7]This is on the CD in `/gisdata/wells_mt.mdb` in Microsoft Access 2000 format

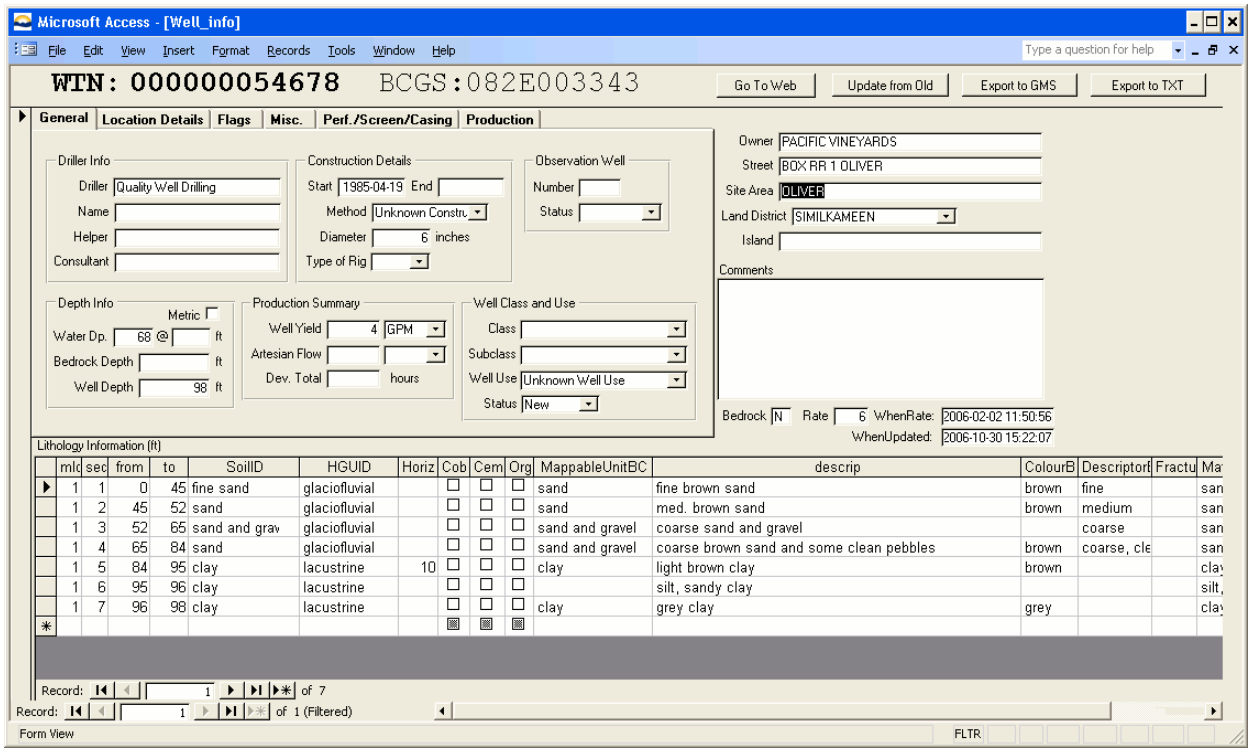

Figure 2.6: Well database interface used for lithology interpretation and classification. Lithologic units are classified both a soil ID, and a geologic facies (in the 'HGU ID' field). Other data for each well can be viewed using the tabs near the top.

The materials and depositional facies were determined from an interpretation of the text descriptions for each layer, and how the borehole relates with surrounding boreholes. Units with ambiguous or diagenetic descriptions, such as "till", "topsoil" or "hardpan" were classified with the assistance of surrounding boreholes, if available.

Digital elevation data were obtained from Natural Resources Canada (2005), which are unprojected 0.75-arc second, Level 1 DEM data.[8] Elevation data were projected on a Transverse Mercator, and interpolated onto 25 m resolution grid for ArcGIS, using bilinear interpolation; and ~50 m resolution TIN (triangular irregular network) for GMS, using linear interpolation.

[8]This is the 1:50000 CDED1 series, which can be accessed at `http://geobase.ca`. At the latitude of the study region, 0.75-arc seconds projects to approximately 22 m north–south by 15 m east–west. Level 1 DEM data are typically generated through photogrammetric methods, using aerial photographs (USGS, 1997)

The 25 m ground elevation grid was used to determine surface slope, slope aspect, flow accumulation, hypsometric curves, and other GIS operations that are needed to determine the catchment hydrology of the region.

Point data (including bedrock contacts, silt tops and water table) were interpolated to ~50 m resolution TIN surfaces, using either *kriging* (e.g., Deutsch and Journel, 1997) or *natural neighbour* methods (e.g., Sibson, 1981). Interpolated TIN surfaces were truncated using a custom Python routine; for example, an interpolated silt surface was "truncated" to be below the ground surface, and above the bedrock surface.[9]

Other geospatial data were obtained from the BC MoE, including: 0.5 m colour orthophoto data, locations of water wells (from WELLS database), and surface hydrology (lakes, rivers). Elevations of the wells were interpolated from the digital elevation data; however, the map position accuracy of the boreholes range from 1 to 100 m (the median is 20 m), which can propagate to the accuracy of interpolated maps derived from the WELLS database that are based on elevation. Surface hydrology map data were modified to honour the orthophoto imagery, such that streams terminated where they could no longer be identified along their stream course.[10]

It must be stressed that the interpretations of the Quaternary deposits presented in the following sections are predominantly based on information from the WELLS database, and need more supporting data and field work to gain more confidence. Furthermore, interpretations of the timing of deglaciation and of depositional environments are subject to change with ongoing Quaternary research of the CIS.

2.7.2. BEDROCK VALLEY

In the Oliver region, there is only a limited number of valley-bottom boreholes that reached bedrock through the fill (Figure 2.7), and no seismic data are presently available. The "Oliver region" used in this study is defined by the area south of Vaseux Lake, and north of Osoyoos Lake, which is underlain by significant depths of unconsolidated material. The region also

[9]GMS presently has a *trunc*(**x**,*a*,*b*) function, which truncates the TIN data values from **x** such that they are $\geq a$ and $\leq b$, where *a* and *b* are constant values. This custom Python routine extends the procedure to allow **a** and **b** to be TIN surfaces, compatible with **x**

[10]The original stream hydrology data are linked and routed together, such that ephemeral and naturally discontinuous streams are connected through straight lines to the nearest water source, such as Okanagan River

includes Meyers Flat, to the north-west, and Inkaneep[11] to the east. The spatial definition of the bedrock boundary was approximated from a GIS analysis of boreholes, digital elevation, slope, and orthophoto data.

The bedrock surface was kriged using a hybrid semivariogram model shown in Figure 2.8. Point sample data include: (1) available borehole bedrock contacts, (2) sampled ground elevation data, where bedrock is assumed to be exposed; and, (3) control points to extend bedrock contact below boreholes that did not reach bedrock, and below the ground surface.

From the available data, it appears the maximum depth of the bedrock surface ranges from approximately 0 to 100 m above sea level (see Figure 2.7). There are no indications that the bedrock is eroded as deeply as in the northern Okanagan, where the bedrock contact is below sea level in many parts of the Valley. However, the bedrock depth can only be verified by deep mid-valley boreholes or from geophysical investigation.

[11]This is the official geographic name; however, it is also popularly known as *Nk'Mip* or *Inkameep*

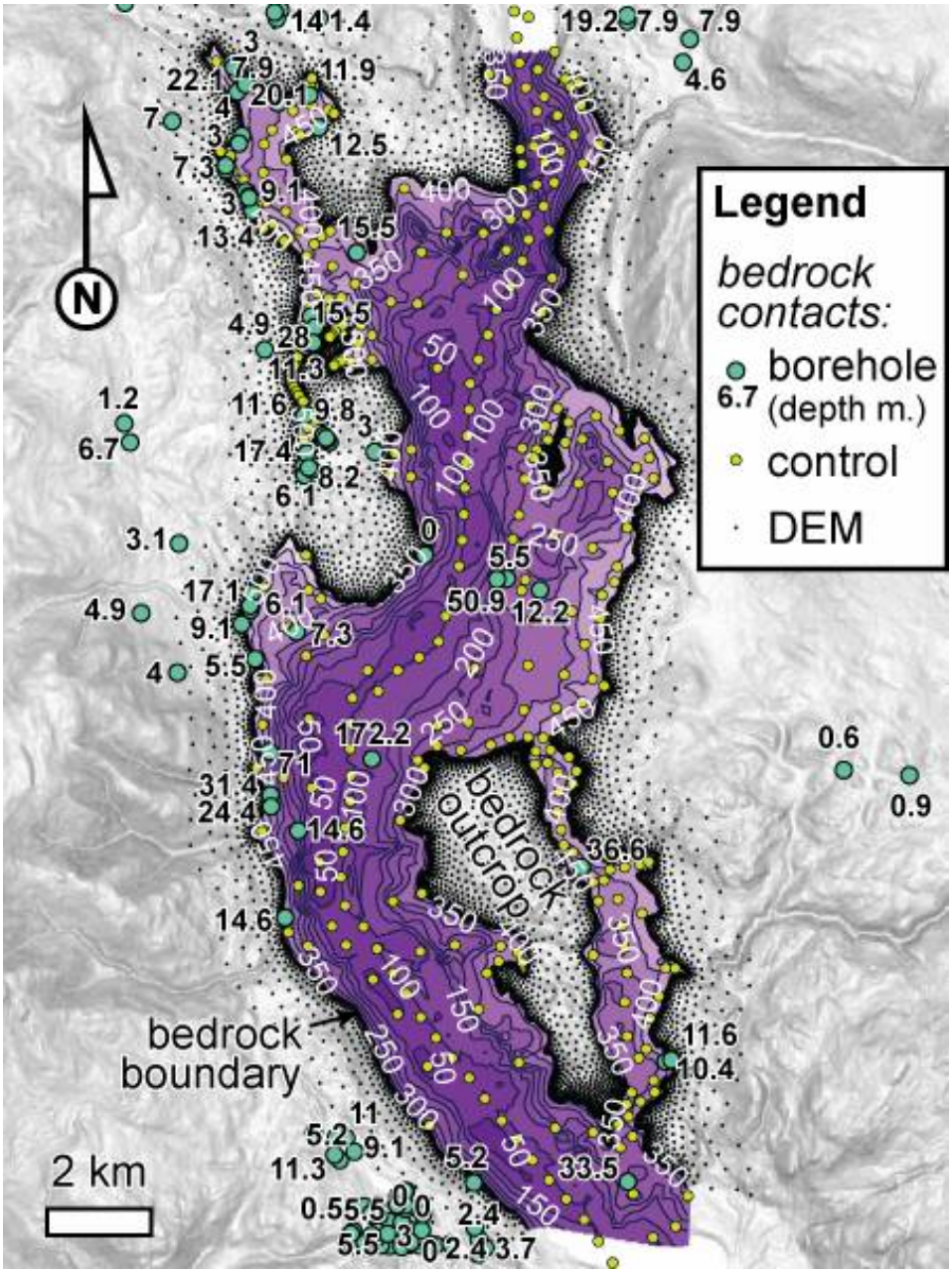

Figure 2.7: Bedrock surface in the Oliver region from borehole data; the bedrock boundary divides predominantly exposed bedrock from significant depths of unconsolidated material.

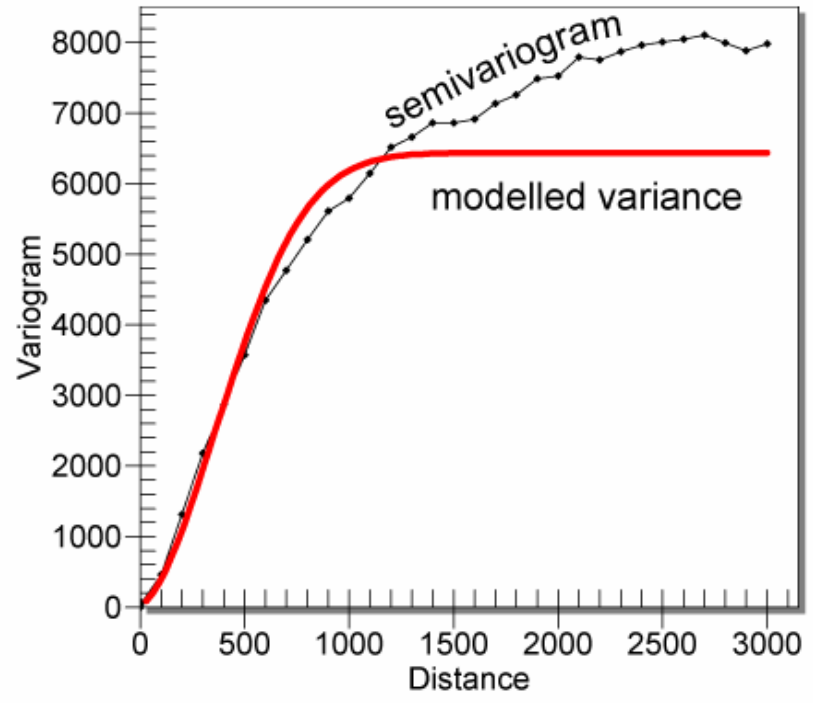

Figure 2.8: Semivariogram and geostatistical model for the bedrock surface. The hybrid model has: (1) nugget of 5; (2) Gaussian model with a contribution of 5926 and a sill of 975; and (3) a spherical model with a contribution of 505 and a range of 374.

2.7.3. QUATERNARY DEPOSITS

The first detailed map of surficial deposits in the southern Okanagan was produced by Nasmith (1962) (see Figure 2.3). In that study, Nasmith interprets a complex assemblage of outwash terraces, kame terraces, and moraines. The map and related interpretations are perhaps too detailed—as it divides regions with similar deposits into multiple depositional environments, which have specific diagenetic contexts that are subject to multiple interpretations. Nasmith's map was used as a guide to further map the basic distributions of materials. The map in Figure 2.9 shows a simpler distribution of surficial deposits, as mapped from borehole, digital elevation and orthophoto data.

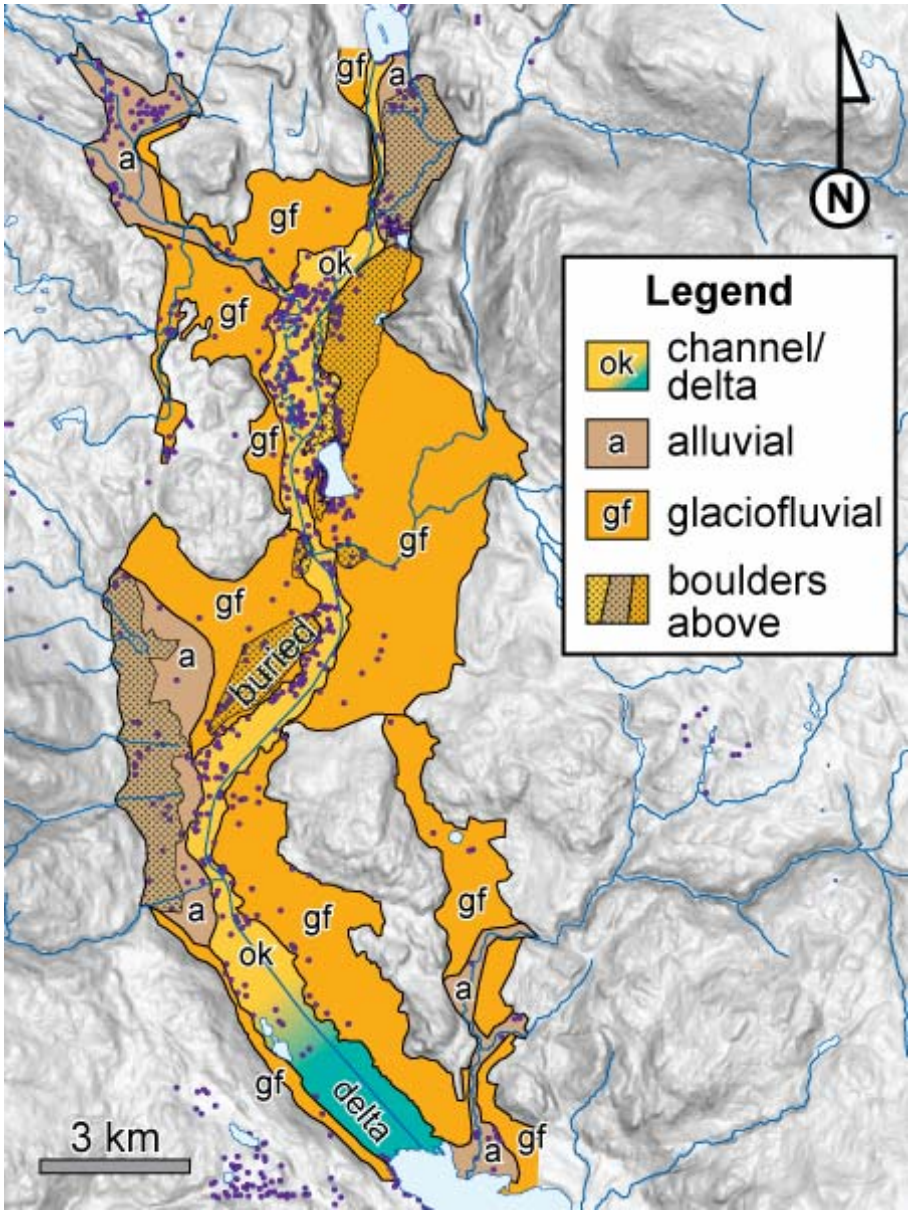

Figure 2.9: Surficial deposits of the Oliver region, showing three primary facies, with accessory boulder deposits. Glaciolacustrine silt and clay (not shown) are generally found below the relatively coarse-grained deposits in this map.

The stratigraphy and interpreted depositional facies in the Oliver region is best described using the depositional system framework (Vanderburgh and Roberts, 1996), with the exception of the subglacial fluvial system (in Figure 2.4), which appears to be absent in the Oliver region. However, all of the conceptual models fail to adequately describe all of the mapped geological materials unique to the Oliver region, so additional depositional environments are proposed

here—specifically the boulder deposits and the drainage currents near McIntyre Bluff during deglaciation.

Geologic cross-sections through the Oliver region are shown in Figure 2.10, which show both the borehole materials with interpretations of their depositional facies, and the water table. The cross-sections were constructed from information in the WELLS database.

2.7.4. GLACIAL TILL DEPOSITS

Many lithologic units in the WELLS database are described by drillers as “till”, “hardpan” or related terminology; however, many of these are, at most, a diamicton. Generally, these units are consolidated or semi-consolidated materials, often containing gravel. The deposits are usually located near the surface, and are either on alluvial fans or along steep valley margins, and many are interpreted here as mass-debris flow deposits, which is part of an alluvial fan facies, described later.

Glacial till appears to be rare in the Oliver area; however, this speculation is based on borehole descriptions, and is influenced by glacial conceptual models. Areas where till deposits are interpreted are at higher elevations, along the sides of the valley, near Meyers Flat and Inkaneep. The deposits are generally a “hard” mixture of clay and gravel, and overlie the bedrock surface. Till deposits appear to be spatially discontinuous, and are found below glaciofluvial and glaciolacustrine materials. To verify a glacial origin of diamicton deposits, detailed sedimentology and age dating (such as photoluminescence dating) are required.

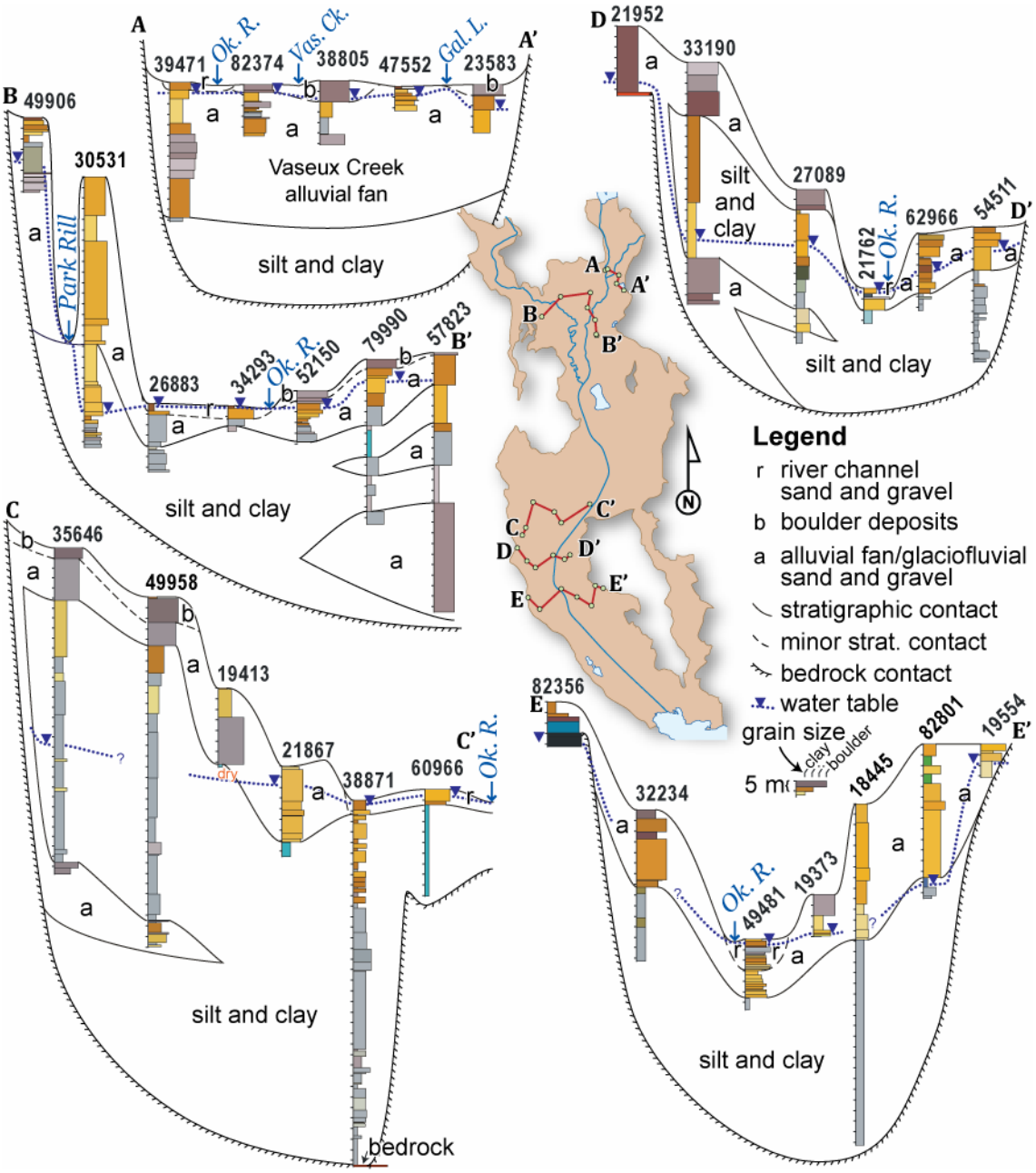

Figure 2.10: Cross-sections through the Oliver region showing textures from the WELLS database, identified by their well tag numbers (WTNs). The width of the columns are proportional to the grain size, and the shading is from the description. Alluvial and glaciofluvial deposits are grouped together in this interpretation, as it is difficult to distinguish between the facies in some boreholes.

2.7.5. GLACIOLACUSTRINE DEPOSITS

Thick silt and clay deposits constitute the majority of unconsolidated valley fill sediment, and are found throughout the study area, up to 700 m above sea level near Richter Pass, and often onlap the bedrock surface (Figure 2.11). Fulton (1965) and Shaw (1977) describe these sediments as rhythmites of silt and clay, which have high-lateral continuity, and decrease upwards in sequence thickness, from several metres to several millimetres. The silt and clay can be interbedded with sand, usually near the valley margins and toward the northern end of the study area. Coarser sand and gravel are also found in discrete beds within the silt and clay unit, and are proximal to alluvial fans and creeks entering the valley. Rare wood and other organic material are found in isolated boreholes, which are usually suspended in fine-grained materials. Similar “white silt” deposits are found throughout Okanagan Valley, Thompson Valley, and similar valleys in the BC Interior.

The fine-grained deposits are interpreted to have been rapidly deposited from sediment suspension in a lacustrine environment in or near a glacier margin (Mullins et al., 1990; Eyles and Mullins, 1991). The coarser sand within this unit is interpreted to have been deposited from minor turbidity flows and slumps along the margins of the valley, while in the northern part of the study region, the sand is interpreted to have been derived from higher-energy water currents near McIntyre Bluff. Higher-energy currents may have occurred from water drainage diversions around possibly stagnant deglacial ice at McIntyre Bluff, where the Okanagan Valley narrows to less than 2 km wide. The diversion of drainage in this region would have changed as the water surface of GLP receded—in particular when the water surface reached the elevation threshold around the overflow channels in Figure 2.12.

The top of the silt and clay was interpolated using natural neighbours (Figure 2.11). The silt contacts in the boreholes were selected as the first significant thicknesses of silt or clay; however, this contact can overlie confined (or buried) sand and gravel aquifers. The silt contact depth is coincidently where many of the water well drillers stopped, as drillers are likely aware of this thick, poorly producing hydrogeologic unit. The silt top surface was trimmed between the bedrock and the ground surface, with an additional ~10 m depth surrounding Okanagan River and Park Rill. The depth adjustment in the interpolated surface around the rivers is to maintain continuity of the sand and gravel deposits above the silt top and adjacent to the rivers.

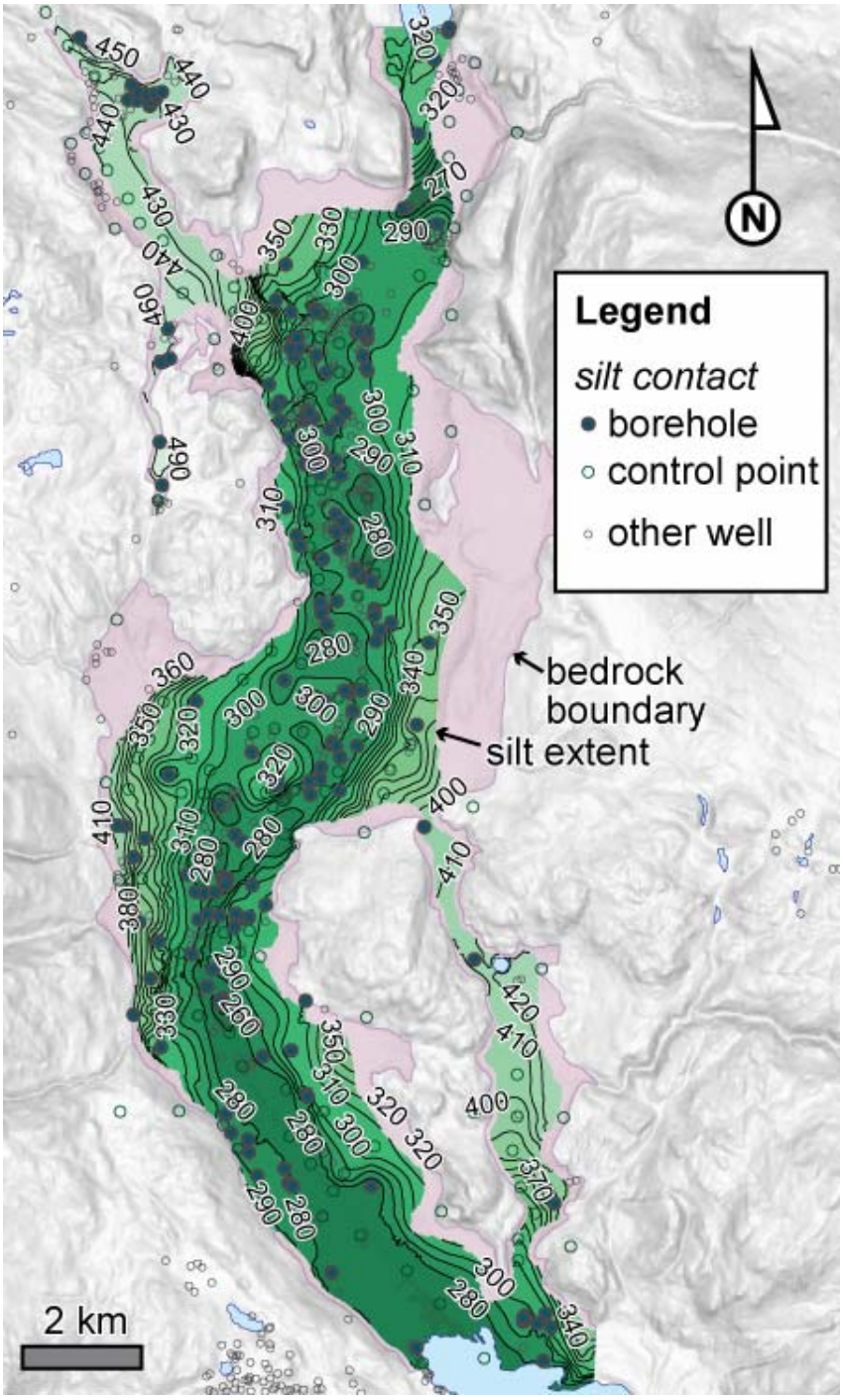

Figure 2.11: Elevation and extent of glaciolacustrine silt and clay, which is predominantly buried beneath glaciofluvial sand and gravel. This surface was interpolated using natural neighbours, using 187 borehole contacts and 146 control points. Control points were added to ensure a reasonable thickness of sand and gravel above the silt to the surface, and also to the interpolated water table surface, described later.

A possible influence of higher-energy currents is evidenced by alternations between sand, silt and clay units in boreholes to the north; some of which have shells (possibly from a lacustrine environment) in the finer material above coarser grained deposits (e.g., WTN 46717, Hodge and Lowen, 1980). The coarse deposits are also found at lower elevations in this area, which may have been a result of high-energy currents due to a drainage diversion.

The top of the silt and clay in Figure 2.11 identifies several isolated topographic high and lows, which could be interpreted as kettle holes, described later. The silt top appears to be deepest at the northern part of the study region, adjacent to Vaseux Creek. This is perhaps due to strong water currents, or possibly due to active alluvial fan (or subaqueous fan) deposition in this region.

2.7.6. GLACIOFLUVIAL DEPOSITS

Sand and gravel deposits are abundant along the sides of the valley, and usually consist of gravel and sand cross-beds with minor finer material present in some locations. The deposits are found throughout the region, and have formed large terraces on either side of the valley (Figure 2.12), and are above the Okanagan River floodplain. Lower-gradient regions and terraces to the north-west have finer-grained sediments, ranging between silt to medium-grained sand.

These glaciofluvial deposits are interpreted to have been deposited near glacial ice, which supplied large volumes of sediment and water. During the deglaciation of the CIS, very large volumes of water would have melted in Okanagan Basin and drained through the Oliver region over several hundred years. The four-major terraces in Figure 2.12 were likely formed as the surface of GLP dropped. The current energy of the water would have also increased, as the water-column depth decreased, resulting in coarser sediments near the top. The terrace immediately south-west of McIntyre Bluff may have preserved backwash water from the main currents, as the sediment consists of sequences of fine- to medium-grained sand and silt.

Glaciofluvial deposits have buried the much finer glaciolacustrine deposits, and the contact between the two geologic facies is an unconformity, as some of the fine material has likely been eroded by the strong currents that deposited the glaciofluvial deposits. This important contact has been reached by many boreholes in the region, and it has a moderately flat contact surface elevation, with local highs and lows (see Figure 2.11). The glaciofluvial deposits have since

been removed or reworked in many regions, such as along the Okanagan River and other creeks.

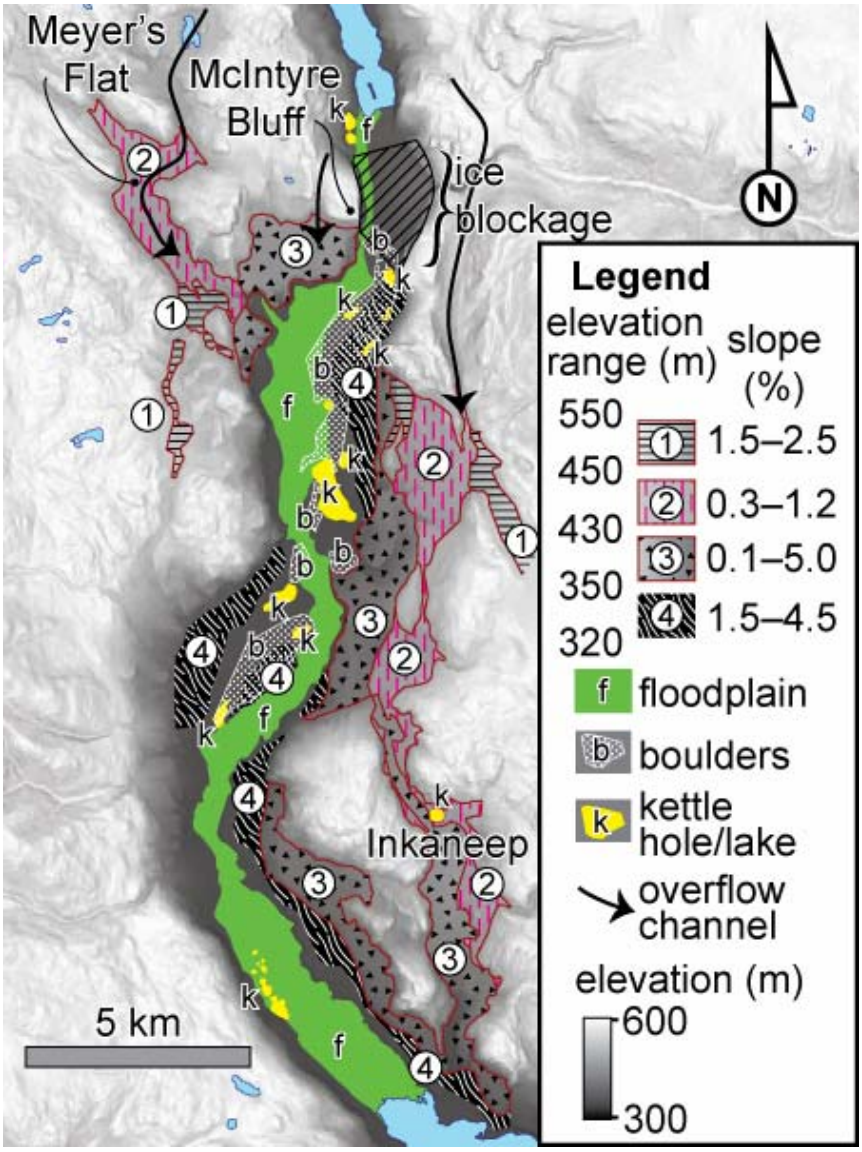

Figure 2.12: Map showing the stepped glaciofluvial terraces along the valley margins, which are interpreted to have been created due to the diversion of water flow around McIntyre Bluff, and the dropping glacial lake level. The distribution of boulders is possibly the result of a breached ice dam near McIntyre Bluff, which may have also redistributed large ice-blocks that would later melt to form kettle holes.

2.7.7. BOULDER DEPOSITS

This anomalous deposit is found at or near the surface in several discrete locations of the Oliver study area (Figure 2.12). It is usually composed of boulders, cobbles, and gravel. Sand is also found in some deposits; however, finer material is generally absent. The boulder deposits appear to overly either sand and gravel, or silt and clay. The deposit, south of Oliver, is buried beneath 6 to ~20 m of sand and other deposits. Other discrete boulder deposits are found near the mouths of creeks along the margins of the valley, above sand and gravel alluvial fans.

These very coarse units can only be transported in a high energy environment. Many of these deposits form the upper sequences of alluvial fans, and are likely deposited through related alluvial processes; however, other discrete boulder deposits in the valley center are not proximal to alluvial fans or valley margin creeks, and require a different transportation process. One possibility is that coarse material accumulated near McIntyre Bluff, along with ice blockage, and was rapidly dispersed when the ice dam breached. In this event, the volume and flow of water would have been potentially very large, and could have transported the boulders, and washed-out any finer materials. In addition, large blocks of ice could have been transported throughout the region south of McIntyre Bluff, and would have created kettle holes and lakes.

2.7.8. ALLUVIAL FAN DEPOSITS

Sand and gravel deposits are generally found near the mouths of creeks along the valley margins, and fan out a few kilometres toward the basin center. The deposits are generally thick, and are often associated with cobbles, and boulders in the upper parts. In isolated sections, the deposits are either cemented or can be classified as a diamicton due the presence of clay, and are often termed by drillers as “hardpan” or “till”.

The deposits are interpreted to be part of an alluvial fan facies, which consists of coarse material deposited from streams and mass-debris flows. Cemented or diamicton units are likely mass-debris flow deposits, which have calcite cements that likely formed shortly after the debris flow event. Calcite cement may have been available from freshly ground and volatile calcite-rich minerals from the parent rocks. Alluvial deposition was active from the time that glaciolacustrine deposition began, and has continued at a slower rate to the present day.

Alluvial deposition also occurred at the same time as glaciofluvial processes, and in many areas it is impossible to distinguish the two facies. As both the glaciofluvial and alluvial facies

generally share similar sedimentological characteristics and timing, these can be mapped as a single unit. Nasmith (1962) recognized and mapped raised alluvial fan deposits, which appear to grade to the former GLP water surface. Although the distinction of two alluvial fan deposits is interesting from a Quaternary geologic perspective, they are treated and mapped as a single depositional facies and material for this study.

2.7.9. RIVER CHANNEL DEPOSITS

These deposits consist of a range of grain-sizes from silt and clay to sand and gravel. Many vertical sections are fining upward sequences, which grade from gravel and cobbles at the base (called a channel lag) to silt and clay at the top (overbank deposits). In addition, silt and clay is found in discrete lenses, which are several metres thick. Peat and other vegetation are found in several boreholes, which extend up to 15 m below the ground surface, near the shores of Lake Vaseux, Lake Osoyoos, Gallagher Lake, Tugulnuit Lake, and near Park Rill. This facies is very continuous, and is adjacent to Park Rill and Okanagan River. Oxbow lakes are commonly found within 1 to 2 m elevation of the present river, and many other buried oxbow lakes are apparent in orthophotos (Figure 2.13). The southern 3 km of Okanagan River flows through a wetland, and has a very low gradient. Okanagan River has a deltaic morphology, as viewed in orthophotos, as it flows into Osoyoos Lake.

This fluvial channel facies was deposited from the Okanagan River and Park Rill, and consists of fluvially re-worked sediment derived from glaciofluvial and alluvial sediments. Deposition is interpreted to have begun when the hydrologic profile of Okanagan River had reached a minimum elevation—possibly after the discharge wained as the CIS melted.

Okanagan River has since aggraded about 15 m, as interpreted from previous vegetation horizons. However, it is cautioned that these organic sediments may have been deposited in deeper water, giving a false horizon and aggradation estimate. Aggradation of this deposit is interpreted to be in response to the accumulation of Vaseux Creek alluvial fan to the north, and Tonasket Creek alluvial fan to the south, near Oroville, Washington. In boreholes where coarse sediments appear to be deeper than 15 m, the deeper deposits may be older glaciofluvial sediments. A contact between the two facies is not easily identifiable due to their similar textures.

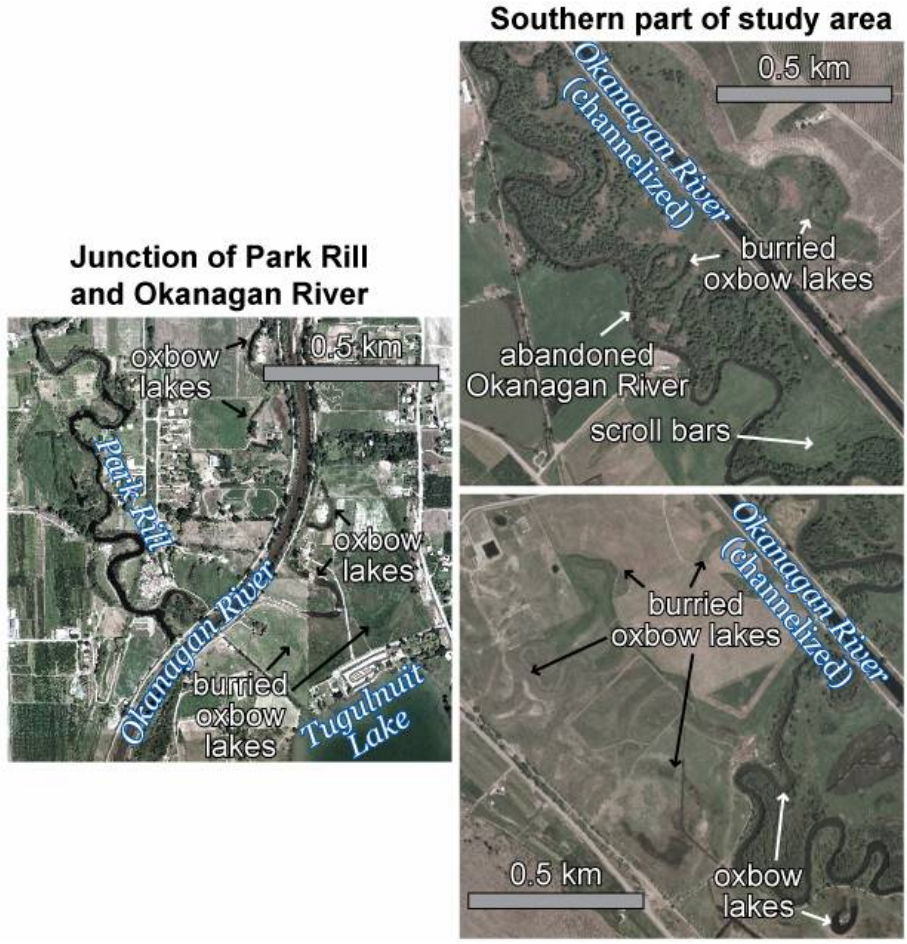

Figure 2.13: Examples of oxbow lakes, buried oxbow lakes found in aerial photos.

Sediment sequences in this facies are that of typical sand and gravel channel deposits, with over-bank silt and isolated oxbow-lake clay plugs. The contacts from channel deposits to glaciofluvial or alluvial deposits are not easily recognized, as they consist of similar materials. This facies is mapped with the assistance of digital elevation data, as it is no higher than perhaps a few metres from the present-day water surface of Okanagan River.

The southern ~3 km of the study area is interpreted to be a delta, which is prograding into Osoyoos Lake. There are limited boreholes in this region (as the water table is very shallow); however, sediments in this region appear to be similar to the other river channel deposits, having gravel channel lag and silt flood plane deposits.

2.7.10. KETTLE LANDFORMS

Several isolated depressions have been identified in both the ground surface topography (see Figure 2.12), and in the silt top surface (see Figure 2.11). The features in the silt top are not identified on the surficial river channel deposits, and they are filled above with sand and gravel deposits. Many of these features appear to be in the same regions where the anomalous boulder deposits are found.

These buried and surficial landforms are interpreted to be either kettle holes or kettle lakes (such as Tugulnuit Lake, Gallagher Lake, and multiple lakes near Deadman Lake). The landform would have developed from rapid sediment deposition on buried ice, which would have later melted to produce depressions in the surface. The depressions in the silt top indicate that stagnant ice blocks may have been present in the valley during glaciolacustrine deposition; however, the size and the distribution of the ice remains unknown due to the apparent absence of deglacial till deposits.

Kettle landforms are also found on the surface topography in the glaciofluvial deposits. Since these appear to be spatially independent from the kettle landforms in the silt, these may have been formed from ice blocks that were transported during glaciofluvial deposition. Due to their proximity to the anomalous boulder deposits, these may have been transported in a related event described previously. Kettle landforms are generally not identified on the Okanagan River flood-plane, as they would have been filled in. One exception is Lake Tugulnuit, which had previously been influenced by Okanagan River (see Figure 2.13).

2.7.11. CHRONOLOGY

An illustration of the possible timing and deposition of sediments during the Quaternary Period is shown in Figure 2.14. The timing of deposition and the volume of valley ice is poorly understood, although it is likely that the majority of sedimentation occurred during the Late Wisconsin glaciation, as the CIS was melting. Preservation of any prior glacial sediments in the Oliver region (e.g., Fulton and Smith, 1978) is inconclusive, since there are no seismic surveys that could indicate any possible unconformities, nor are there any reliable and direct stratigraphic age estimates (e.g., *in situ* organic material from interglaciations).

Two nearby radiocarbon date locations are selected for chronology of Holocene-aged sediments: (1) a wood fragment from Penticton at a depth of 51 m and an age of 9070±80 years

before present (BP) (GSC-3601; McNeely and Clague, 1996); and (2) a series of radiocarbon dates from organic material between 8.5 and 11.5 m below the bottom of Tugulnuit Lake, with dates ranging from 3780±50 to 3860±50 years BP (Rück et al., 1998). The radiocarbon date from Penticton is likely a waterlogged wood fragment that was deposited in GLP, and represents one of the first signs of flora in Okanagan Basin after the last glaciation. The series of radiocarbon dates from the bottom of Tugulnuit Lake are likely timed with over-bank flooding of Okanagan River, which briefly flowed into the lake.

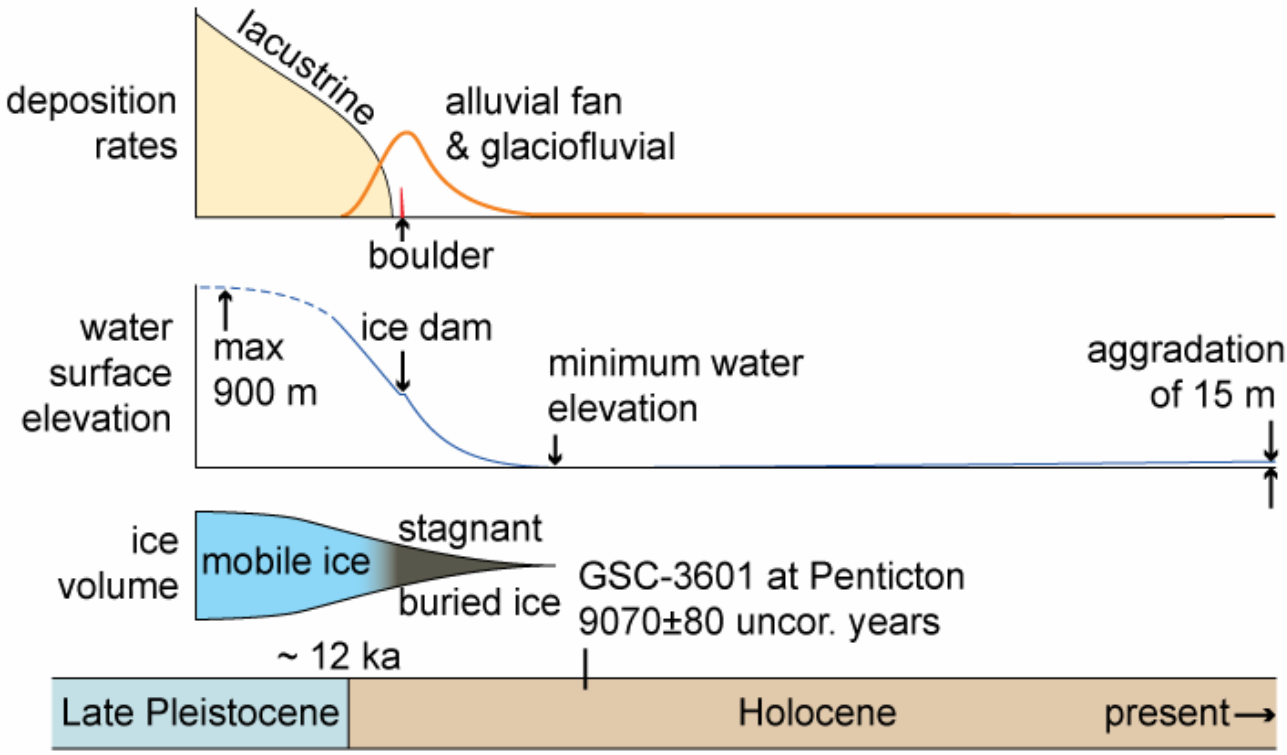

Figure 2.14: Conceptual diagram of deposition in the Oliver region during the Quaternary Period. Depositional rates have greatly diminished from their former rates, after the disappearance of the CIS. The transition of deposition from glaciolacustrine to glaciofluvial is partly due to the declining water surface elevation, which controlled the water energy. As the stagnant and buried ice volume melted, kettle lakes and holes appeared on the surface. The radiocarbon date indicates the first sign of flora in the region after the last ice age.

3. HYDROSTRATIGRAPHY

3.1. BC AQUIFER CLASSIFICATION

In the study region, the BC MoE has mapped four aquifers using the WELLS database (Berardinucci and Ronneseth, 2002). In this region, two types of aquifers are mapped: highly-vulnerable unconfined and low-vulnerable confined aquifers (Figure 3.1). The mapped aquifers are described in "worksheets", available through the BC MoE, and are summarized below.

Aquifer 254 is located in the southern half of the study area, and is a shallow sand and gravel aquifer, which is underlain by thick silt and clay deposits. The median depth to water is 3.1 m, and the median production rates in the aquifer are 3.8e-3 m³/s (60 USgpm[12]). This aquifer is said to be recharged by the Okanagan River, irrigation and precipitation.

Aquifer 255 is in the northern half of the study area, and consists of sand and gravel with boulder deposits, and is also underlain by silt and clay. This aquifer is predominantly unconfined, although some deeper wells in this region are completed in confined sand and gravel aquifers below the silt and clay deposits. The median depth to water is 11.6 m, and the median production rates are 9.5e-4 m³/s (15 USgpm). This aquifer is recharged from the Okanagan River and from precipitation.

Aquifer 256 is along the western side of the valley, and is a deep confined sand, gravel aquifer. It is the only aquifer in the Oliver region with a low vulnerability rating, due to the water depth and the presence of confining beds consisting of cemented and finer grained deposits. The median depth to water is 9 m, and the median well yield is 1.9e-4 m³/s (3 USgpm). It is recharged from precipitation, and the adjacent creeks.

Aquifer 257 is located at Meyers Flat, at higher elevations in the north-west part of the study region. This moderately developed unconfined aquifer consists of variably cemented sand and gravel deposits, and is underlain by silt, diamicton and bedrock at variable depths. The median depth to water is 8 m, and the median well yield is 2.5e-3 m³/s (40 USgpm). The aquifer is said to be recharged from precipitation, although Park Rill flows through the center of the mapped aquifer.

[12]US liquid gallon per minute; 1 USGPM ≈ 6.31e-5 m³/s ≈ 5.45 m³/day

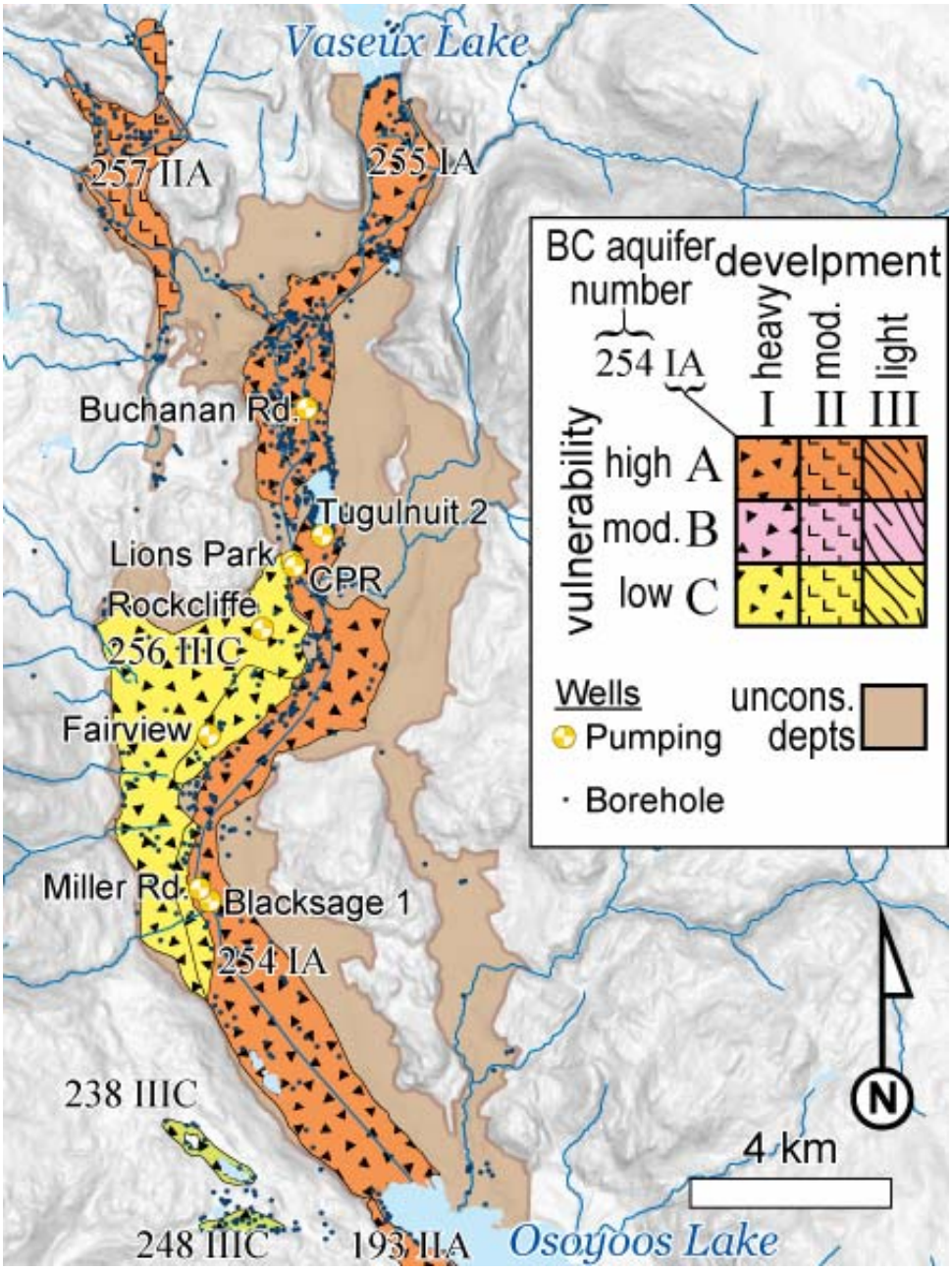

Figure 3.1: BC aquifer classification map, described by Berardinucci and Ronneseth (2002). The unconsolidated deposits surrounding the mapped aquifers are either dry or undeveloped (thus unrecognized).

3.2. HYDROSTRATIGRAPHY

Hydrostratigraphic units can be defined by combining several depositional facies having similar sediments with assumed hydrogeological properties. In particular, geologic units that are generally comprised of sand and gravel (river channel, glaciofluvial and alluvial facies) or silt and clay (glaciolacustrine facies) can be combined and treated as single hydrogeologic units.

The simplification of stratigraphy can help reduce the complexity of groundwater model construction; however, the heterogeneity of the materials can affect flow paths, and the delineation of capture zones to production wells. Heterogeneity is the degree of spatial variation of materials and their associated hydrogeologic properties within a region. All of the units express some degree of heterogeneity, such as: (1) rhythmites of silt and clay in the glaciolacustrine deposits, (2) cementation and presence of boulders in the alluvial fan deposits, and (3) presence of fine-grained buried oxbow lake sediments within the fluvial channel deposits. These heterogeneities can be addressed in groundwater modelling by employing stochastic techniques of the material properties as discussed later.

The important hydrogeologic units in the Oliver region are:

Silt and clay: consisting of the lacustrine deposits; this unit has poor groundwater production potential, due to the low hydraulic conductivity and storage properties; it is interpreted as an aquitard;

Sand and gravel: consisting of the (1) river channel, (2) glaciofluvial, (3) and the alluvial deposits; this unit has high groundwater production potential; however, it is generally dry if it is far from a river or creek;

Boulder: these anomalous deposits can potentially have very high production potentials, and may provide buried conduits for water flow, if they are below the elevation of a nearby river.

3.3. WATER TABLE

A map of the water table elevation (Figure 3.2) was defined using the water depth as reported in the WELLS database, and calculated from the difference of well elevation and the water depth. However, this method of defining water table elevation can present problems, since the water depths in each well were obtained at different dates (between 1922–2004) and measured using different methods. Furthermore, some measurements are influenced from the development and purging of the well, while other measurements are in confined aquifers, which may not adequately represent the water table elevation.

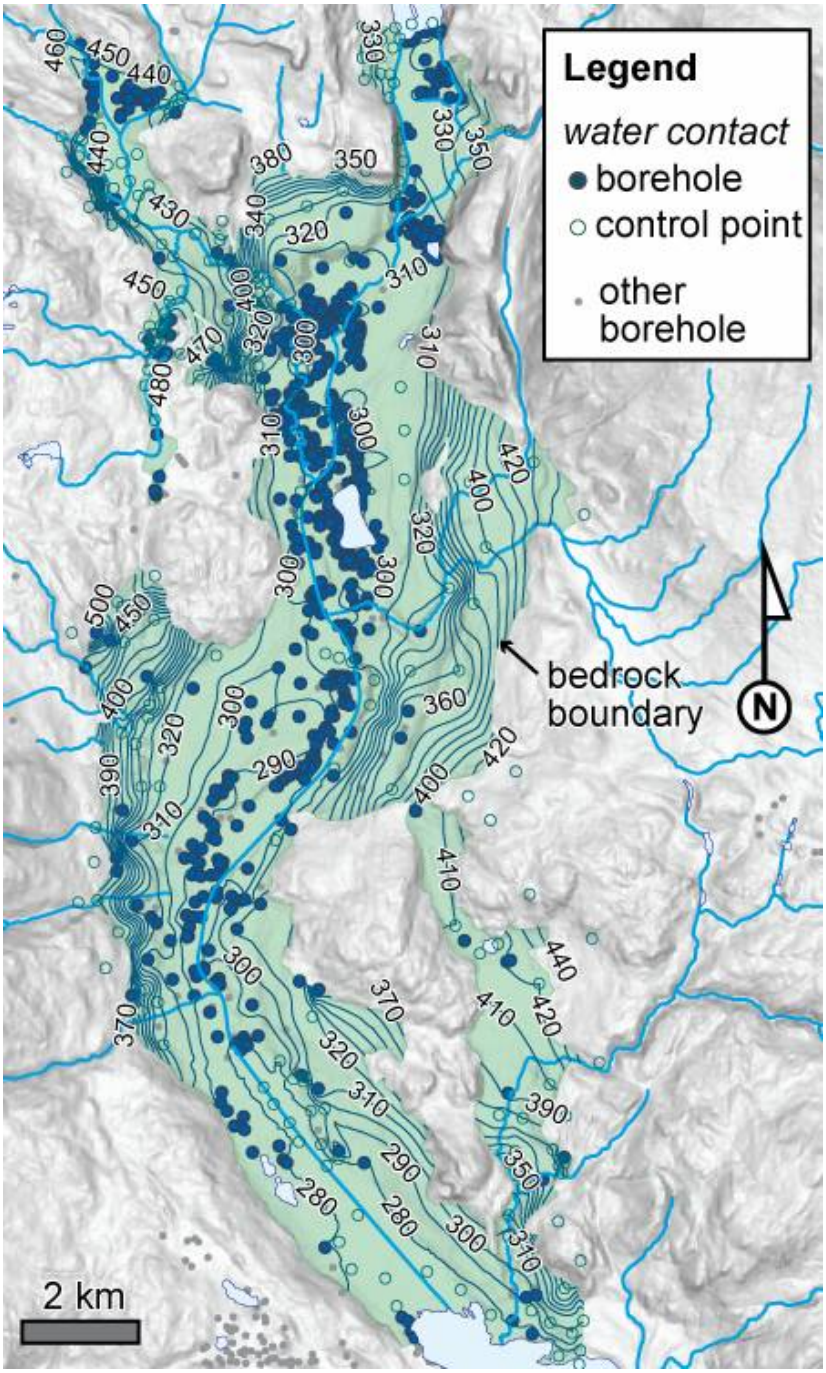

Figure 3.2: Map of water table elevation, interpolated with the natural neighbour interpolation method using 569 data points from the WELLS database, and an additional 202 control points. It should be cautioned that this map is technically a potentiometric head map, as some of the wells on the valley side are in confined aquifers.

From the water table elevation map, it can be observed that the water table is relatively flat in the valley bottom, and is close to the elevation of Okanagan River. Along the valley margins, near the bedrock outcrops, the water table is at a higher elevation; however, the exact profile of

the water table from the valley bottom to the bedrock margin is difficult to define without detailed data. At higher elevations along the benches, it is assumed that both the depth of the bedrock and silt influence the depth of the water table, such that if the water table is shallow, then the depth of the silt or bedrock contact is at a nearby depth (unless already defined in the borehole lithology).

3.4. AQUIFER GEOMETRY AND LAYERS

Despite the abundance of highly-permeable sediments, locations of aquifers in the Oliver region are highly dependant on the groundwater table depth and the proximity to surface water features, such as Okanagan River. There are two forms of aquifers in the study area: (1) upper unconfined, and (2) lower or confined aquifers. The upper aquifer is adjacent to Okanagan River, and is the most productive and accessible aquifer in the study region. Much less is known about the lower confined aquifers, as they are disconnected from each other, and fewer boreholes have defined their geometry.

3.4.1. UPPER UNCONFINED AQUIFER

The main aquifer in the study region is the upper unconfined sand and gravel aquifer adjacent to Okanagan River. The upper aquifer is the same as Aquifers 254 and 255 in Figure 3.1. The majority of water wells (including all of the municipally controlled wells) are completed in this aquifer, since it has a very high specific capacity. Many of the water well records in the WELLS database are dug-wells, as this aquifer is at a shallow depth near surface water features.

Upper unconfined sand and gravel aquifers are also present at higher elevations in the study region, along the valley margins. This includes (but is not limited to) Aquifer 257 in Figure 3.1 at Meyers Flat. These aquifers have a much more limited total capacity, and are likely to be highly influenced by local streams. Aquifer tests from Meyers Flat (Kalyn, 1983) indicate that these sediments have similar hydraulic properties as the aquifer adjacent to Okanagan River.

The saturated thickness of the upper sand and gravel (Figure 3.3) is determined from the difference in the water table elevation (see Figure 3.2) and the top of the uppermost silt and clay contact (see Figure 2.11). The aquifer thickness, b, is directly proportional to the transmissivity, T, through the relation $T=Kb$, where K is the hydraulic conductivity of the aquifer. The saturated

thickness is important for providing adequate horizontal groundwater flow through the unconfined upper aquifer; e.g., from a river to a pumping well. A thin saturated aquifer would have a limited ability for the well to access groundwater recharged through the river.

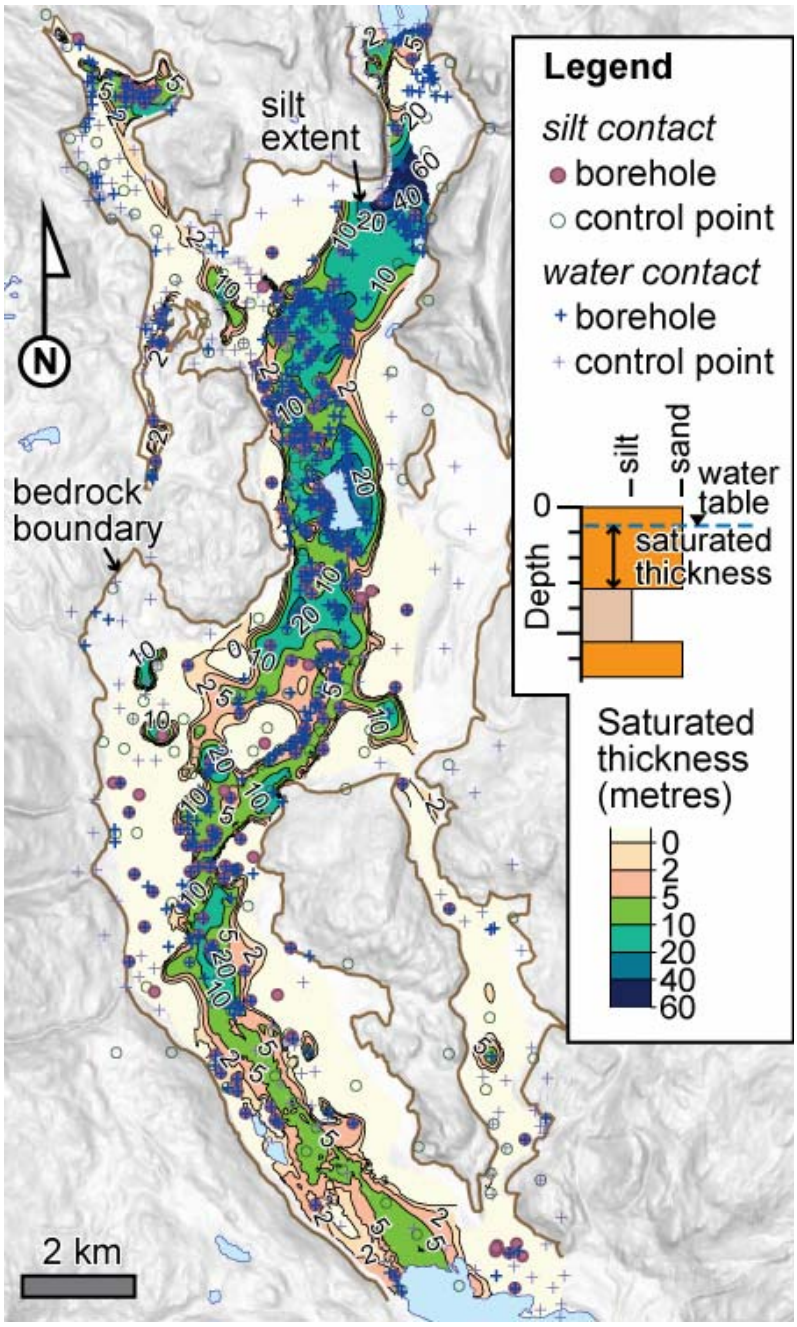

Figure 3.3: Saturated thickness of upper sand and gravel aquifer, b, as calculated from the difference of the water table, and the uppermost silt top. This map does not consider confined aquifers beneath the uppermost silt contact, which is why there are many producing wells found where b=0. Interpretations to the reliability of this data are dependant on borehole data, and should only be considered most reliable where both silt and water table contacts are available.

The map in Figure 3.3 should be consulted with discretion, as it is derived from two interpolated datasets; thus it may only be reliable in regions where data points from both sets are nearby. However, regions with sufficient data points show that the saturated thickness of the upper aquifer adjacent to Okanagan River varies from a few metres to 20 m or more, which is influenced most by the silt top elevation. Some areas with isolated zones of high saturated thicknesses can be associated with kettle holes in the silt top, such as near Rockcliffe, Fairview, Miller Rd., and other production wells.

The presence of boulder deposits also appears to influence high specific capacities for many wells in the upper aquifer. These boulder deposits are mappable in several zones, and can potentially offer very high hydraulic conductivities (if saturated).

3.4.2. LOWER CONFINED AQUIFERS

The upper glaciofluvial units in the northern valley bottom contain layers of fine sand, which make some of the wells partially confined (e.g., WTNs 53199, 46717). These finer-grained confining deposits appear to be discontinuous, and may have resulted from varying water currents in GLP during the Late Pleistocene.

Deep confined sand and gravel aquifers are found along the valley margins, which are in alluvial deposits. This includes Aquifer 256 in Figure 3.1. Many of these alluvial fan deposits interfinger the glaciolacustrine deposits at depth, and extend only a few hundred metres toward the valley center. These aquifers are likely to be most influenced by ephemeral streams. As these streams have also deposited the alluvium, they are likely to be hydraulically connected.

4. RECHARGE MODELLING

4.1. INTRODUCTION

The approach used to simulate recharge is similar to that employed in previous studies by Scibek and Allen (2006a, 2006b) to investigate the impacts of future predicted climate change on groundwater recharge. As such, the full approach used a combination of computer models including: (1) GCMs (global climate models) for current and future-predicted climate change periods; (2) Statistical Downscaling Model (SDSM) to statistically downscale temperature from GCMs; (3) LARS-WG to stochastically generate weather and evapotranspiration data; (4) ROSETTA to estimate the hydraulic properties of soils from given soil measurements; and (5) HELP for simulating surface and subsurface hydrology from climate and soil data.

Historic climate data are generated synthetically using a stochastic weather generator. For the climate change analysis, the absolute changes in temperature, and the relative changes in precipitation and solar radiation, were determined using a downscaling technique and directly from the GCMs, respectively. These changes were used to shift the climate in the weather generator.

This section of the report provides an overview of the methodology and results, and presents the results for the current (historic) recharge. It does not discuss the various GCMs, nor the downscaling that was used to predict shift terms for future climate change. Details concerning the complete methodology and results for different climate change models and periods are provided elsewhere (Toews, 2007).

Recharge results are obtained for a grid with 100 m resolution, using geospatial data from each location, including soil, land use, surface slope, groundwater depth, and leaf area index (LAI).

4.2. OBSERVED WEATHER DATA

Daily measurements of precipitation and temperature are available throughout much of the Okanagan, and are provided by the Meteorological Service of Canada (Environment Canada, 2002). Station names and locations are listed in Table 4.1. Hourly global solar radiation data are available at Summerland and Mt. Kobau, west of Oliver, and hourly wind velocity and relative humidity data from Osoyoos, south of Oliver. These climate variables are used to (1) calibrate the stochastic weather generator, (2) downscale GCM climate variables, and (3) provide

meteorological data to estimate evapotranspiration.

Temperature and precipitation normals for Oliver are shown in Figure 4.1. The diurnal variability of temperature in Figure 4.1a is greatest during the summer (as indicated by the thick vertical lines), while the largest variability in seasonal mean temperature is during the winter time (as indicated by the heights of the 1st and 3rd quartiles of the boxplots). Outlier temperature minima between November and February are likely indicative of cool arctic climate systems. Maximum temperatures in the Oliver region peak near July 27. Precipitation normals (Figure 4.2b) are bimodal, with higher precipitation normals during summer and winter months. Precipitation normally occurs in the form of snow between December and January.

Table 4.1: Weather stations used from Okanagan Basin.

Station name	ID	Location	Elev. (m)	Years
Oliver*	1125760	49°10' N,119°34' W	315	1938–*present*
Oliver STP	1125766	49°11' N,119°33' W	297	1924–2004
Mt Kobau Observatory†	1125223	49°07' N,119°41' W	1862	1966–1980
Osoyoos CS	1125852	49°02' N,119°26' W	283	1990–*present*
Summerland CDA*†	1127800	49°34' N,119°39' W	455	1916–1995
Summerland CS	112G8L1	49°34' N,119°39' W	434	1990–*present*

*Primary stations for daily temperature and precipitation

†Station with hourly solar radiation

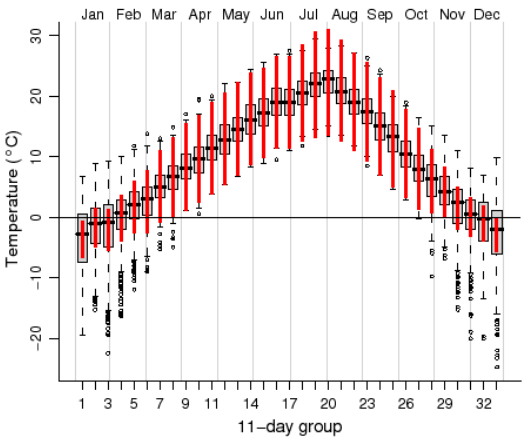

(a) Temperature; thick vertical lines represent diurnal variability between daily T_{min} T_{max}

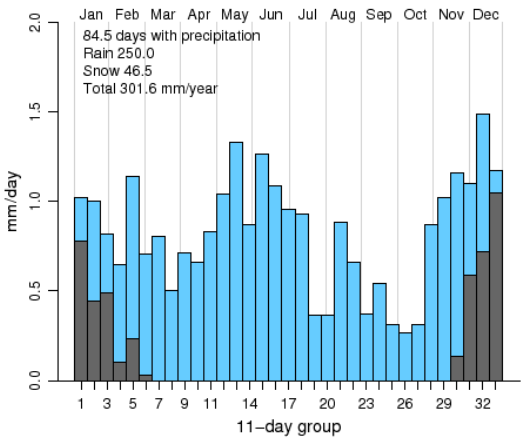

(b) Precipitation; showing rain and snow fractions

Figure 4.1: Temperature and precipitation normals of Oliver, between 1961–2000.

4.3. METHODS

4.3.1. STOCHASTIC WEATHER GENERATION

Weather and evaporation data were generated stochastically generated using LARS-WG (Semenov and Barrow, 1997). This weather generator is calibrated using daily precipitation, maximum and minimum temperature, and global solar radiation. The calibration process uses conditional relationships between the observed parameters. For example, realistic temperature and solar radiation values are generated depending if the day is considered rainy or dry. Recurrence of precipitation is determined using a first-order Markov chain.

Data from Summerland between 1962 and 1995 were used to calibrate LARS-WG, since all the required climate variables were available at this location. Although Summerland is 50 km to the north of Oliver, the two locations share a similar climatology, and are both in the valley-bottom of Okanagan Basin. The slight climate variability between the two locations is compensated by determining shift factors from the climate normals calculated using concurrent historical data (see Toews, 2007).

Synthetic weather was generated for 200 years. Output synthetic data include daily maximum and minimum temperature, precipitation, solar radiation and potential evapotranspiration. Synthetic 'historic' climate from LARS-WG is confirmed to reproduce the 1961–1990 normals from Oliver for measured temperature and precipitation normals (see Toews, 2007).

4.3.2. SPATIAL DATA

Input spatial data, used both directly and indirectly to model recharge, are shown in Figure 4.2. An extensive valley-bottom soil database was used to determine both the spatial variation and vertical assemblage of soil horizons in the Oliver region (Wittneben, 1986; Kenk and Sondheim, 1987). The database identifies 91 primary soil types from the valley-bottoms of the Okanagan and Similkameen regions. This GIS database represents soil coverages with polygons, which identify the dominance of up to three primary soil types in each polygon (Figure 4.2a), which are weighted by deciles. Physical and chemical measurements were recorded from type-section pits (~1.5 m deep) for each primary soil type. Each soil type is described with up to eight layers, and layer data include bulk density, available water content, soil chemistry measurements, and percentages of: coarse material (>2 mm), sand, silt, clay, and organic matter. Soil drainage was obtained from the bulk properties assigned to each soil type (Figure 4.2b).

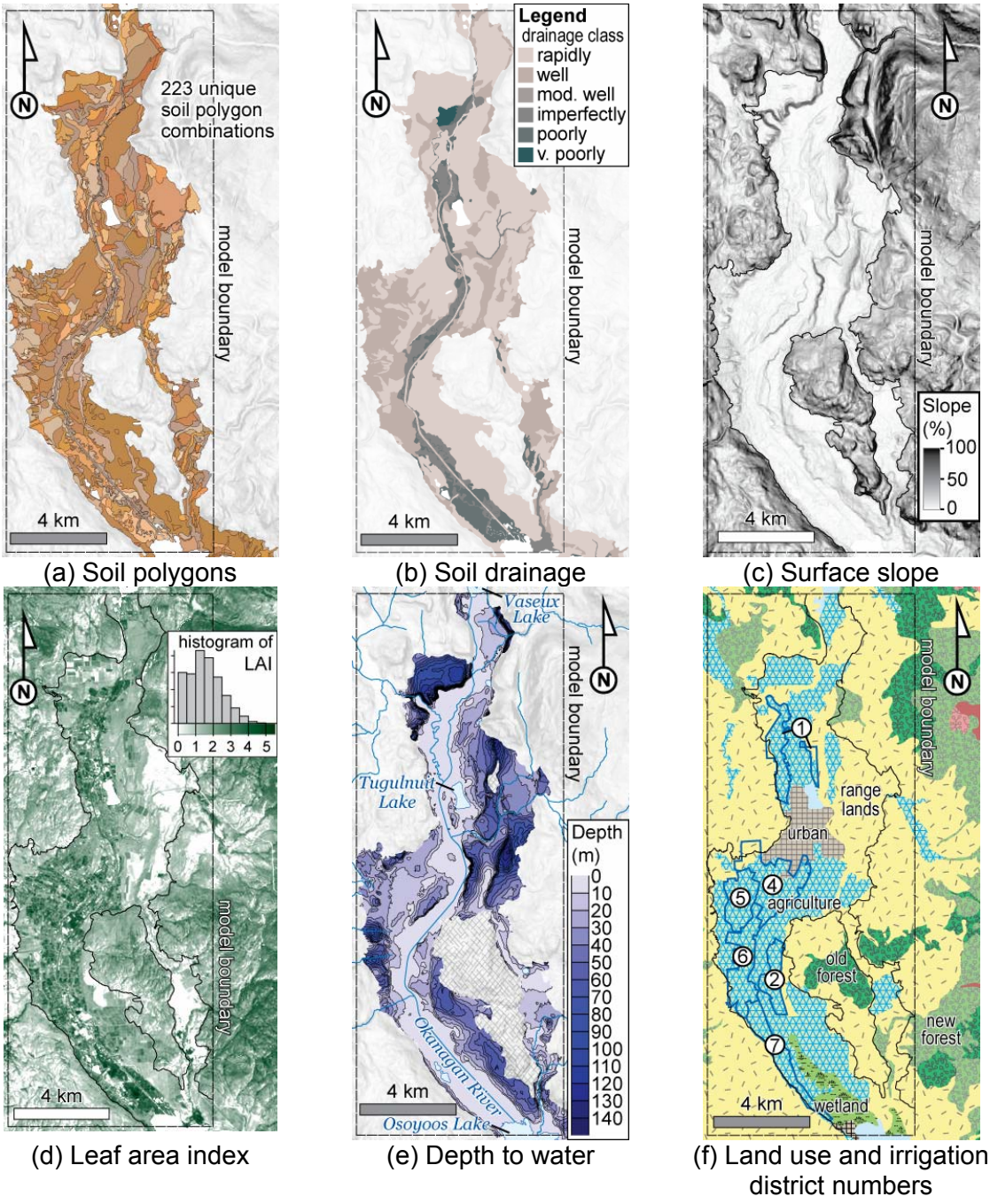

Figure 4.2: Spatial input variables for HELP model.

Level 1, 1:50000 series (0.75-arc second resolution) digital elevation data (Natural Resources Canada, 2005) were used to determine surface slope (Figure 4.2c). Leaf area index (LAI) was estimated from Landsat 5 TM imagery acquired on August 8, 2005 (Soffer et al., 2007), and algorithms were calibrated from ground measurements made in August of 2005 and 2006 (e.g., Fernandes, 2003; Leblanc et al., 2005). LAI data were originally gridded at 30 m resolution

(Figure 4.2d), but were regridded to a coarser 100 m resolution. Depth to water table (Figure 4.2e) was determined using differences between ground elevation and interpolated water table elevation. Water table elevation data were interpolated using natural neighbours (e.g., Sibson, 1981) on a 100 m grid using water depth records in a water well database (BC MoE, 2006), and well elevations determined from digital elevation data using their coordinates. Vector-based 1:250000 land use data (Yazdani et al., 1992), and locations of irrigation districts (T.Underwood; pers. comm. 2006) are shown in Figure 4.2f.

4.3.3. IRRIGATION

Irrigation was added to precipitation in irrigation districts (Table 4.2) located in the Oliver region using proportions of crop types, and daily climate and evapotranspiration data from LARS-WG. There are six irrigation districts in Oliver (identified in Figure 4.2f) with monitored irrigation uses. The two dominant crop classes are orchard (including peaches, cherries and apples) and vineyards (grapes). The proportion of crop type in each irrigation district is identified in Table 4.2 and were generalized from maps by Neilsen et al. (2004).

Table 4.2: Irrigation districts, coverage types, and average annual water use between 2000–2005 (T.Underwood; pers. comm. 2006). Irrigation efficiency, N_D, is determined from these averages.

Name	No.	Coverage fraction		Area	Avg. water use	Avg. rate	N_D
		orchard	vineyard	(m^2)	(m^3/year)	(mm/year)	–
Mud Lake	1	0.8	0.2	2831376	3143968	1110	1.8
Blacksage	2	0.8	0.2	1839441	2570480	1397	2.2
Rockcliffe	4	0.8	0.2	4858991	4789357	986	1.6
Fairview	5	0.8	0.2	2567433	2347473	914	1.5
Hester Ck.	6	0.5	0.5	3622108	2340087	646	1.2
Mt. Kobau	7	0.8	0.2	2828661	2489884	880	1.4

Average rates of actual applied irrigation can be calculated for the various irrigation districts using estimates of the amount of water used, and the total area of the respective irrigation district. However, average rates do not provide a realistic measure of the actual daily irrigation rates, because on some days it actually rains. Therefore, an approach was developed to calculate the daily applied irrigation based on the precipitation and evaporation data from LARS-WG. The approach relies on estimates of seasonal crop water demand.

Allen et al. (1998) describe *crop water demand* as the water that a given crop will require to compensate the evapotranspiration loss, while the *irrigation water requirement* is defined as the difference between the crop water demand and effective precipitation. Irrigation may also include additional water for leaching of salts. Seasonal crop water demand was estimated using crop water demand coefficients, K_c, from Neilsen et al. (2006):

$$K_c = 6.770 \times 10^{-8} d^3 - 6.466 \times 10^{-5} d^2 + 0.01407 d - 0.1149 \quad \text{for orchard trees} \quad (4.1a)$$

$$K_c = 2.161 \times 10^{-7} d^3 - 1.434 \times 10^{-4} d^2 + 0.02616 d - 0.1602 \quad \text{for grapes} \quad (4.1b)$$

where d is the day of the growing season, which begins at 1 and accumulates to the end of the growing season. The start of the growing season in the spring is established after 5 consecutive days where T_{mean}>10^{o}C, and ends in the fall after 5 consecutive days where T_{mean}<10^{o}C (Neilsen et al., 2006). In addition, the growing season was limited to begin at earliest mid-March and at latest late-October, as plant growth is limited by the photoperiod, regardless of temperature.

Daily irrigation rates, I_r (in mm/day), were calculated using:

$$I_r = N_D \times K_c \times E_p - P \quad (4.2)$$

where N_D is an efficiency factor for each irrigation district, E_p is daily potential evapotranspiration, and P is daily precipitation; the last two variables are from LARS-WG and have units mm/day. If I_r is negative (e.g., from excessive precipitation), it was reset to zero for that day. K_c coefficients were weighted by relative proportions of vineyard and orchard tree crops in each irrigation district. N_D was determined from trial and error to obtain similar measured average irrigation rates in Table 4.2 using the historic synthetic climate data. The values of N_D (above 1.0) indicate that most crops are likely over irrigated for their respective crop water demand. The average crop water demand for orchard trees is 717 mm/year and for vineyards it is 408 mm/year using the same synthetic historic climate data set.

4.3.4. RECHARGE MODELLING

HELP model

Version 3.80D of the HELP model (Berger, 2004), which is a revised and updated version of the original HELP model by Schroeder et al. (1994), was used to estimate recharge. HELP models surface and near surface hydrologic processes critical for estimating recharge, including:

accumulation of solid precipitation (snow and ice) on the surface; surface runoff/infiltration; estimated and potential evapotranspiration; transpiration in relation to the growth and decay of vegetation; soil freeze/thaw from air temperature, and; water flow through discrete layers of variably saturated soil. The model uses vertical (1D) soil profiles, and simulates the leakage at the base of the profile. If the base of the soil column is set equal to the water table depth, the leakage across this boundary is effectively the groundwater recharge. HELP has been used in many groundwater recharge studies (e.g., Gogolev, 2002; Allen et al., 2004; Jyrkama and Sykes, 2005; Scibek and Allen, 2006a, 2006b).

It is recognized that the HELP hydrologic model is not the best-available model for simulating recharge processes. Scanlon et al. (2002) compared several hydrology similar codes, and rated HELP lower than others, such as UNSAT-H (Fayer, 2000), and SHAW (Flerchinger, 2000). The main drawback of HELP is that it employs a storage-routing unsaturated flow process. Other codes generally solve Richards' equation through finite-differences, where water may move up or down, depending on the matric potential gradient. The HELP model uses a few critical assumptions: (1) water may only escape upwards (as evapotranspiration) if it is within the evaporative depth zone, which is a non-physically-based depth parameter of the model, but often specified by the user to coincide with the rooting depth; and (2) water drained from the base of the evaporative depth zone will eventually be routed to the base of the model. Furthermore, the timings and threshold of freeze/thaw of the soil layers in HELP is calculated based on an empirical dataset from a limited number of studies from the United States and Germany. It is unknown how well these empirical relationships hold for the soils and climate in the Okanagan region.

Despite the shortcomings, the HELP model was selected for many reasons: (1) its simplicity and speed—a soil profile with 200 years of climate data can be simulated in seconds, rather than hours; (2) it utilizes daily climate data needed for climate change simulations; (3) it simultaneously models multiple hydrologic processes, including soil freeze/thaw; and (4) it can be used to compare with other similar investigations that have used the same model in different climate regimes (e.g., Scibek and Allen, 2006a).

Because HELP is a 1D model, spatially-distributed recharge estimates require simulations for each unique combination of physical parameters that might influence recharge. These include soil (and its depth layering), vegetation, slope and water table depth. Consequently, then study area was discretized into 100 m grid cells for recharge analysis, which covered a 2100 m by

1100 m region, with 10102 active cells (and unique HELP simulation). LAI and water depth were used directly, as they were gridded to match the modelling domain. Polygon coverages of soil and land use data were interpreted through a weighted approach. Each grid location (*i*,*j*) can have *k* {1,2,...} categories, which are weighted by the surface area occupied by each category:

$$W_k = \frac{A_k}{\sum A_k} \quad \text{where } \sum W_k = 1 \qquad (4.3)$$

which is multiplied with each *k* parameter value, and summed to arrive at a single value for each grid location.

One of the major limitations of using a 1D recharge model is that surface (and sub-surface, if important) water routing from one grid cell to the next is not accounted for by the model. Thus, this excess water will not be routed to adjacent down-gradient cells. For this reason, use of a 1D recharge model is not particularly well suited to areas with moderately steep to steep topography. However, it this particular study area, the valley bottom is generally flat, and the soils well drained, so that there will be little surface runoff, and little lateral flow within the vadose zone; only vertical flow.

HELP uses daily mean temperature, total daily precipitation and total solar radiation as weather inputs. In this study, weather time series and evapotranspiration input parameters (Table 4.3) were assumed to be constant throughout the modelling domain. However, unique precipitation time series were generated for each irrigation district, which include daily irrigation application rate (Equation 4.2) as influenced by both the crop type and irrigation efficiency.

Table 4.3: Input parameters used in HELP.

Parameter		Value
Latitude		49.15 °N
Relative humidity (quarterly)	JFM:	72%
	AMJ:	52%
	JAS:	51%
	OND:	80%
Wind Speed		6km/hr

Vegetation and runoff

Runoff curve numbers (USDA, 1986) were calculated for each grid location based on vegetation and soil texture, which are arbitrarily quantified by Schroeder et al. (1994). A vegetation number, V_n, can range from 1.0 for bare ground to 5.0 for an “excellent” stand of grass; and a soil texture

number, T_n, can range from 1.0 for coarse sand to 15.0 for clay. Values for V_n were interpreted from land use through Table 4.4, while T_n was first approximated from soil drainage (Figure 4.2b), then modified by adding values of T_n in Table 4.4. The intention of these adjustments is to increase the potential for runoff on more developed land uses. Finally, runoff curve numbers were adjusted according to surface slope (Figure 4.2c). The complete methodology to calculate runoff curve number is very similar to the "computed curve number" available in the graphical interface for HELP (see Toews, 2007).

Values for the evaporative depth zone, E_z, were obtained from land use, using Table 4.4. These values are approximated to be similar to rooting depths of vegetation expected in the land use regions.

Table 4.4: Influence of land use on vegetation cover, V_n, soil texture number, T_n, and evaporative depth zone, E_z (cm).

Land use	V_n	T_n	E_Z
Agriculture	3.2	+1	100
Old Forest	4.5	0	200
Range Lands	1.8	0	35
Recreational	3.2	+2	40
Urban	2.2	+4	40
Wetlands	3.5	0	40
Young Forest	4.3	0	100

Soil layers

Soil columns were dynamically created across the site to represent the unique spatial soil data combinations. Each soil column was defined using 1 to 9 vertical percolation layers, because it is assumed that only vertical flow is present. Soil profiles built for each grid square using weighted spatial and depth averages of hydraulic properties determined from the soil database (Figure 4.3).

Soil hydraulic properties for each soil horizon were estimated using the ROSETTA computer program (Version 1.2), which implements hierarchical pedotransfer functions (Schaap et al., 2001). The H3 artificial neural network model was selected, which uses measured bulk density and percentages of sand, silt and clay. The model directly calculates saturated hydraulic conductivity, K_s, saturated and residual water contents, θ_s and θ_r, respectively, and van Genuchten (1980) water retention curve parameters α and η. Porosity, η, was set equal to θ_s.

Field capacity (θ_{fc}, where suction pressure, $|\psi|$, is 33 kPa≅337 cm of water) and wilting point (θ_{wp}, where $|\psi|$=1500 kPa≅15306 cm) were calculated using:

$$\theta(\psi) = \theta_r + \frac{\theta_s - \theta_r}{\left[1 + \left(\alpha \cdot |\psi|\right)^n\right]^{1-1/n}} \qquad (4.4)$$

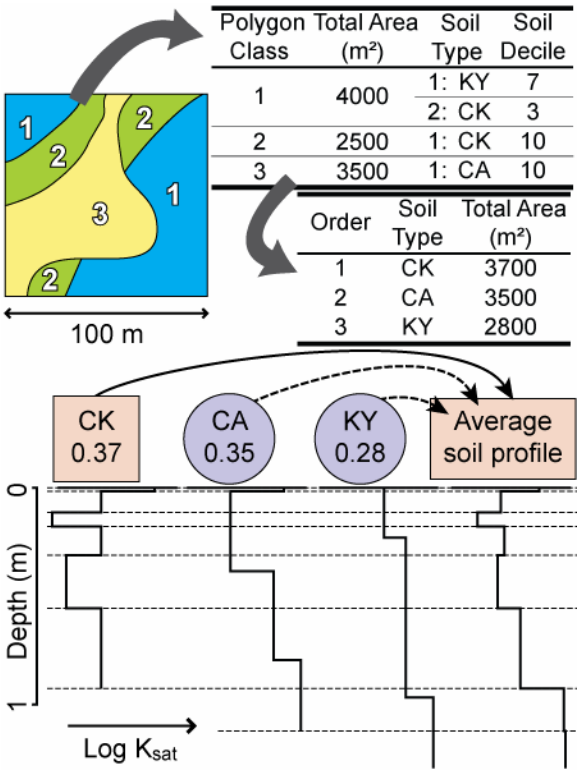

Figure 4.3: Illustration of the soil database for a 100 m grid cell. This example shows three-different soil coverages comprising varying proportions of soil types, which are combined using area-weighted means. The illustration on the bottom shows the depth-weighted average soil profile of log*K* that is used to represent the grid cell. Here, the dominant soil type 'CK' is used as a template, and "inherits" the properties of 'CA' and 'CK', depending on their relative abundances. The resulting soil profile has eight layers.

Hydraulic properties for organic soil layers were determined independently using estimates from peat (Päivänen, 1973; Silins and Rothwell, 1998), as soil texture data were unavailable for these horizons. Saturated hydraulic conductivity was estimated using the linear relation (Päivänen, 1973):

$$\log_{10}(K_s) = 2.8 - 10 r_b \qquad (4.5)$$

where K_s is saturated hydraulic conductivity (cm/day), and r_b is bulk density (Mg/m^3), which ranged between 0.22 and 0.36 Mg/m^3. The water retention parameters were approximated by

fixing $\theta_s \leftarrow$ 0.85 (close to porosity), $\theta_r \leftarrow 0$, and $\eta \leftarrow 1.4$ (Silins and Rothwell, 1998). The α shape parameter was adjusted in Equation 4.5 to obtain, $\theta_{fc} - \theta_{wp} \cong \theta_a$ where θ_a is the available water content from the soil database.

Where the water table extends below the base of the soil profile (>~1.5 m), average aquifer values were used to append a bottom layer, which extends to the water table (Figure 4.2e). This bottom layer, if appended, has a K_S of 0.1 cm/sec and ϕ of 0.25, as approximated from multiple pump tests in the regional sand and gravel aquifer (Toews, 2007). Water retention parameters θ_{fc} and θ_{wp} were approximated to be 0.045 and 0.018, respectively (Rawls et al., 1993).

Soil moisture was first initiated automatically[13] (1 year model spin-up), but model spin-up was extended by running 200 years of climate data, while only keeping the last 100 for analysis. A longer spin-up time was needed to initialize soil moisture, as simulations using tall soil columns generally underestimated recharge during the early time series.

4.4. RECHARGE RESULTS

Maps showing geometric mean of K_S for all soil layers and calculated runoff curve numbers are shown in Figure 4.4. Mean annual results using a 'historic' synthetic climate without irrigation are shown in Figure 4.5. Mean annual recharge rates in Figure 4.5a have a median of 45 mm/yr, with first and third quartiles of 15 and 60 mm/yr, respectively. These values are approximately 20% of the annual precipitation. The parameters with most control on recharge are the near-surface soil hydraulic properties, including K_S, and water retention parameters θ_{fc} and θ_{wp}. This control is apparent from the similarity of between maps of annual recharge and geometric mean of K_S.

Runoff (or infiltration excess; Figure 4.5b) is very comparable to runoff curve numbers (Figure 4.4b). Runoff is computed by HELP to be a minor component of the annual water budget; however, this is possibly underestimated due to the limitations of runoff simulation using daily time-step data (Scanlon et al., 2002).

[13]Soil moisture is initiated in HELP by first setting the moisture to field capacity, then running the first year of data twice, ignoring the first year of results (Schroeder et al., 1994, Section 3.6)

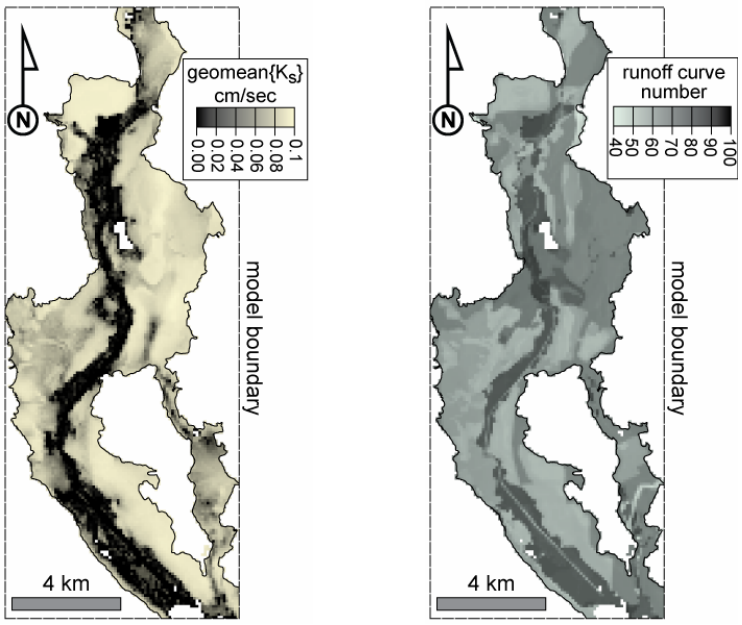

(a) Geometric mean of K_S (b) Runoff curve number

Figure 4.4: Soil and surface properties.

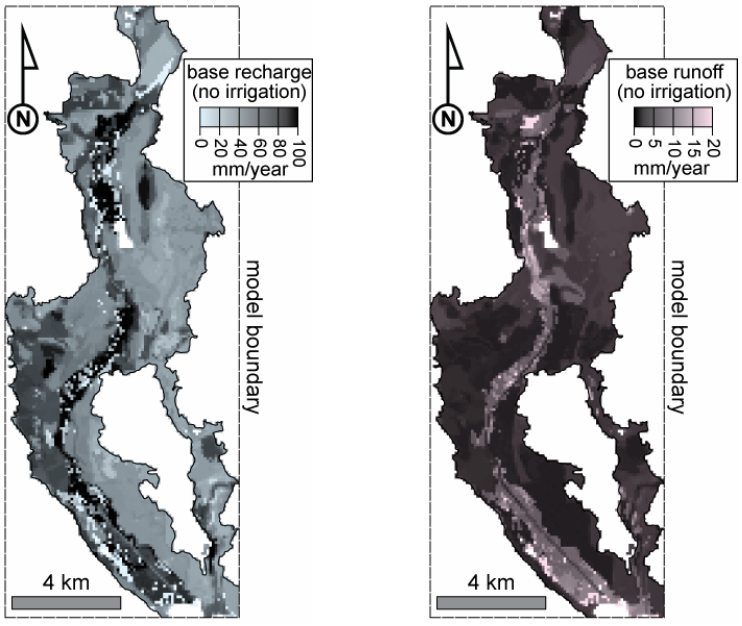

(a) Recharge (b) Runoff

Figure 4.5: 'Historic' mean annual recharge and runoff, without irrigation.

Monthly recharge rates are displayed both without irrigation in Figure 4.6a, and with irrigation in

Figure 4.6b. Natural recharge arrives at the water table at different times of the year, which is influenced by the depth to water. This delay is due to the time of transport through the soil, which is proportional to the height of the soil column. If the soil is fully saturated ($\theta = \phi$), HELP simulates the flow of water through the soil column length, *dl*, with a unit hydraulic gradient (*dh*/*dl*=1) and a delay, *dt*, of:

$$dt = \frac{dh\phi}{\mathrm{K}_s}. \qquad (4.6)$$

Simulations using irrigation have a significant increases on net recharge in the irrigation districts. Zones 6 and 7 (identified in Figure 4.2f) have the lowest recharge of these zones, averaging 250 and 450 mm/yr, respectively. Irrigation zone 2, the most intensely irrigated district, has the highest net recharge of 1000 mm/yr.

Irrigation return flow is the ratio of annual recharge to irrigation plus precipitation. Results for the baseline synthetic climate are shown in Figure 4.7. Irrigation return flow is very dependant on the efficiency of irrigation (N_D), which was adjusted to meet the observed application amounts. Where the N_D is close to 1.0 (perfect efficiency), irrigation return amounts are close to 0.2, while in less efficient districts this return fraction is nearly 0.6. From an irrigator's perspective, this loss contributes higher energy costs associated with pumping the water.

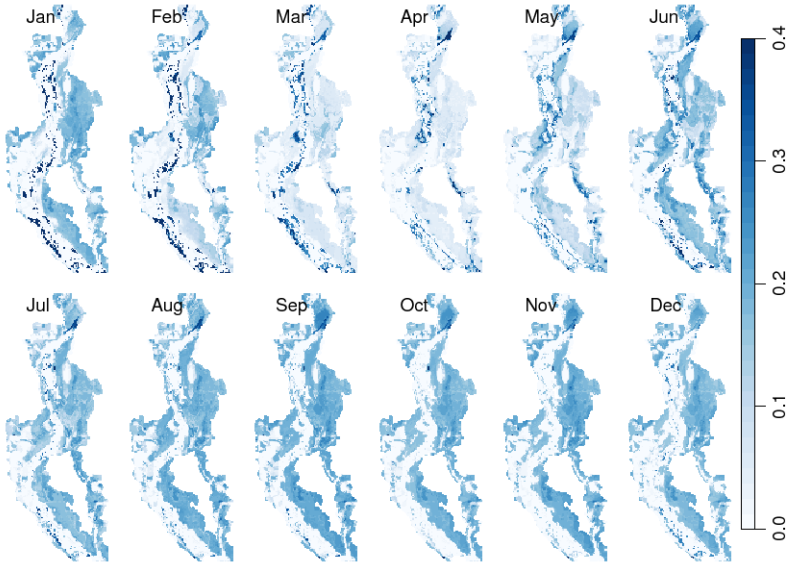

(a) Without irrigation

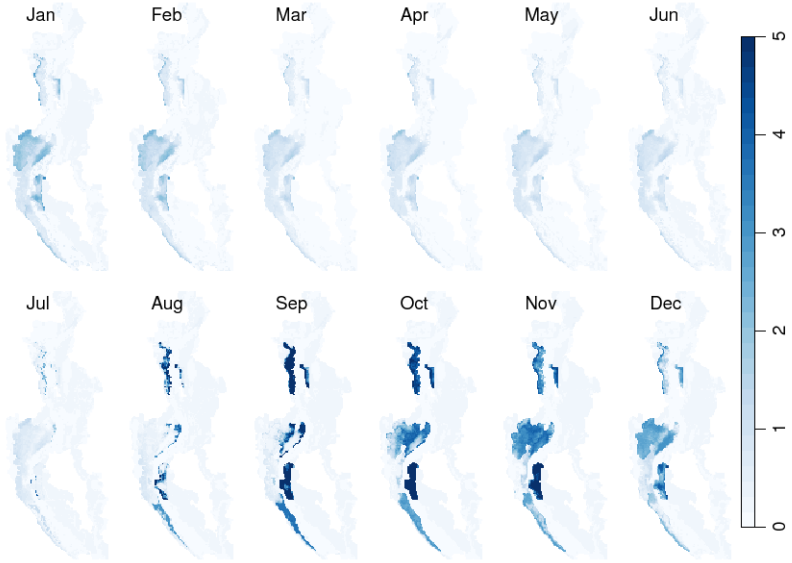

(b) With irrigation

Figure 4.6: Monthly recharge in historic climate (mm/day). Note the scale change between figures.

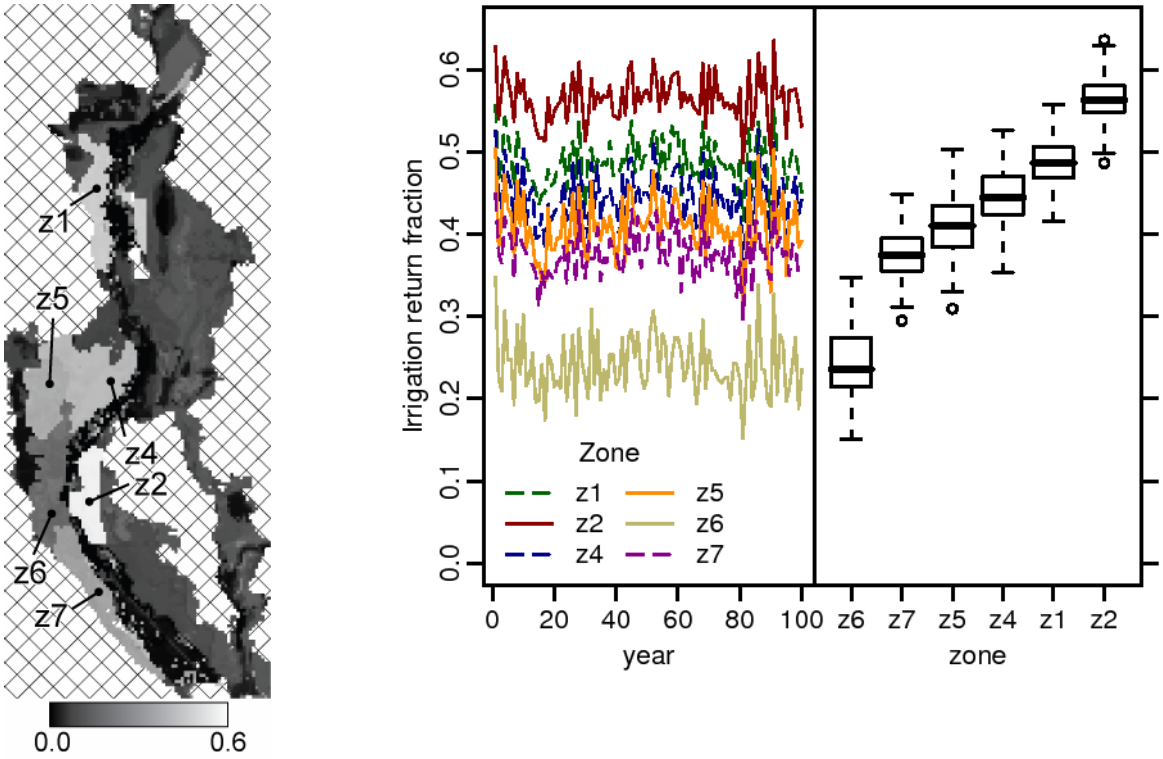

(a) Average return flow

(b) Annual return flow fractions from locations in each irrigation district

Figure 4.7: Irrigation return flow (fraction of recharge to input precipitation and irrigation) in the historic climate state.

Comparison of model results to observed data

Water level variations in observation wells[14] No. 332, located in irrigation district 2 (Figure 4.8a), and No. 282, located outside of soil data extent (~5 km north-west of the region) with no irrigation influence, are provided for comparison (Figure 4.8b). These measured levels have an annual periodicity that has comparable timing to the HELP model recharge. Figure 4.9 shows irrigation (with precipitation) and recharge responses at the same location as Obs. Well No. 332. Although the water levels are influenced by nearby pumping water wells used primarily for irrigation, this comparison shows that both recharge rates and water levels are lowest in early summer, and increase sharply near the end of summer. Water levels in this irrigation district reach their peak in November, presumably after accumulation of recharge (i.e., integration of recharge rates in Figure 4.9b). In contrast, water levels outside of the irrigation district (Figure 4.9a) peak in spring during the freshet, and are at their lowest during winter.

[14]See http://www.env.gov.bc.ca/wsd/data_searches/obswell/wellindex.html

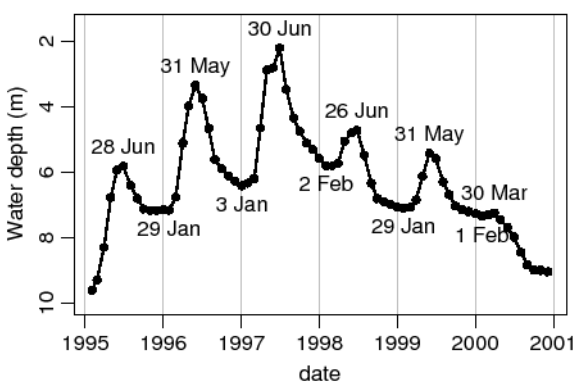

(a) Observation Well 282; non-irrigated region

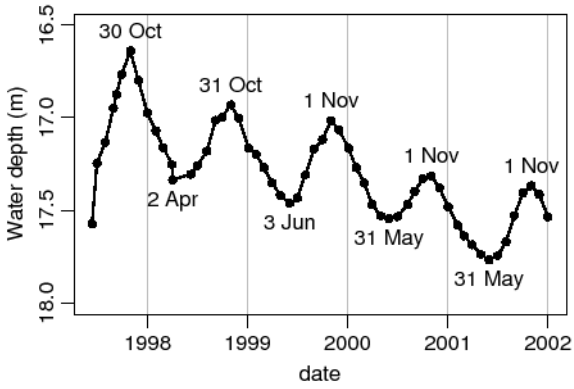

(b) Observation Well 332 in irrigation zone 2

Figure 4.8: Measured water levels in groundwater observation wells.

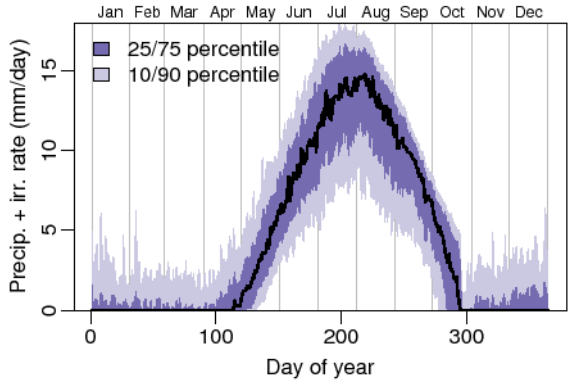

(a) Precipitation and irrigation rate

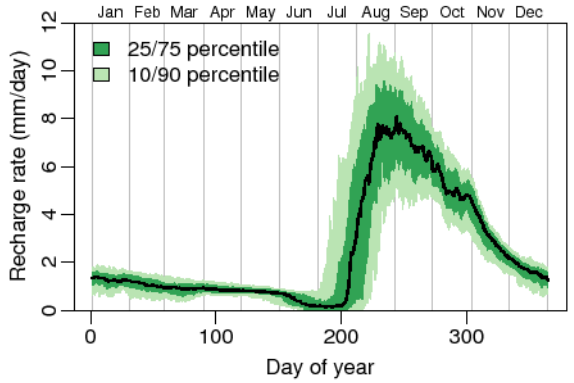

(b) Recharge rate

Figure 4.9: HELP simulation in irrigation district 2 at the same location as Obs. Well 332.

5. HYDROGEOLOGY AND GROUNDWATER FLOW MODEL

5.1. INTRODUCTION

A regional-scale deterministic groundwater model was developed for the southern Okanagan, which extends from the south end of Vaseux Lake to the north end of Osoyoos Lake. The model was developed first as a steady-state model, calibrated to August stresses, which are regarded as low-flows. The model was then converted to a transient model, which has monthly stress periods for two years.

5.2. CONCEPTUAL MODEL

5.2.1. HYDROSTRATIGRAPHY

The generalized valley bottom hydrostratigraphy, shown in Figure 5.1, consists of coarse sand, and gravel with boulders near the surface, which form an unconfined aquifer. These sediments also extend along the valley margins and continue to depth forming confined or partially confined aquifers. The surface sediments are underlain by fine lacustrine silt and clay of limited permeability, which overlie bedrock that is assumed to be impermeable.

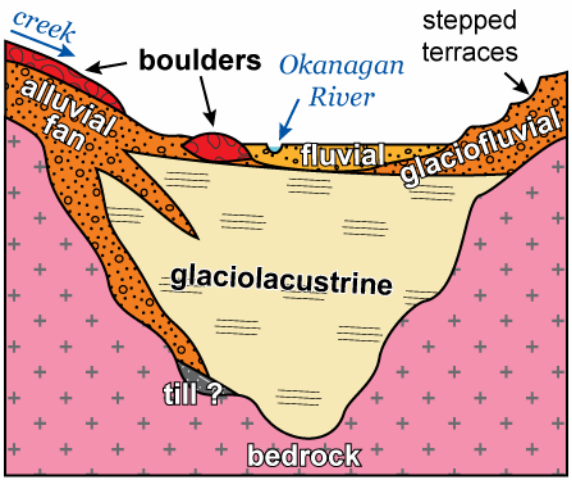

Figure 5.1: Generalized stratigraphy of the Oliver region, in a representative west–east section through the bedrock valley. The upper sediments consist of sand and gravel glaciofluvial, alluvial and reworked fluvial channel sediments. Boulder deposits are also found in discrete locations. The upper coarse sediments are underlain by silt and clay glaciolacustrine sediments.

5.2.2. AQUIFER HYDRAULIC PROPERTIES

Most of the high-producing water wells (BC MoE, 2006) in the Oliver region are completed in the upper sand and gravel aquifer, adjacent to (and vertically below) Okanagan River. Table 5.1 shows well name, and respective well tag numbers (WTN), their seasonal usage, and average pumping rate. The information of pumping rates were provided by Foley et al. (2005).

Table 5.1: Production water wells in the Oliver region, which are identified in BC using well tag numbers (WTN).

Well name	WTN	Seasonal usage	Aquifer type	Average pumping rate	
				(USgpm*)	(m^3/s)
Buchanan Rd.	21873	summer	unconf.	402	2191
Fairview	21867	year-round	unconf.	425	2317
Blacksage 1	49481	summer	unconf.	2000	10902
Rockcliffe	82376	year-round	unconf.	1500	8176
Miller Rd.	84724	year-round	unconf.	1092	5952
Tugulnuit 2	83008	summer	unconf.	1200	6541
Town	29205	?	?	?	?
Lions Park	83010	year-round	unconf.	1230	6705
CPR	83011	year-round	unconf.	1000	5451
BCFGA 1	53199	summer	semi-conf.	300	1635
BCFGA 3	46717	summer	semi-conf.	550	2998
Deer Park Fire	82374	emergency	unconf.	1501	8182
Deer Park Dom.	82375	year-round	unconf.	108	589

*US gallon per minute; 1 USgpm = 5.45 m^3/day = 6.31 × 10^{-5} m^3/s

Pumping test data are available for some of these wells, which provide hydraulic property estimates for the sand and gravel aquifer, such as transmissivity, T, hydraulic conductivity, K_S, and specific yield, S_y (Table 5.2). The storage coefficient, S, is estimated to be about 5.7 × 10^{-5} (Hodge and Lowen, 1980).

Hydraulic conductivity, K_S, was calculated from T using an estimate of the saturated thickness, b, of the unconfined aquifer (using $T = K_s b$). The saturated thickness represents the difference in elevation between the silt contact and the water table. The geometric mean was used where multiple estimates of T were available. Figure 5.2 shows a probability distribution of the hydraulic conductivity values from the sand and gravel aquifer, which have a log-transformed

mean of 2.4×10^{-3} m/s or 204 m/day.

Table 5.2: Hydraulic properties from pumping tests conducted at production wells: transmissivity, *T*, saturated aquifer thickness, *b*, hydraulic conductivity, K_S, specific yield, S_y and aquifer test method(s).

Well name	T (m^2/day)	b (m)	K_S (m/day)	K_S (m/s)	S_y	Method* (Reference†)
Buchanan Rd.	9439	20.7	439	5.1×10^{-3}	0.16	TR (F)
Fairview	9546	26.5	359	4.2×10^{-3}	–	TR (F)
Blacksage 1	5200	24.8	210	2.4×10^{-3}	–	
Rockcliffe	15310	25.3	605	7.0×10^{-3}	0.38	J, TR
Miller Rd.	1465	11.9	123	1.4×10^{-3}	0.18‡	TR (G1)
Tugulnuit 2	9500	11.9	800	9.3×10^{-3}	0.10	TR (G2)
Town	6495	8.8	737	8.5×10^{-3}	0.22‡	TR
BCFGA 1	204	4.6	45	5.1×10^{-4}	–	RD (H)
BCFGA 3	492	6.6	75	8.7×10^{-4}	–	RD (H)
Deer Park Fire	450	20.6	22	2.5×10^{-4}	–	RD (P)
Deer Park Dom.	5000	21.3	235	2.7×10^{-3}	–	RD (P)

*TD, Theis drawdown; TR, Theis recovery; J, Jacob; RD, residual drawdown

†F, (Foweraker, 1969); M, (Callan, 1971); H, (Hodge and Lowen, 1980); P, (Arengi and Badry, 1993); G1, (Allard, 2004); G2, (Foley et al., 2005)

‡Estimated from pumping well using the Neuman (curve matching) method—not reliable

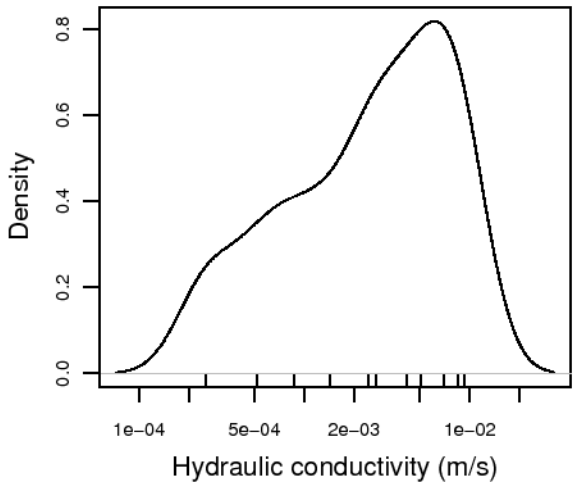

Figure 5.2: Probability distribution of the hydraulic conductivity of the sand and gravel aquifer from pumping test results in Table 5.2. The geometric mean is 2.4e-3 m/s.

No hydrogeological test data are available for the silt and clay aquitard, as it is a low-producing hydrogeological unit. Hydraulic conductivities in the silt and clay are estimated to be between 0.1 to 10 m/day, or 1.2×10^{-6} to 1.2×10^{-4} m/s, and specific yield values are estimated to be

about 0.02 (e.g., Domenico and Schwartz, 1998).

If the hydraulic property estimates are reasonable for the sand and gravel unconfined aquifer and the silt and clay aquitard, then there are approximately two-orders of magnitude difference in the hydraulic conductivity at the contact between the upper sand and gravel and lower silt and clay materials, so this contact may act as an impermeable (no-flow) boundary for simple models and analytical solutions of groundwater flow (Anderson and Woessner, 1992).

Similarly, the underlying bedrock is assumed to have very low bulk permeability, so it is considered impermeable. However, this assumption may be incorrect, as it is known that the bedrock is highly fractured (in outcrop exposures at high elevation), and water seepage has been observed along parts of the Okanagan Valley Fault system (Grasby and Hutcheon, 2001). Whether the bedrock fracturing extends to depth is uncertain, but nonetheless likely. Furthermore, a large hydraulic gradient exists between the uplands and the Okanagan Valley Fault system, which has an elevation difference of 1100 m. However, as the fault system is beneath hundreds of metres of sediment, this flow cannot be verified nor easily quantified. Investigation to the bulk permeability of the bedrock and the contribution of groundwater flow through the bedrock surface is in progress (Voeckler, PhD candidate, University of British Columbia, in progress).

5.2.3. DIRECT RECHARGE

Direct areal recharge to the aquifer occurs from infiltration of precipitation and irrigation return flow. Details of direct recharge modelling were discussed previously in Section 4.0.

Irrigation return flow was also modeled. Often, this is only approximated from the volume of water used for irrigation; for example, Allen et al. (2004) used 20%. Details concerning irrigation input were discussed in Section 4.0, where irrigation was calculated from crop water demand coefficients, and daily time-series of evapotranspiration and precipitation data. Irrigation return is variable from year-to-year, and changes significantly between irrigation districts.

5.2.4. PUMPING WELLS

Monthly production rates were available for 2005 only (Table 5.3 and Figure 5.3). Measurements were made at pumping stations near one or more production wells, so only one well was used to represent multiple wells; in particular: Lions Park was merged to CPR, Tugulnuit 2 was used to represent other Tugulnuit wells, and Blacksage 2 was used to represent Miller Road.

Table 5.3: Average well production rates for 2005, all units are m^3/day.

	CPR & Lions†	Rockcliffe domestic	Tugulnuit	Buchanan Road*	Fairview domestic*	Blacksage domestic*	Monthly totals
Jan	2247.1	1.3	0.0	0.0	1357.5	0.0	3605.9
Feb	1334.8	2124.0	0.0	0.0	779.9	0.0	4238.7
Mar	1626.0	1959.0	0.0	4.4	948.2	0.0	4537.6
Apr	3120.2	1877.7	0.0	441.3	1260.2	4493.5	11192.8
May	3535.3	3795.1	0.0	0.4	1153.6	7312.9	15797.3
Jun	2609.8	4558.8	0.0	54.8	1123.0	8034.8	16381.1
Jul	4459.8	4952.2	130.5	336.9	1204.6	12360.0	23444.0
Aug	4367.5	4437.7	3901.4	1550.7	1224.2	12447.2	27928.7
Sep	3133.4	4501.4	341.9	0.0	1141.4	8238.3	17356.5
Oct	3094.4	1441.6	0.0	17.0	740.1	4254.6	9547.7
Nov	2852.9	0.0	0.0	1.8	1045.4	241.7	4141.8
Dec	2344.9	316.4	0.0	0.0	1205.3	0.0	3866.6
Ann	2906.3	2497.6	370.5	203.1	1100.8	4816.1	11894.3

†Meter reported not to be accurate

Source: B. Hamilton, pers. comm. 2006

*Meter only read on a periodic basis

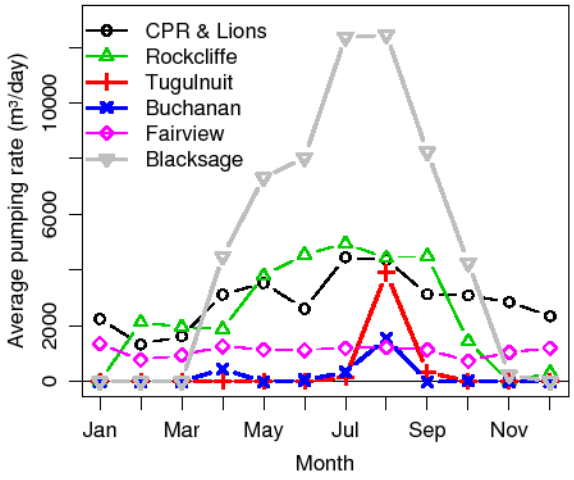

Figure 5.3: Well production rates for 2005, see Table 5.3.

5.2.5. SURFACE WATER HYDROLOGY

Hydrologic data used in this analysis, including lake stages and flow rates in rivers and streams, are listed in Table 5.4.

Table 5.4: Hydrological gauging stations (HYDAT CD, Environment Canada, 2001).

Station name	ID	Location	Years
Lake stage elevations			
Vaseux Lake near the outlet	08NM243	49°16′25″N,119°31′24″W	1991–*present*
Osoyoos Lake near Osoyoos	08NM113	49°01′43″N,119°27′37″W	1946–*present*
River or creek flow rates			
Okanagan River near Oliver	08NM085	49°06′53″N,119°33′50″W	1944–*present*
Vaseux Creek above Dutton Ck.	08NM015	49°15′44″N,119°28′27″W	1919–1982
Vaseux Creek above Solco Ck.	08NM171	49°14′58″N,119°19′16″W	1970–*present*
Inkaneep Creek, upper station	08NM082	49°07′10″N,119°21′40″W	1941–1950
Inkaneep Creek, lower station	08NM012	49;07;00N,119;29;30W	19191950
Testalinden Creek near Oliver	08NM130	49;07;13N,119;35;25W	19651968
Testalinden Creek in canyon	08NM164	49;07;17N,119;35;53W	19691986

5.2.5.1 Lakes

The primary control of hydrology in the region is from Vaseux Lake to the north, and Osoyoos Lake to the south; the two lakes are connected by Okanagan River. The stages for these lakes are controlled by McIntyre Dam for Vaseux Lake (Figure 5.4a) and by Zosel Dam at Osoyoos Lake in Oroville, Washington (represented by Figure 5.4b measured at Osoyoos, BC). Mean monthly deviations from annual mean lake elevations are shown in Table 5.5).

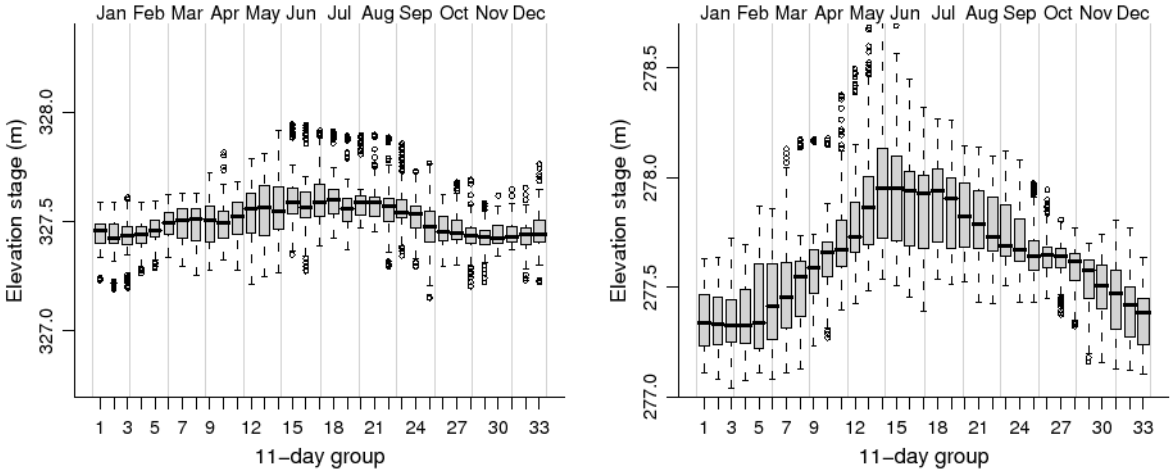

(a) Vaseux Lake (08NM243), 1991–2003 (b) Osoyoos Lake (08NM113), 1977–2003

Figure 5.4: Stages of lakes at both ends of Okanagan River.

Table 5.5: Monthly median stages (m), and the deviation from the annual median.

	Vaseux Lake		Osoyoos Lake	
	median	**deviation**	**median**	**deviation**
January	327.433	~0.063	277.331	~0.303
February	327.450	~0.046	277.331	~0.303
March	327.507	+0.011	277.500	~0.134
April	327.503	+0.007	277.650	+0.016
May	327.556	+0.060	277.833	+0.199
June	327.576	+0.080	277.945	+0.311
July	327.581	+0.085	277.920	+0.286
August	327.582	+0.086	277.772	+0.138
September	327.528	+0.032	277.671	+0.037
October	327.444	~0.052	277.640	+0.006
November	327.427	~0.069	277.550	~0.084
December	327.439	~0.057	277.406	~0.228
Annual	327.496		277.634	

There are also many small (~1 km) lakes along the valley bottom and valley sides, such as Tugulnuit Lake,[15] Gallagher Lake, and Deadman Lake. These water bodies do not have any major streams flowing in or out of their surface (with the exception of Tugulnuit Lake, which has a gravity-fed pipe down to Okanagan River). It is interpreted that all of these lakes are sustained through groundwater.

[15]This is the official geographic name; however, *Tuc-el-Nuit Lake* is also very common

5.2.5.2 Rivers

Okanagan River is the main surface water body in the region. The river is controlled by the *Okanagan Flood Control System*, which consists of channelized reaches and flow structures, and was constructed between 1950–1957 to reduce damages from seasonal flooding (Schubert, 1983). The river flow is controlled by McIntyre Dam, near the outlet of Vaseux Lake, where some of the flow is also diverted into the SOLID[16] irrigation channel. While the upper reach of Okanagan River is natural (unaltered channel; 5.6 km in length), the remaining 2/3 is channelized, from 1 km north of Oliver to Osoyoos Lake. The channelized portion was over-excavated, and river banks were constructed from emplaced local materials (Hodge, 1978). There are thirteen vertical drop structures[17] to slow the flow and control the grade (Figure 5.5), each with about 1 metre elevation drop.

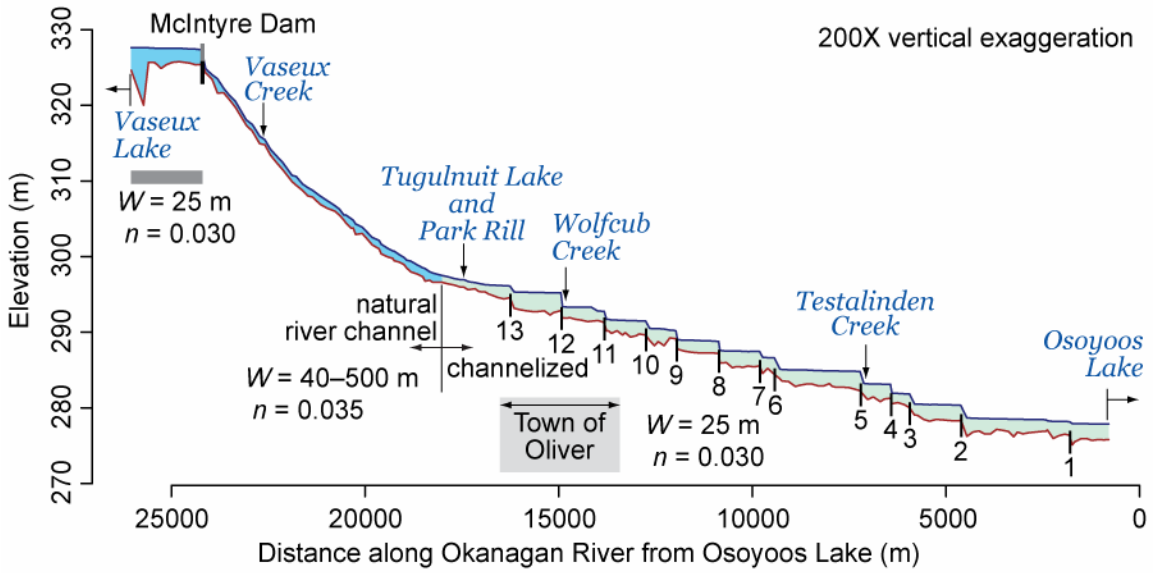

Figure 5.5: Elevation profile of Okanagan River, showing stage and river bottom, locations of numbered vertical drop structures and McIntyre Dam, approximate channel widths, *W*, and Manning's roughness coefficient, *n*; surveyed June 9–23, 1980 (Schubert, 1983; Nichols, 1993).

Historical flow data from a Water Survey of Canada station near Oliver are shown in Figure 5.6. Stage–discharge calibration data are not available, so seasonal fluctuations of river stages were approximated using changes in the surface elevation of Vaseux Lake (Figure 5.4, Table 5.5), although it is recognized that there is no direct correlation between these two levels due to large

[16]Southern Okanagan Lands Irrigation District; formerly called SLOP or South Okanagan Lands Project
[17]Located on the CD at gisdata/ok_riv_struct.shp

difference in hydrology between the lake and river channel.

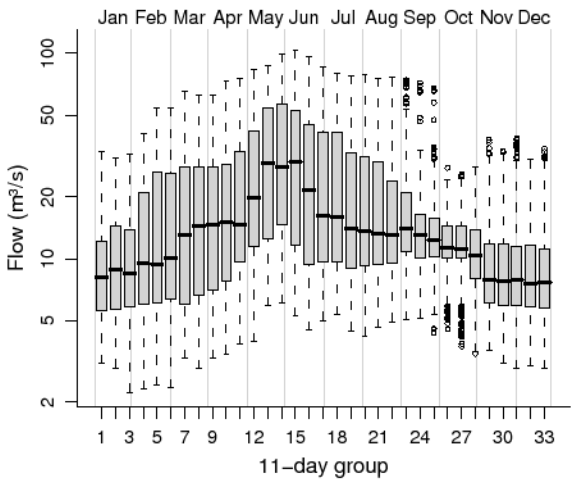

Figure 5.6: Flow in Okanagan River at Oliver (ID: 08NM085), 1957–2004.

5.2.5.3 Streams

The majority of the streams entering the Oliver region are ephemeral, and do not extend far down into the valley in available orthophotos. The stream catchments to the bedrock interface were shown in Figure 2.2. It is assumed that some of these small streams directly recharge groundwater at the bedrock/valley-fill interface, since they disappear partway down the valley over unconsolidated material.

The incoming annual flow from each stream, $\hat{Q}_{Ann}$, was approximated using an empirical correlation with the catchment area to the valley fill margin, A_B (Table 5.6; see Figure 2.2), and the median annual discharge. This estimate was further adjusted to incorporate the hypsometric curves (or distribution of elevations) unique to each catchment:

$$H_f = \sum_{z=1}^{n} h(z)\left[P_l\left(z - 275\right) + 1\right] \qquad (5.1)$$

where H_f is the hypsometric factor for each stream catchment, $h(z)$ is a density histogram of the catchment elevations in 50 m increments (where $\sum h(z) = 1$), z is the mid-point of the elevation band, and P_l is the precipitation lapse rate relative to the valley bottom elevation (~275 m), which was determined to be 6×10^4 m^{-1} (Toews, 2007) (or 60% increase in mean precipitation per 1 km rise in elevation). The quantity H_f considers the increased precipitation at higher elevations, and how this influences different catchments with different distributions of elevations.

Higher values of H_f indicate that the streamflow is more influenced from increased precipitation at higher elevations.

Table 5.6: Hydraulic parameters from stream catchments, shown in Figure 2.2; items are sorted by their hypsometric factor, H_f; A_B is the area of the basin to the bedrock margin; estimated annual flow, $\hat{Q}_{Ann}$, is described later.

Stream name	A_B (km^2)	H_f –	$A_B \cdot H_f$ (km^2)	$\hat{Q}_{Ann}$ (1 × 10^6 m^3/yr)
Vaseux	290.0	1.76	510.4	47.25
Inkaneep	160.7	1.62	260.8	24.14
Hester	9.2	1.60	14.6	1.35
Testalinden	12.3	1.58	19.6	1.81
Tinhorn	3.6	1.57	5.7	0.53
Reed	18.4	1.54	28.4	2.63
Wolfcub	54.1	1.49	80.8	7.48
Park Rill	83.0	1.48	123.2	11.41
Orofino	10.8	1.47	15.9	1.47
Togo	2.4	1.43	3.4	0.31
Victoria	13.1	1.42	18.5	1.72
Atsiklak	10.9	1.40	15.3	1.41
Burnell	8.1	1.35	10.9	1.01
Kearns	39.8	1.24	49.5	4.58

Annual flow data from Water Survey gauges were determined using available data, which span over different time periods, and years with insufficient data were excluded from analysis. Summary statistics are listed in Table 5.7. Figure 5.7 shows boxplots of the annual flow data which are plotted against $A_B \cdot H_f$, or the area to the gauge adjusted by H_f. The zero-intercept best-fit line through the median values, weighted by counts is:

$$\hat{Q}_{Ann} = 92581 \frac{\mathrm{m}^3}{\mathrm{year} \cdot \mathrm{km}^2} \cdot A_B \cdot H_f \qquad (5.2)$$

where $\hat{Q}_{Ann}$ is the annual estimate of flow (m^3/yr) from a stream catchment with area A_B (km^2), and hypsometric factor H_f. The inclusion of H_f in Equation 5.2 improves the R^2 correlation statistic from 0.7987 to 0.8642. The line of best-fit, shown in Figure 5.7 passes through the range of historical annual flows, so it may be considered realistic. This correlation is an underestimate of total catchment flow, since hyporheic flow and other shallow groundwater bypasses stream gauges, which only consider surface water flow. Estimates of $\hat{Q}_{Ann}$ for all catchments are in Table 5.6, calculated using Equation 5.2.

Table 5.7: Statistics from annual measured streamflow data; A_g is the area to each individual gauge; Q_1 and Q_3 are the first and third quartiles, respectively.

Short	ID	A_g	$A_B \cdot H_f$	Annual flow (1×10^6 m^3/yr)					
		(km^2)	(km^2)	count	min	Q_1	median	Q_3	max
Tes1	08NM130	13.0	20.6	4	0.31	0.42	0.51	0.72	1.18
Tes2	08NM164	13.0	20.6	13	0.22	0.42	0.60	1.17	2.52
InkUp	08NM082	70.4	114.2	9	0.85	1.61	3.92	6.74	13.02
InkMid	08NM012	164.0	266.1	19	2.37	5.35	8.54	13.35	29.70
VasUp	08NM171	117.0	205.9	33	11.56	20.27	29.63	37.52	46.96
VasMid	08NM015	255.0	448.8	27	18.90	31.22	42.95	53.08	76.10

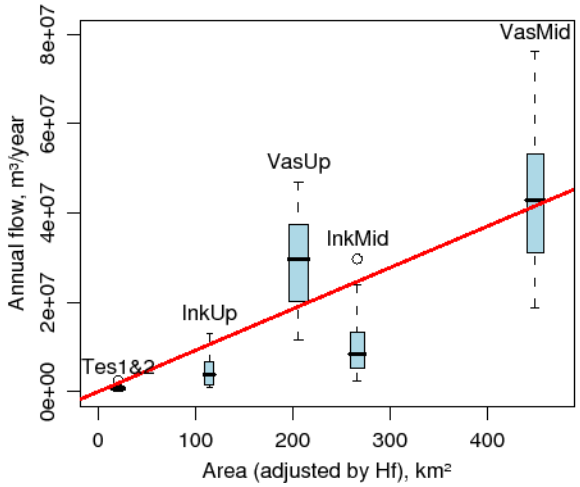

Figure 5.7: Analysis of annual stream flow data with catchment area, adjusted by H_f. Widths of boxplots are proportional to the square root of the count of annual flow values. The line of best-fit with median values (center of boxplot) is shown, which was used to calibrate Equation 5.2.

It interesting to remark that the correlations of basin flow with area are best using maximum values, and are poorest using minimum annual values (Table 5.7). This is perhaps because there are fewer losses of surface water in the catchment during high-flow years, and more variable losses of surface water in low-flow years.

The seasonal signal of creek flow was estimated using data from the Upper Vaseux Creek gauging station (ID 08NM015), which was selected since it assumed that the creek bottom is close to bedrock and would best represent total flow in the catchment. Other stations have very

similar seasonal signals in both timing and shape. The seasonal signal was represented using a normalized seasonal distribution, D_t (Table 5.8):

$$D_t \frac{Q_t}{\sum(Q_t \cdot \Delta t)} \qquad (5.3)$$

where Q_t is the mean flow rate for time *t* in a season (such as in a 5-day period or a month), and Δt is the number of days in *t*. The normalized seasonal distribution curves are illustrated in Figure 5.8 for 5-day and monthly distributions. The normalized seasonal distribution is used to estimate seasonal flow at all creeks, given an annual flow [m^3/day]:

$$\hat{Q}_t = \frac{\hat{Q}_{Ann} \cdot D_t}{365 \text{ days}} \qquad (5.4)$$

Table 5.8: Monthly normalized distribution values, D_t (scaled 1 × 10^{-3} for display), for flow at Upper Vaseux Creek.

Jan	Feb	Mar	Apr	May	Jun	Jul	Aug	Sep	Oct	Nov	Dec
0.371	0.345	0.429	2.804	13.350	9.764	2.802	0.766	0.547	0.615	0.555	0.386

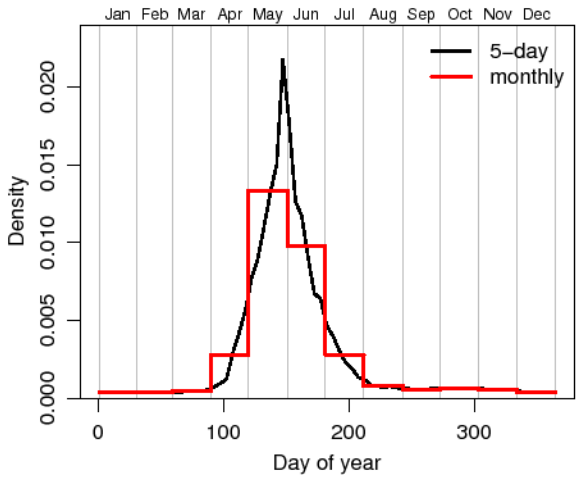

Figure 5.8: Normalized seasonal distribution of flow at Upper Vaseux Creek gauge, above Dutton, 1970–2003 (ID 08NM015). Both 5-day and monthly curves represent a normalized seasonal distribution, D_t, which each integrate to 1 over a year.

5.3. GROUNDWATER FLOW MODEL

GMS version 6.0 (Owen et al., 1996; EMRL, 2005) was used for both the 3D stratigraphic construction and to simulate groundwater flow using MODFLOW-2000, version 1.15.00 from August 6, 2004 (Harbaugh et al., 2000). GMS allows the user to define a groundwater model using a conceptual model approach, whereby properties and boundaries are defined spatially using vector-based arcs, polygons and points. These can represent, for example, aquifers, rivers, and wells, which contain specific boundary condition data, such as material properties, stage and pumping rates. The conceptual models are then translated to a finite difference grid by the location of the elements on the grid, and then translating the boundary condition information to the respective MODFLOW modules.

Conceptual models for steady-state and transient boundary conditions were defined, which, respectively, represent low-flow conditions expected in mid-summer (represented by August) and for each month of a two year period (24 stress periods of 28 to 31 days). Two years with identical stresses in each year were simulated to compare changes between the two years. Four time steps were simulated in each stress period using a time step multiplier of 1.2, which total to 96 simulated time steps over 730 days.

5.3.1. MODEL DOMAIN AND GRID DESIGN

The finite difference grid, shown in Figure 5.9, has 256 rows, 98 columns and 9 layers. The horizontal grid spacings range between 50 to 100 m, with telescopic grid refinement focused around pumping wells. This resolution is sufficient to define cones of depression around the production wells, since the surrounding materials have high transmissivities. Many consulting reports indicate drawdowns in pumping wells on the order of tens of centimetres.

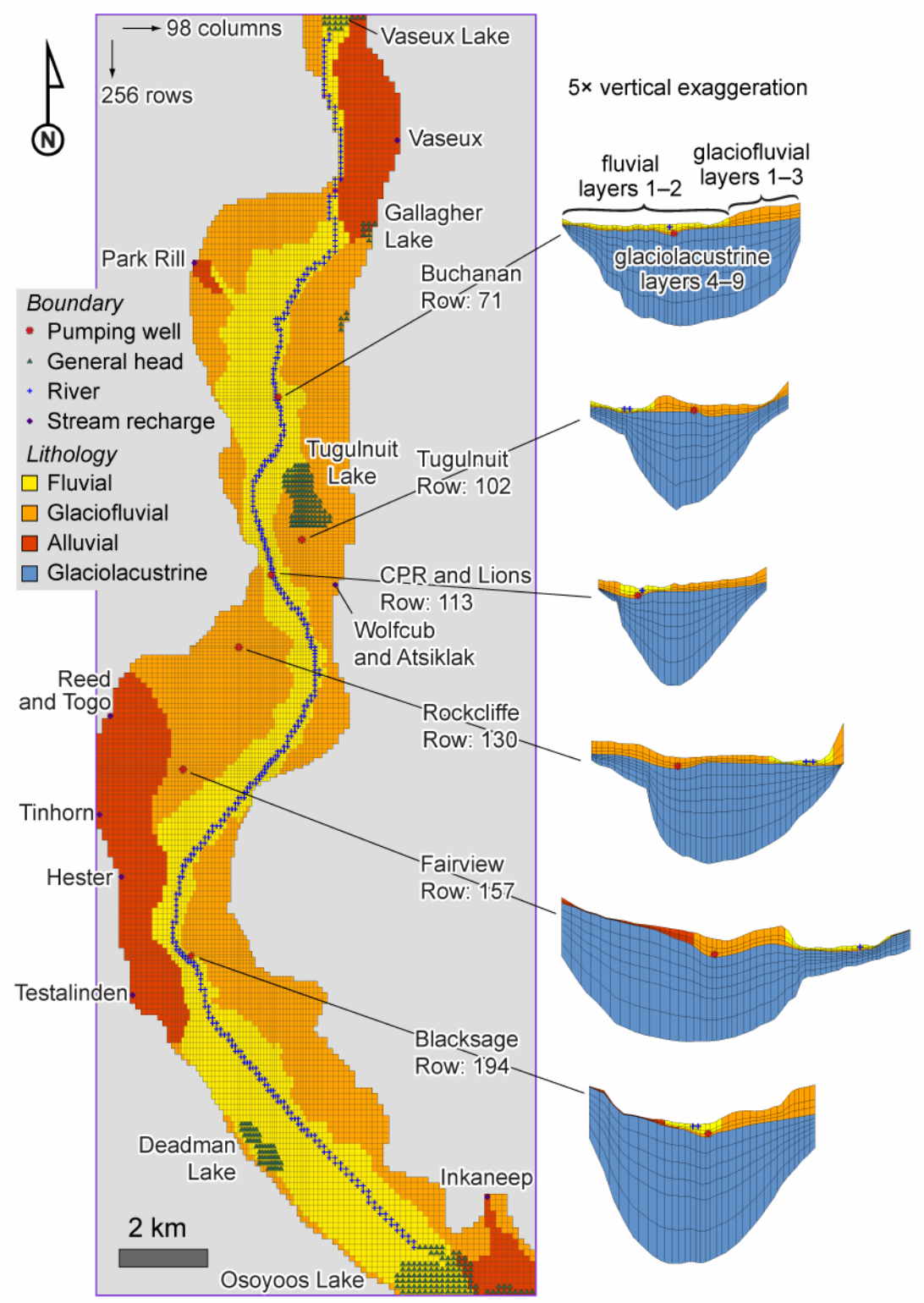

Figure 5.9: Regional model grid, materials and boundary conditions. The vertical profiles are shown at each pumping well, and have a slightly larger scale than the plan-view, and a vertical exaggeration of 5.

The upper surface of the grid was interpolated from Level 1 digital elevation data (Natural Resources Canada, 2005); the top of layer 4 was interpolated using the silt top, as shown in Figure 2.11; the bottom of layer 9 was interpolated using the bedrock surface, as shown in Figure 2.7. The top three layers contain alluvial and glaciofluvial materials, and have vertical spacing fractions of 1/2, 1/4 and 1/4, from top to bottom. The uppermost layer is thicker than the others, since it is typically dry for most of the region above the flood plane, and it contains boundary data for the river and lakes, which require sufficient vertical space for the boundary bottoms.[18] The Okanagan River fluvial materials are in the top two layers only, and are usually underlain by glaciofluvial deposits for layer 3. Layers 4 to 9 are glaciolacustrine silt and clay materials, which have vertical spacing fractions of 1/8 for layers 4–7, and 1/4 for layers 8–9.

The bedrock is considered to be impermeable and was defined using the bottom and sides of the model domain, which are simulated as a no flow boundaries by MODFLOW. The outer region of the model was defined such that the lowermost grid cell was saturated under August steady-state conditions. MODFLOW cannot simulate processes that extended too far up along the raised benches, since the majority of this is unsaturated material. A more advanced code, such as FEFLOW (e.g., Dierscha and Perrochetb, 1999) would be more ideal to simulate these regions and groundwater conditions.

5.3.1.1 Materials and flow package

The Layer Property Flow (LPF) Package was used to simulate groundwater flow in MODFLOW. The materials were defined using zones (array IDs), as shown in Figure 5.9. The package was configured to calculate interblock transmissivity using the harmonic mean, and all layers were set to be “convertible” (as opposed to “confined,” where transmissivity is constant). Wetting was enabled for all layers, and is detailed later.

Material properties were initially set to values indicated from aquifer tests. Horizontal hydraulic conductivity and vertical anisotropies were later adjusted during calibration using steady-state conditions with August model stresses, and are found later in Table 5.10. Horizontal anisotropy factors, K_x / K_y, for all materials were set to 1.0, since this anisotropy is not expected to change horizontally. Vertical anisotropy factors, K_h / K_z, were varied for each material. Vertical

[18]The digital elevation data used for the upper surface does not always correlate with the hydrology boundaries from river surveys, and often the digital elevation data is influenced by tops of vegetation and buildings. For this reason, the digital elevation data are often overestimated, which consequently overestimate the bottom limits of the layer containing the bottom of river and lake boundaries.

anisotropies for fluvial sediments are higher than surrounding materials, as suggested from other studies (e.g., Chen, 2000). Alluvial vertical anisotropy was also higher than other materials, since many of the material descriptions describe “hardpan” deposits, which are interpreted to have come from mass transport flow deposits and, thus, likely have lower hydraulic conductivity. Also, a higher vertical anisotropy may help raise the water table along the benches, which is observed in some parts of the region.

5.3.2. HYDROLOGICAL BOUNDARY CONDITIONS

Surface elevations for lakes were approximated from 0.75-arc second Level 1 digital elevation data (Natural Resources Canada, 2005), unless otherwise specified. Each type of surface water boundary was simulated using different MODFLOW packages, since each boundary condition has different mass-balance interactions with the aquifers. Park Rill was not simulated, as attempts us define it using the Drain Package appeared unrealistic, and added to problems with simulation convergence.

5.3.2.1 Recharge

Mean monthly recharge was applied to the upper layer in the model. Monthly recharge results in Section 4.0 consisted of 100 years (1200 months) of gridded 100 m recharge rates, which were archived in multidimensional netCDF array files. These netCDF files were translated using a Python script[19] to a simple text file, which can be imported as a transient 2D scatter point file in GMS. The 2D transient points were then linearly interpolated to the irregular 2D grid with the same spacings as the MODFLOW model. This way, the interpolated grid can be used directly as a array for the Recharge Package (RCH) in MODFLOW. This package was configured to receive a recharge flux to the highest active cell. Recharge fluxes used for this model also include considerable contribution from simulated irrigation return flow, as shown in Figure 4.6b.

5.3.2.2 River

Okanagan River has regulated flow from Vaseux Lake to Osoyoos Lake, which was modified using the monthly deviations of stage at Vaseux Lake (see Table 5.5). As this river flows year-round, it was simulated using the River Package (RIV1). Boundary conditions were assigned to layer 1 of the model. River stage and bottom elevations of Okanagan River were defined from a detailed survey (Schubert, 1983). River stages were set to Osoyoos Lake levels if they were less than this lake. These adjustments were were implemented in GMS using a Python script,[20]

[19]Located on the CD at programs/monthlync2xys.py
[20]Located on the CD at programs/gms_fixed2ts.py

since the river stage was defined at 191 nodes from the survey data.

The riverbed conductance was initially set to 10 $m^2d^{-1}m^{-1}$, which is lower than the surrounding hydraulic conductivities of the fluvial deposits. This value was adjusted during calibration.

5.3.2.3 Streams

Development of the model initially used the Stream Package (STR) (Prudic, 1989); however, it was difficult to maintain a model that could converge with reasonable model error, and without significant oscillation in convergence. The STR package is limited in that fluxes cannot pass from the top layer, through upper dry cells to the highest active cell (if the highest active cell is several layers beneath the boundary), which is a likely scenario in the study region. The updated and much improved Streamflow-Routing Package (SFR2) (Niswonger and Prudic, 2005) was also not used, since it is not supported in GMS. This MODFLOW package was redesigned to overcome some of the limitations described above, such as simulating unsaturated flow beneath streams.

As a substitute solution, stream flow rates were applied in the Recharge Package (RCH), which applies a specified flux to the highest active cell. Flow rates from each stream, estimated in m^3d^{-1}, were converted to recharge fluxes using the area of a grid cell selected on the edge of the model nearest to the stream. Locations of the cells and the areas are listed in Table 5.9. A limitation of this method is that it is not possible to separate the contribution of flow from streams in the flow budget, since it is included with recharge. The fluxes were included in the 2D array of recharge using a Python script,[21] which uses the stream flow estimates in Table 5.6 with the seasonal response in Table 5.8 and the area of the grid cell in Table 5.9.

[21]Located on the CD at programs/gms_addcreeksto2D.py

Table 5.9: Application of streams to MODFLOW Recharge Package.

Creek name	Grid location		Area
	row	column	(m^2)
Vaseux	23	74	9789.76
Park Rill*	45	22	5413.70
Wolfcub†	116	63	6552.39
Reed‡	145	3	8799.79
Tinhorn	167	1	9769.76
Hester	178	5	9769.76
Testalinden	203	7	9668.22
Inkaneep	239	90	9834.56

*Plus tributaries: Burnell, Victoria, Orofino and Kearns

†Including Atsiklak Creek

‡Including Togo Creek

5.3.2.4 Lakes

All the lakes in the region were simulated using the General Head Boundary (GHB) Package. The Lake Package (LAK) was not used, as this was exceedingly more complex and posed more complications in attempt to construct a stable numerical model. Water levels, indicated in Table 5.5, were used for the transient stages. The conductance for the polygon boundary was initially set to $10 m^2 d^{-1} m^{-1}$, which was adjusted during calibration.

5.3.2.5 Pumping wells

Pumping wells were simulated using the Well (WEL) Package, using the monthly pumping rates for 2005 in Table 5.3. The depth range of screens for each well are detailed in Section 6.0, which are translated and distributed along 1 to 3 cells in the upper layer of the MODFLOW grid.

5.3.3. SOLVER AND REWETTING

The geometric multigrid solver (GMG) was used (Wilson and Naff, 2004). This is an advanced MODFLOW-2000 solver based on the preconditioned conjugate gradient (PCG) algorithm. The solver was optimized for transient non-linear groundwater flow.[22] Optimal model solutions were achieved by setting the inner iteration residual convergence criterion to 0.001, the outer iteration head change convergence criterion to 0.01, a damping parameter of 0.51 with adaptive

[22]A groundwater model is considered *nonlinear* if it includes Cauchy boundary conditions or head dependant nodes, such as the MODFLOW River Package

damping for remaining iterations, using ILU smoothing with semi-coarsening of the multigrid preconditioner along all dimensions.

Rewetting is a method used in MODFLOW where “dry” cells can be converted to “wet” or a variable head cell if the head in surrounding cells is high enough to trigger the rewetting (McDonald et al., 1991). This method is used since MODFLOW is a saturated-flow code, and considers “dry” cells as “no-flow” cells since it can not simulate complicated unsaturated groundwater flow. Cell rewetting was activated for all cells in the model – the model must simulate flow with fluctuating water levels in a transient simulation. Rewetting also presents difficulties with convergence, since the convergence error used in solving the groundwater flow equation is prone to oscillation, as cells are converted between “wet” and “dry” within iterations of each time step. To avoid oscillation in the convergence, rewetting was enabled only from underlying cells (as opposed to neighbouring cells), and the head was calculated using the threshold of 12.0 with a wetting factor of 0.5, and an iteration interval of 3.

5.3.4. MODEL CALIBRATION, MATERIAL PROPERTIES, AND FLOW BUDGET

Calibration was performed on a steady-state model (described next section) using approximations of hydraulic properties of the materials and boundary conductances described previously. The model was calibrated iteratively by modifying independent hydraulic properties, and taking note of the model error between observed and simulated hydraulic heads from 430 water wells, and their locations within the modeling domain. A similar procedure was then used for modifying the conductances to the river and general head (lake) boundaries. Final calibrated values for hydraulic conductivities are listed in Table 5.10. Conductances of 10 $m^2d^{-1}m^{-1}$ and 20 $m^2d^{-1}m^{-1}$ provided the best-fit calibration for river and general head (lake) polygon boundaries, respectively.

Table 5.10: Hydrologic properties of materials used for regional model, determined through calibration (described later) of the August steady-state model to groundwater well heads.

Name	Materials	K_h (m/day)	$\frac{K_h}{K_z}$	S_s (1/m)	S_y	n
Fluvial	Sand, some gravel	200.0	5.0	5×10^{-4}	0.25	0.3
Alluvial	Sand, gravel, clay	50.0	10.0	1×10^{-4}	0.2	0.3
Glaciofluvial	Sand and gravel	400.0	3.0	1×10^{-4}	0.2	0.3
Glaciolacustrine	Silt and clay	0.5	3.0	1×10^{-2}	0.1	0.3

The calibrated steady-state model is evaluated using residuals between computed and observed heads, where out of 430 wells, 243 have a negative residual (model underestimates observed) and 187 residuals are positive. The normalized Root Mean Square Error is 6.4%. A plot of the residuals is in Figure 5.10. In this model, the hydraulic head is underestimated along the benches, while it is within reasonable error elsewhere. The flow budget for the steady-state model is summarized in Table 5.11.

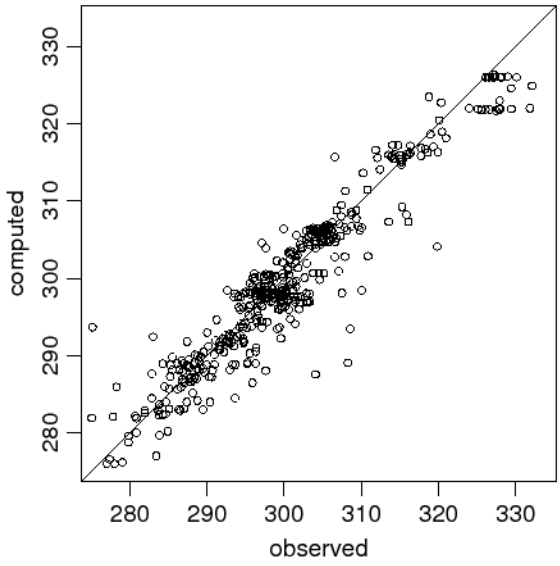

Figure 5.10: Steady-state calibration of regional model, showing a cross-plot of observed and computed heads from 430 wells. The normalized RMSE is 6.4%.

Table 5.11: Steady-state flow budget for regional groundwater model (all active cells). The difference between total in and out flow is 86.31 m^3, or 0.08%.

Source/sink	Flow in		Flow out	
	m^3	%	m^3	%
General heads	31074	28.79	~10447	9.88
Rivers	45029	41.73	~69406	64.26
Wells	0	0.	~27929	25.86
Recharge	31812	29.48	0	0.
Σ	107915	100.00	~108002	100.00

5.3.5. TRANSIENT SIMULATIONS

Transient simulations were undertaken using the heads from the steady-state solution as an initial condition.[23] The two-year transient simulation was then repeated three times, using the heads of the previous simulation as the starting heads for the next. This looping of simulation allows the model to settle into a seasonal pattern, which has minor differences of head and flow rates from the first year to the second. In analysis, this could be regarded as a seasonal steady-state, since the difference of total in and out flows are nearly zero, specifically 50.03 m^3 or 0.0087%. This process was completed using the "current" or "base" recharge and stream flow conditions. The transient flow budget is shown in Figure 5.11.

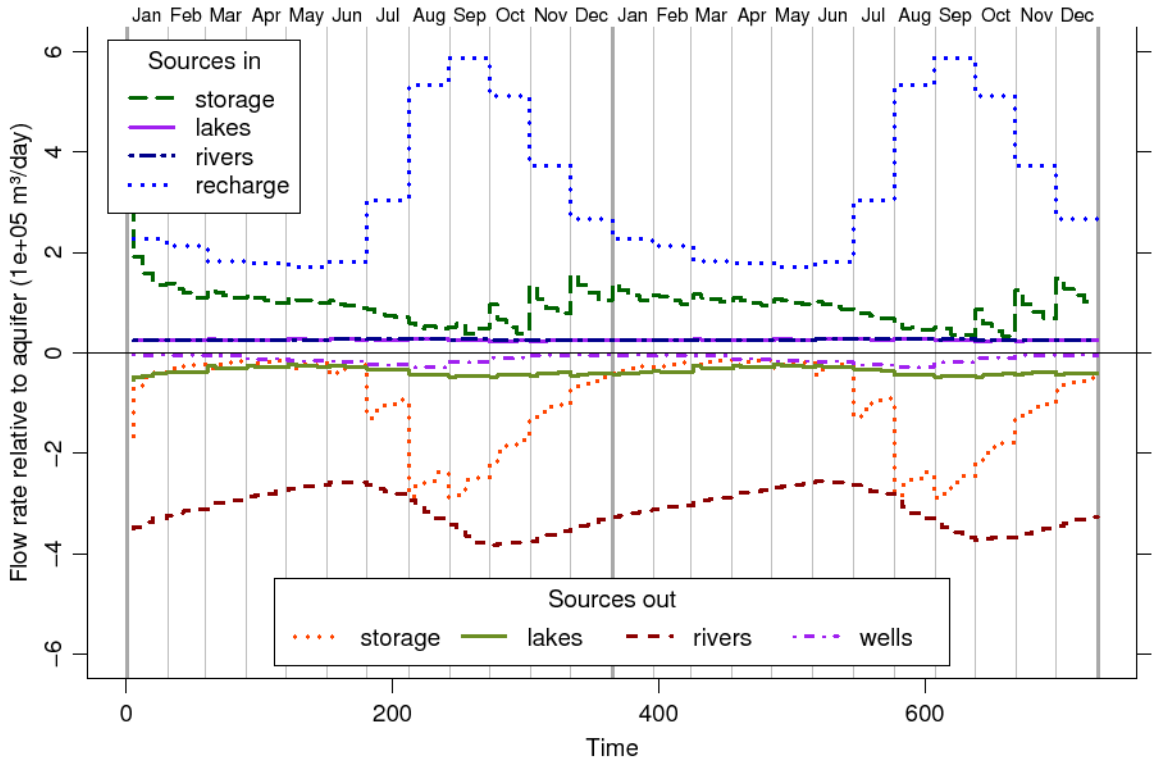

Figure 5.11: Transient flow budget for regional groundwater model using the base or "current" climate conditions for all active cells. Negative budgets indicate flow out of the aquifer, while positive budgets indicate flow into the aquifer.

[23]Dry cells were removed and re-interpolated using neighbouring heads. In GMS, this was done by converting the heads from the last time step to 3D scatter points, then re-interpolate the points to the 3D grid using the inverse distance weighted (Shepard's) method with the nearest 8 points. This method replaces the dry head value, a dummy number −888.0, with realistic values of head (even if the head is below the cell bottom elevations).

The transient annual flow budget was calculated through integration of the second-year, using the trapezoid rule:

$$F \equiv \frac{f_1 + f_2}{2} dt_1 + \frac{f_2 + f_3}{2} dt_2 + \frac{f_n + f_{n+1}}{2} dt_n \quad (5.5)$$

$$F = \sum_{i=48}^{95} \left[\frac{f_i + f_{i+1}}{2} \left(t_{i+1} - t_i \right) \right] \quad (5.6)$$

where F is the total annual flow in m^3/yr, dt is the time step duration in days, and f is the flow budget, in m^3/day. The indices 48 and 95+1 select day 365 and 730, respectively. The transient annual flow budget is given in Table 5.12.

Table 5.12: Transient annual flow budget for current and future periods. The flow numbers represents the area under the curves in Figure 5.11, from January to December of the second year. Totals appear independently for flows of each climate condition.

Source/sink	Flow in		Flow out	
	1×10^6 m^3/yr	%	1×10^6 m^3/yr	%
Storage	32.536	19.66	~34.881	21.08
General heads	9.619	5.81	~13.167	7.96
Rivers	9.604	5.8	~113.115	68.35
Wells	0	0	~4.341	2.62
Recharge	113.746	68.73	0	0
Σ	165.506	100	~165.504	100

The model water budget results show that recharge from precipitation and irrigation dominates the input to the aquifer (roughly 68% of the total water budget). Water from lakes and rivers accounts for approximately 10% of the inflow to the aquifer. Water input to storage is 20%. The change in storage (inflow minus outflow) is roughly zero, as would be expected for such a seasonal steady-state simulation. Losses of groundwater to lakes and rivers accounts for a much higher percentage than the inflow (76%), while wells extract only 3% of the annual water budget.

A water table map was also generated from the model using the heads from the highest active cell in the 3D finite difference grid (Figure 5.12). The water table elevation ranges from 280 to 355 m.a.s.l. along the Vaseux Lake to Osoyoos Lake corridor. The water table rises up slightly in proximity to the benches.

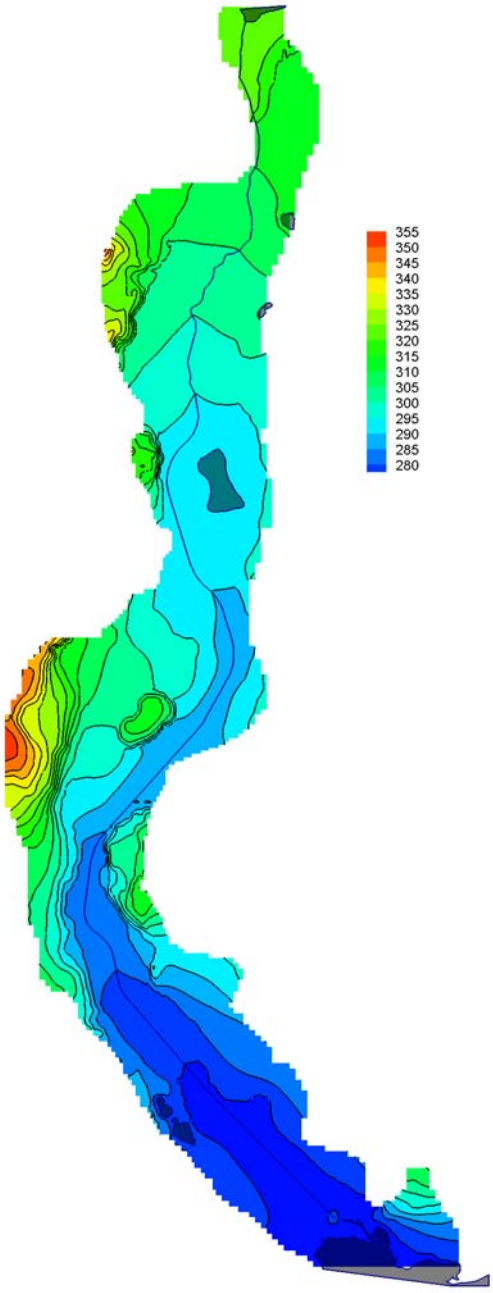

Figure 5.12: Water table map created from the hydraulic head values for the highest active cells in the model domain

6. CAPTURE ZONE ANALYSIS

6.1. INTRODUCTION

A capture zone analysis was undertaken for the municipal groundwater wells for the Town of Oliver and the surrounding region. The capture zones completed as part of this study will offer an alternative to the calculated fixed radius (CFR) capture zones currently used in the land use allocation model (Foley et al., 2005). Also, the zones will be used for wellhead protection planning as identified in the Concept Plan for Oliver.[24]

A well capture zone is the spatial region surrounding a production water well, in which water will flow into the well within a period of time (Anderson and Woessner, 1992). Essentially, the zone is based on a time of travel (TOT) calculation. There are a number of methods to determine TOT, including: (1) arbitrary fixed radius or calculated fixed radius methods (these two methods only give reasonably accurate results if the hydraulic gradient is zero or very low); (2) analytical methods based on the parabolic shape of the capture zone when there is a measurable regional hydraulic gradient; and (3) numerical methods based on particle tracking simulations. The most rigorous are the numerical methods, which rely on a calibrated groundwater flow model. In a numerical simulation, imaginary particles are released at the well screen, and tracked backwards within the model to determine their origin at specified times. The locus of the points of origin at any particular time defines the capture zone for that time. Typically, 1, 5 and 10 year captures zones are computed.

Defining the spatial extent of well capture zones can help land use management and land use planning in respect of designating land use activities within well capture zones that are effectively benign so as to avoid potential risks to the quality of groundwater produced from the well. For example, a land use decision may be explicitly based on trying to avoid placing a potentially risky development, such as a gas station, within the capture zone of a well. For existing land use, the capture zones may aid in emergency response planning. For example, if a gasoline spill were to occur within the well capture zone area, the well could be shut down.

The spatial extent of a well capture zone is partially dependent on the heterogeneity of the

[24]http://www.sgog.bc.ca/content.asp?contentID=156

hydraulic properties of the aquifer, which influence the groundwater flow directions. For example, gravel lenses can act as conduits where water can travel faster than in surrounding finer-grained materials, such as sand and silt. In contrast, clay plugs found in association with in-filled oxbow lakes in this study area may cause the flow to diverge towards nearby “faster” sediments. Consequently, zones with high conductivities are more susceptible to contamination since more water passes through these materials, and because transit times are faster. Thus, the spatial distribution of materials in the aquifer can lead to non-uniform capture zones that require a numerical model be constructed.

The most common method for model construction relies on defining layers, and assigning hydraulic properties to those layers as was done in the regional model discussed in the previous chapter. More sophisticated hydrostratigraphic models can effectively capture some spatial variability in the materials, such that lenses or changes in material type are incorporated into the different model layers (e.g., Abbotsford regional model described by Scibek, 2005). This latter approach tends to capture some degree of heterogeneity at some spatial scale. In either case, the model and the computed capture zones are deterministic, which simply means that they are based on fixed model parameters defined for specific homogeneous or heterogeneous layers. When there is uncertainty in the distribution of materials, there is equal uncertainty in the computed capture zone. In this case, probabilistic capture zones are best computed.

In this particular study area, the upper aquifer consists dominantly of sand and gravel; however, other finer- and coarser-grained materials are also present. These materials represent glaciofluvial, alluvial and channel deposits. Silt and clay lenses are interpreted as in-filled oxbow lakes and over-bank deposits of the channel facies deposited by Okanagan River (see Figure 2.13). The variation and distribution of these materials contribute to the significant heterogeneity of the hydraulic conductivity in this aquifer. Furthermore, the materials in the upper aquifer are only known at sparse locations, from the borehole data, and not continuously throughout the aquifer. Thus, a geostatistical technique was used in this study to stochastically produce multiple realizations of continuous aquifer materials from statistical parameters derived from the existing borehole data. The multiple aquifer material realizations were then used to simulate groundwater flow, from which the probabilities of flow paths from each realization were analyzed to establish probabilistic capture zones around each well.

6.2. LOCAL SCALE GROUNDWATER MODEL CONSTRUCTION

A three-layer local scale groundwater flow model was constructed in GMS 6.0 (Owen et al., 1996; EMRL, 2005). A local scale was selected for the well capture zone analysis in order to capture the heterogeneity in the surficial aquifer materials. Steady-state groundwater flow was simulated using MODFLOW 2000, Version 1.14.00 (Harbaugh et al., 2000).

The heterogeneity of the aquifer materials in the upper two layers was stochastically generated using transition probabilities determined from the borehole data, using T-PROGS (Carle and Fogg, 1996, 1997; Carle, 1999). Transition probabilities are used in indicator geostatistics to quantify how one material change to another over spatial distances. These probabilities are used with vertical (1-D) Markov chains, which are a stochastic process that is used to predict materials in 3-D. Both the transition probabilities and Markov chains are calibrated from classified soil materials in 438 boreholes (BC MoE, 2006) measured at 0.3 m vertical lag spacings to 10.8 m. The classifications were: (1) silt, (2) sand, (3) sand and gravel, and (4) gravel. Boulder deposits were classified as gravel, and clay deposits as silt. This decision to limit the number of classifications was based on a need to minimize the range of hydraulic conductivity values in the modelling domain.[25]

Vertical transition probabilities and fitted Markov chain model results are shown in Figure 6.1. The graphs are arranged in a matrix. Each graph shows the probability that material *R* will change to material *C* over different lag distances, where *R* is the material in the rows, and *C* is the material in the columns. A lag distance is simply a fixed spacing between two arbitrary points, at which the materials at each end are compared. The measured material proportions and fitted lens lengths are provided in Table 6.1, which have a best-fit with the observed transition probabilities. The fitted vertical embedded transition probabilities (e.g., Carle, 1999) are:

$$\mathbf{\Pi} = \begin{bmatrix} - & 0.35 & 0.4 & 0.25 \\ 0.2 & - & 0.6 & 0.2 \\ 0.25 & 0.55 & - & 0.2 \\ 0.2 & 0.5 & 0.3 & - \end{bmatrix}$$ for silt, sand, sand & gravel, and gravel

[25]MODFLOW models cannot converge if the range of hydraulic conductivity properties is too diverse; there are at least five or more orders of magnitude in K_S between clay and boulder deposits.

Table 6.1: Measured material proportions and fitted Markov chain models.

Material	Proportion	Lens length	Lens ratios	
		Vertical (*Z*)	Strike (*X*)	Dip (*Y*)
Silt	0.0695	2.5	8.0	12.0
Sand	0.3017	6.0	10.0	10.0
Sand and gravel	0.3866	7.8	8.0	12.7
Gravel	0.2422	9.0	8.0	12.0

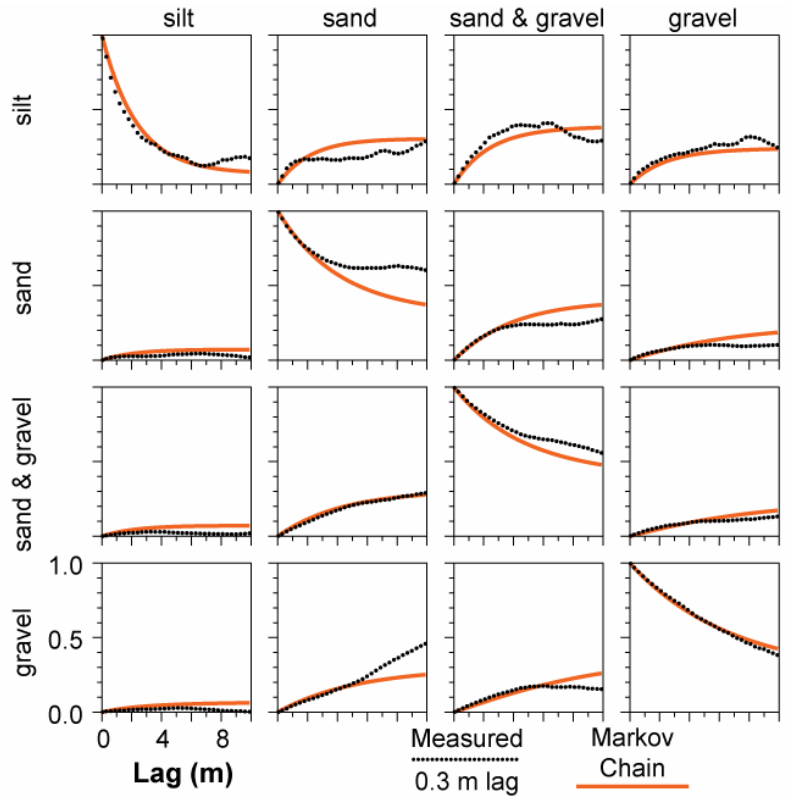

Figure 6.1: Vertical transition probabilities from the borehole data, and fitted transition probability models. To interpret this matrix of graphs: each graph shows the probability that material *R* will change to material *C* over different lag distances, where *R* is the material names in the rows, and *C* is the material names in the columns. A lag distance is simply a fixed spacing between two arbitrary points, at which the materials at each end are compared.

In practice, horizontal Markov chains and transition probabilities are not determined, as the borehole data are too sparse along horizontal dimensions. Statistical parameters for the horizontal directions are thus assumed to be a scaled ~10x from the vertical (strike and dip values in Table 6.1), as it is expected the geological facies are more laterally continuous in horizontal directions. The *y*-direction (north–south) lens ratios for silt and gravel are slightly larger than in the *x*-direction (east–west), since it is expected that these lenses are in the same

general alignment with Okanagan River.

Thirty conditional simulations of aquifer materials were generated (see examples in Figure 6.3), through which groundwater flow was ultimately modelled. These three-dimensional grids of aquifer material realizations are *conditional* in the sense that they honour both the transition probabilities and borehole data.

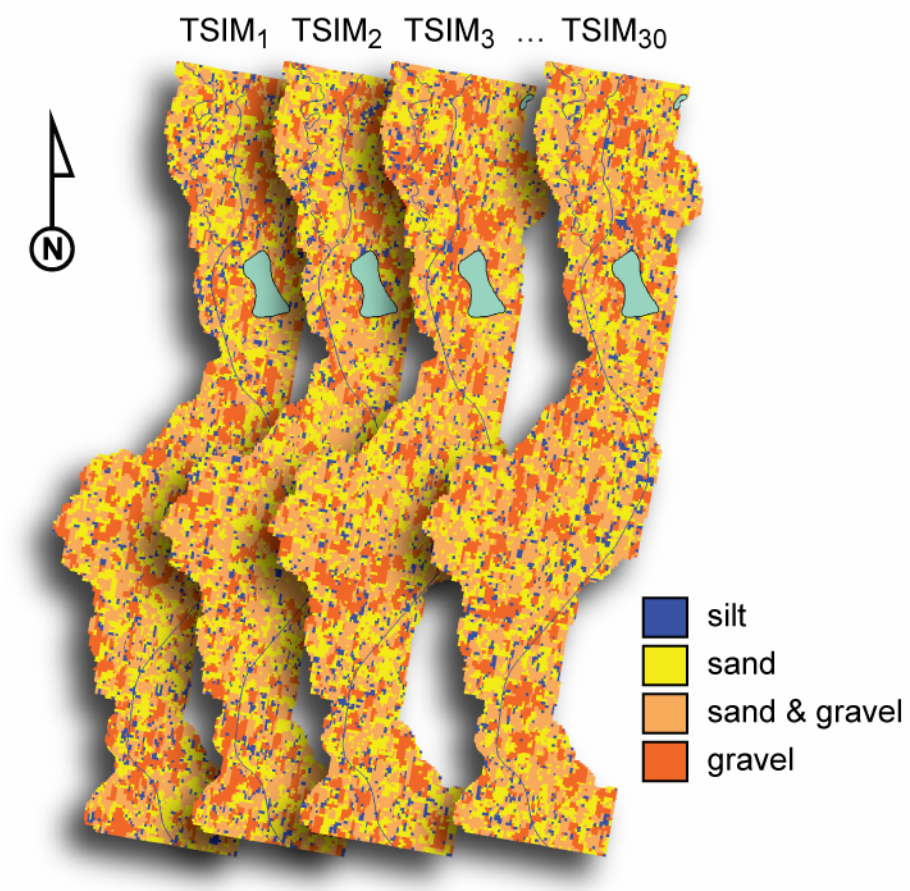

Figure 6.2: Realizations of aquifer materials from TSIM (subprogram of T-PROGS). These conditional simulations honour both transition probabilities and borehole data.

6.2.1. GRID DESIGN AND MATERIAL PROPERTIES

The finite difference grid for the groundwater model (Figure 6.4) has 313 rows, 119 columns and three layers. Horizontal grid spacing is 50 m and refines to 20 m near pumping wells. The upper two layers have equal thicknesses, which span through the upper aquifer. The top of the upper aquifer is defined from digital surface elevation data (Natural Resources Canada, 2005) to the

silt top (see Figure 2.11). Layer 3 is represented by the thick silt, which extends down to the bedrock (see Figure 2.7).

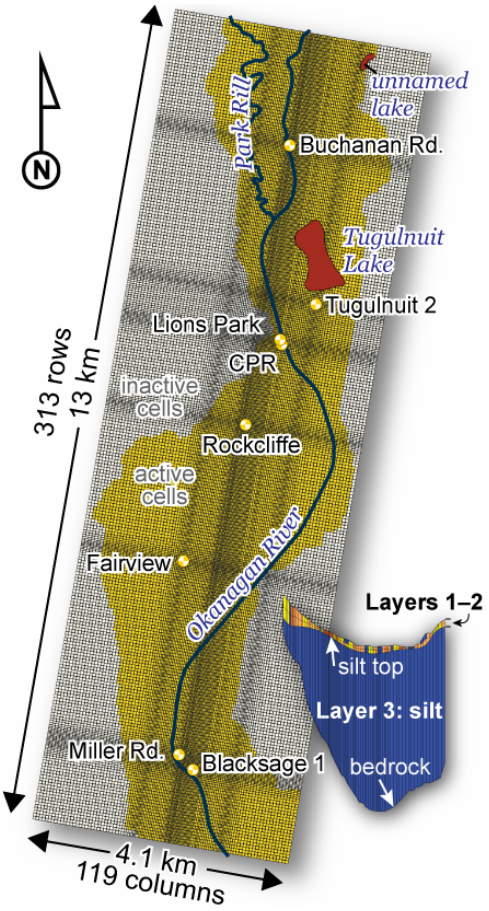

Figure 6.3: Groundwater model grid and boundary conditions.

As for the regional scale model, pumping test data for several production wells were used to provide estimates of the hydraulic properties for the sand and gravel aquifer. The hydraulic property estimates were the same as those used in the regional model as given in Table 5.2. Also, as for the regional scale model, hydraulic conductivities for the silt and clay were estimated to be between 0.1 to 10 m/day, or 1.2e-6 to 1.2e-4 m/s, and specific yield values were estimated to be about 0.02 (e.g., Domenico and Schwartz, 1998).

The layer-property flow package (LPF) was used to represent the materials using convertible layer types. Horizontal anisotropy for all materials is assumed to be homogeneous (1.0), despite

possible small-scale longitudinal imbrication of sedimentary materials along the length of Okanagan River. Vertical anisotropy for all materials was assumed to be 2.0, although other studies suggest that this values is an underestimate (e.g., Chen, 2000).

Vertical leakage correction was removed, and cell wetting parameters were disabled, as this allowed the model to converge. The final material properties achieved through calibration are described in Table 6.2.

Table 6.2: Hydrologic properties of materials used for capture zone analysis; horizontal hydraulic conductivity, K_h, and porosity, n.

Material	K_h (m/s)	K_h (m/day)	n
Silt	5.8e-5	5	0.2
Sand	5.8e-4	50	0.3
Sand & gravel	4.6e-3	400	0.3
Gravel	1.2e-2	1000	0.3

6.2.2. BOUNDARY CONDITIONS

Recharge flux (RCH) was applied to the highest active cell (Figure 6.4), and was obtained from the average annual recharge. Irrigation return flow was not considered for this particular model; only natural precipitation was used in recharge modelling.

Each type of surface water boundary was simulated using a different MODFLOW package, since each boundary condition has different mass-balance interactions with the aquifers. Okanagan River and Park Rill were simulated using the river package (RIV), while Tugulnuit Lake and a small unnamed lake were simulated using the general head boundary (GHB). The RIV and GHB boundary conditions were simulated in layer 1. River stage and bottom elevations of Okanagan River were defined from a detailed survey (Schubert, 1983). The river stage elevations for Park Rill were estimated from available digital elevation data, with a river depth estimate of 1 metre. Conductances were set to 400 $m^2day^{-1}m^{-1}$ and 20 $m^2day^{-1}m^{-1}$ for RIV and GHB, respectively, as these values are within the same order of magnitude of the aquifer materials (with correction for units) and allowed convergence of the model. A sensitivity analysis of river bed conductance parameters showed they have minimal influence on exchange of water through the RIV boundary condition.

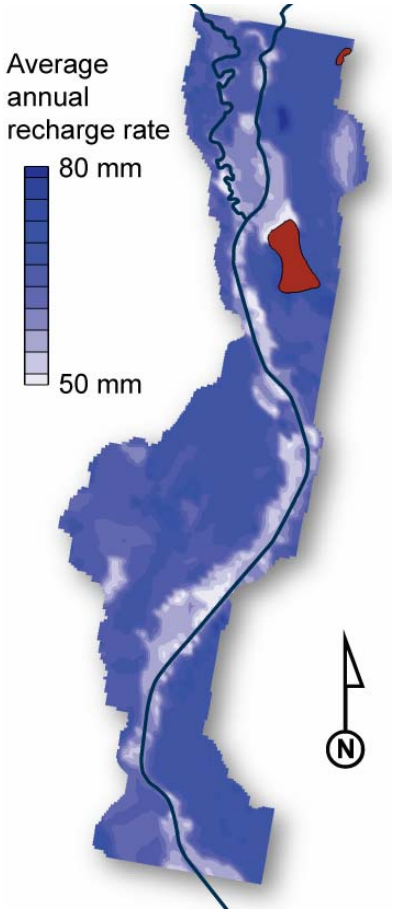

Figure 6.4: Annual recharge rate. Does not include irrigation return flow.

Most of the high-producing water wells (BC MoE, 2006) in the Oliver region are completed in the upper sand and gravel aquifer, adjacent to (and vertically below) the Okanagan River. Eight municipal production wells were simulated in layer 2 (and in layer 1, for some wells where the screen overlapped) using typical pumping rates from consulting reports and supplemented with well yield data from the WELLS database where needed. Table 6.3 shows well name, and respective well tag numbers (WTN), average pumping rate and screen interval for those wells considered for the capture zone analysis. The information of pumping rates was provided by Foley et al. (2005).

Table 6.3: Municipal production water wells used for the capture zone analysis, and their pumping rates.

Well name	WTN	Average pumping rate		Screen depth (m)	
		(USgpm)	(m^3/s)	from	to
Blacksage 1	49481	2000	1.26e-1	11.6	25.7
Miller Rd.	84724	1092	6.89e-2	14.8	18.0
Buchanan Rd.	21873	402	2.54e-2	17.4	22.1
Fairview	21867	425	2.68e-2	26.8	34.1
Lions Park	83010	1230	7.76e-2	18.3	23.2
CPR	83011	1000	6.31e-2	9.1	13.6
Rockcliffe	82376	1500	9.46e-2	15.0	24.4
Tugulnuit 2	83008	1200	7.57e-2	10.4	14.3

6.2.3. SIMULATION AND PROBABILISTIC CAPTURE ZONES

The steady-state model was solved using the PGC2 solver, with both head change and residual volume criteria set to 0.01. Steady-state flow simulations were performed for each aquifer material instance. Of the 30 groundwater simulations, two did not converge. River mass balances converge with minimal residual (sum of squared weighted residuals is 1.7e-29).

The model is reasonably calibrated with respect to observed water table points (Figure 6.5), with many observed points underestimated along the valley margins. The higher observed water table along the sides are difficult to simulate with this model, and would require: (1) additional boundary conditions (e.g., streams at valley sides) to raise their elevation; (2) higher recharge rates; or (3) lower hydraulic conductivities.

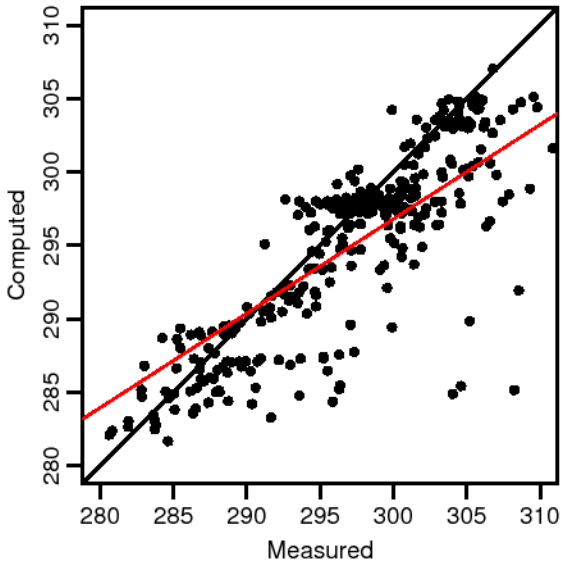

Figure 6.5: Observed vs. computed hydraulic heads, with R^2=0.5717.

6.3. RESULTS

Probabilistic capture zones were determined in GMS using eight particles distributed within each cell, which were traced to each pumping well through MODPATH. Capture zones were determined for 60, 365 and 3650 days.

Probabilistic capture zones for 60 and 365 days are shown in Figure 6.6. The 3650 day (or 10 year) capture zones are not shown, since these have less reliability and for many wells are no different than the 1-year zones. The contours that define the capture zones indicate the probability that water in the saturated aquifer will reach the pumping well within the designated time. Time of travel above the water table (in the unsaturated zone) is not considered, although from recharge modelling this can range anywhere between a few weeks to months, depending on depth to water and hydraulic conductivities.

Details for each well are summarized as follows:

Blacksage 1 and Miller Rd.: these capture zones are highly influenced by nearby reaches of Okanagan River. The proximity of this boundary condition appears to constrain the capture zone, such that the differences between the 1 and 10 year capture zones are very minor.

Buchanan Rd.: this capture zone is influenced by nearby Okanagan River and by the higher water table to the east (influenced by the unnamed lake in this model). The forked geometry

of the capture zone appears to be influenced by localized deposits of finer- and coarser-grained deposits, as found in the boreholes and simulated through T-PROGS.

Fairview: this well appears to obtain water through the underlying silt, thus having a capture zone with limited extent. The modeled capture zone is highly influenced by the silt top elevation, which is lower at this location. However, this well appears to also be in a region with boulder deposits, and may have a more complicated subsurface path that cannot be practically modeled without a more detailed survey.

Lions Park and CPR: these capture zones are highly influenced by nearby Okanagan River, and also partially influenced by Lake Tugulnuit. The 10 year capture zones are elongated towards Lake Tugulnuit about 0.5 times the extent of the 1 year zones.

Rockcliffe: the geometry of this capture zone is mostly controlled by the silt top elevation, which appears to have a localized northward trench, interpreted to be a kettle hole that extends near Okanagan River. This well has the highest pumping rate of all wells and the surrounding aquifer has the highest measured transmissivity in the Oliver region. Boreholes 800 m north-east of this well (e.g., WTN 19573) indicate the presence of deeper coarse gravel and boulder deposits, which could be connected, to some degree, to Okanagan River.

Tugulnuit 2: this capture zone has an overall lower probability, as materials in this region of the upper aquifer are highly variable, resulting in a number of different material realizations from T-PROGS and different flow path realizations. The 10 year capture zone is nearly identical to the 1 year capture zone.

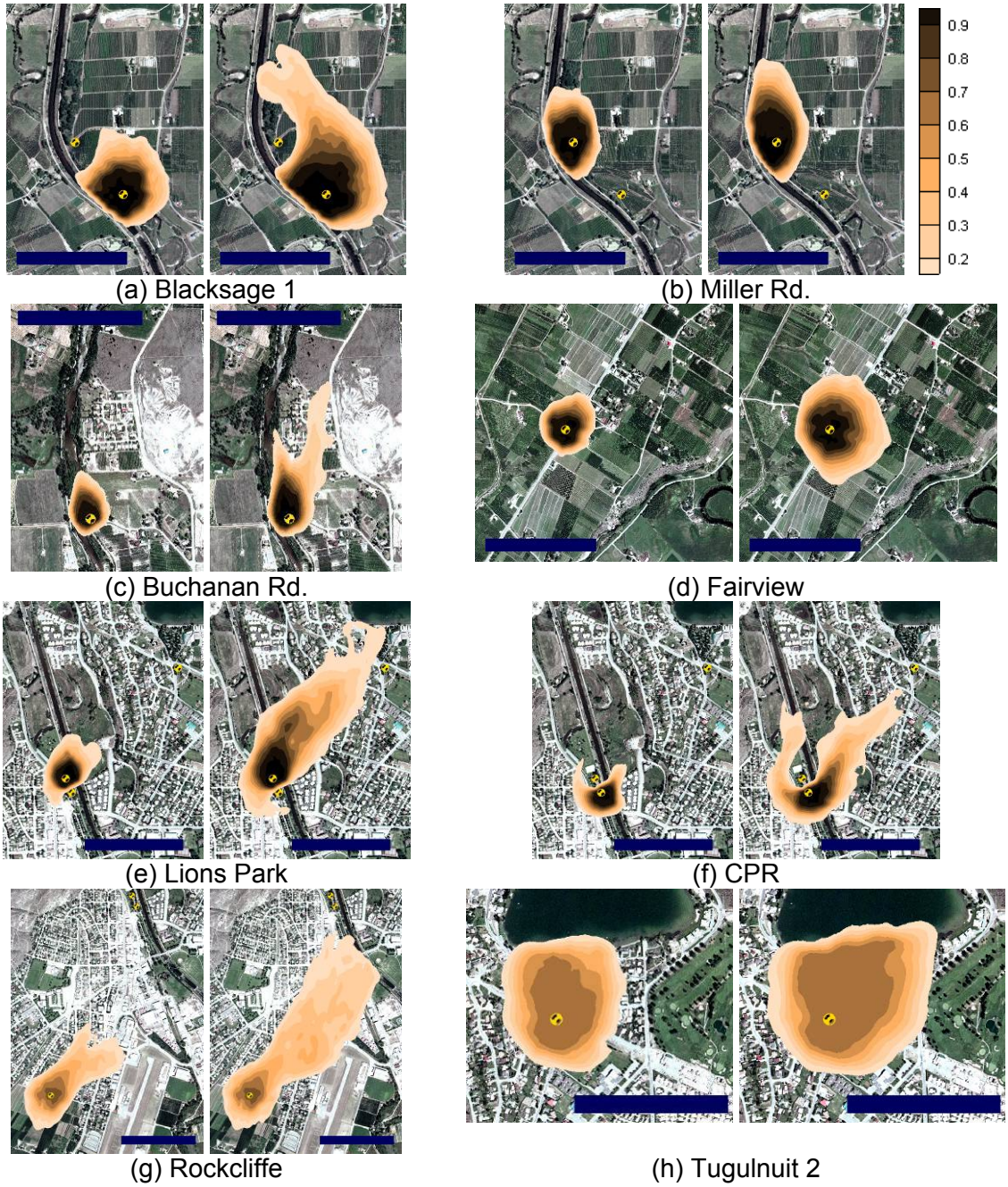

Figure 6.6: Probabilistic capture zones for the Oliver region, for 60 and 365 days. Shaded contours indicate the probability that water in the aquifer will reach the pumping well within the simulation time. Scale bar width is 500 m.

6.4. DISCUSSION

The capture zones determined in this study have a wide range of outcomes, which are influenced by unique hydrogeologic conditions surrounding each pumping well, such as the placement near Okanagan River or Lake Tugulnuit, subsurface hydrogeology, or placement to

other nearby wells. Circular capture zones, as determined using the CFR method by Foley et al. (2005), are comparable to several of the capture zones in this study. These similar capture zones include those around Fairview and Tugulnuit 2 pumping wells, and they also have similar dimensions to zones surrounding Blacksage 1 and Miller Rd. pumping wells. However, circular CFR capture zones are very different for the Rockcliffe, Lions Park and CPR pumping wells. These capture zones are elongated in the opposite direction of groundwater flow, with minimal capture zone exposure in the direction of groundwater flow.

The geometry and ranges of probabilities in each capture zone are influenced by the heterogeneity of aquifer materials, as approximated from groundwater simulations through stochastic realizations of aquifer materials. Capture zones around Rockcliffe, and Tugulnuit wells are larger, and have less-defined probabilities overall due to the high variability of geologic materials found in the boreholes near these regions. In contrast, the capture zone surrounding Buchanan Rd. is influenced by boreholes north of the pumping well with more continuous assemblages of materials.

Defining capture zones based on a probabilistic approach are particularly beneficial where there is a significant lateral groundwater flow, as these can have a large influence on the geometry of the zone. Also, probabilistic capture zones, by definition, convey more information of the spatial probabilities at which water will reach the well. These probabilities are influenced by the heterogeneity of the aquifer and surrounding boreholes. However, this method also requires a large number of boreholes, and the model development can take considerable time to construct.

7. CONCLUSIONS

The geology and hydrostratigraphy of the south Okanagan Region near the Town of Oliver, BC, consists of valley fill deposits overlying bedrock. The maximum depth of the bedrock surface ranges from approximately 0 to 100 m above sea level. There are no indications that the bedrock is eroded as deeply as in the northern Okanagan, where the bedrock contact is below sea level in many parts of the Valley.

Fine-grained glaciolacustrine silt and clay deposits are found at depth are overlain by (1) alluvial sand and gravel near creeks, sometimes bound with clay; (2) isolated boulder deposits near the center of the valley; (3) glaciofluvial sand and gravel along the benches and above the flood plain; and (4) fluvial sand and gravels along Okanagan River, which are fluvially-reworked sediments from the region. With the exception of the glaciolacustrine sediments, all the materials have high hydraulic conductivities, generally over 50 m/day. Buried kettle holes identified in the subsurface may indicate increased transmissivity, which is desirable for high production rates.

The main aquifer in the study region is the upper unconfined sand and gravel aquifer adjacent to Okanagan River. Upper unconfined sand and gravel aquifers are also present at higher elevations, along the valley margins. Regions with sufficient geological data show that the saturated thickness of the upper aquifer adjacent to Okanagan River varies from a few metres to 20 m or more (up to 60 m), which is influenced most by the silt top elevation. Some zones of high saturated thicknesses can be associated with kettle holes in the silt top, such as near Rockcliffe, Fairview, Miller Rd., and other production wells. The upper glaciofluvial units in the northern valley bottom contain layers of fine sand, which make some of the wells partially confined. These finer grained confining deposits appear to be discontinuous. Deep confined sand and gravel aquifers are found along the valley margins, which are in alluvial deposits. Many of these alluvial fan deposits interfinger the glaciolacustrine deposits at depth, and likely extend less than several hundred metres toward the valley center. These aquifers are likely to be most influenced by ephemeral streams.

Spatially-distributed recharge was modeled using available soil and climate data with the HELP hydrology model. Mean annual recharge rates have a median of 45 mm/yr, with first and third quartiles of 15 and 60 mm/yr, respectively. These values are approximately 20% of the annual

precipitation. Recharge simulations using irrigation yield significant increases in net recharge in the irrigation districts, from 250 mm/yr to 1000 mm/yr.

A regional deterministic groundwater flow model was constructed in MODFLOW for the region extending from Vaseux Lake to Osoyoos Lake. Both a steady-state and transient model were run and calibrated to observed hydraulic head data. Groundwater in the Oliver region is regulated and maintained from Okanagan River and the bounding lakes. The water table is generally flat throughout the region, and ranges in elevation from 280 to 355 m.a.s.l. along the Vaseux Lake to Osoyoos Lake corridor. The water table rises up slightly in proximity to the benches. Model results suggest that a large proportion of the water budget is sustained through recharge. Much of the recharge is from irrigation return flow.

Capture zones for municipal groundwater wells were determined using a local-scale groundwater model. These capture zones are similar to zones determined using the calculated fixed radius method. The capture zones determined using the numerical model are most effective where the groundwater flow rates are greatest, such as where there is a high hydraulic gradient and/or hydraulic conductivity.

8. REFERENCES

Allard, R., 2004. Well construction and capacity testing, new production well PW04-1 Oliver, British Columbia. Tech. Rep. 04-1140-020, Golder Associates, Ltd., Kelowna, BC.

Allen, D.M., Mackie, D.C., Wei, M., 2004. Groundwater and climate change: a sensitivity analysis for the Grand Forks aquifer, southern British Columbia, Canada. Hydrogeology Journal 12, 270–290.

Allen, D.M. 2001. Groundwater and Climate: A Case Study for the Grand Forks Aquifer, Southern British Columbia. Final Report prepared for the Groundwater Section, Water Management Branch, B.C. Ministry of Environment, Lands and Parks, Victoria, B.C., Queen's Press, March 2001, 227 pp.

Allen, D.M. 2000. Numerical Modelling of the Grand Forks Aquifer, Southern British Columbia. Final report prepared for the Groundwater Section, Water Resources Branch, British Columbia Ministry of Environment, Lands and Parks, Victoria, B.C., Queen's Press, March 2000, 126 pp. ISBN 0-7726-4374-1

Allen, R. G., Pereira, L. S., Raes, D., Smith, M., 1998. Crop evapotranspiration — guidelines for computing crop water requirements. FAO Irrigation and Drainage Paper 56, Food and Agriculture Organization of the United Nations, Rome, Italy.

Anderson, M.P., Woessner, W.W., 1992. Applied Groundwater Modeling: Simulation of Flow and Advective Transport, 2nd Edition. Academic Press, San Diego, CA, USA.

Arengi, J.T., Badry, A., 1993. Performance and capacity evaluation of new community water well, Deer Park Mobile Home Park near Oliver, BC. Tech. rep., Pacific Hydrology Consultants Ltd., Burnaby, BC.

BC MoE, 2006. WELLS: Water well database. BC Ministry of Environment, Victoria, BC. Website.
http://aardvark.gov.bc.ca/apps/wells/

Berardinucci, J., Ronneseth, K., 2002. Guide to using the BC aquifer classification maps for the protection and management of groundwater. BC Ministry of Water, Land and Air Protection, Victoria, BC, Canada.
http://www.env.gov.bc.ca/wsd/plan_protect_sustain/groundwater/aquifers/

Berger, K., 2004. The Hydrologic Evaluation of Landfill Performance (HELP) model: engineering documentation for HELP 3.80 D — Enhancements compared to HELP 3.07. Tech. rep., Institute of Soil Science, University of Hamburg.
http://www.geowiss.uni-hamburg.de/i-boden/suppengdochelp380d.pdf

Callan, D.M., 1971. Groundwater development SOLID no. 3 system, Oliver, BC. File 0249723, Water Investigations Branch, BC Water Resources Service, Department of Lands, Forests, and Water Resources, Victoria, BC.

Carle, S.F., 1999. T-PROGS: Transition probability geostatistical software, Version 2.1. University of California, Davis, CA, USA.

Carle, S.F., Fogg, G.E., 1996. Transition probability-based indicator geostatistics. Mathematical Geology 28 (4), 453–476.

Carle, S.F., Fogg, G.E., 1997. Modeling spatial variability with one and multidimensional continuous-lag Markov chains. Mathematical Geology 29 (7), 891–918.

Chen, X., 2000. Measurement of streambed hydraulic conductivity and its anisotropy. Environmental Geology 39 (12), 1317–1324.

Clague, J.J., 1991. Quaternary glaciation and sedimentation. In: Gabrielse, H., Yorath, C.J. (Eds.), Geology of the Cordilleran Orogen in Canada. No. 4 in Geology of Canada. Geological Survey of Canada, Ch. 12, pp. 419–434.

CSSC, 1978. The Canadian system of soil classification. Publication 1646, Canada Soil Survey Committee, Resource Branch, Canadian Department of Agriculture, Ottawa, ON, Canada.

Deutsch, C.V., Journel, A.G., 1997. GSLIB: Geostatistical Software Library and User's Guide, 2nd Edition. Oxford University Press, New York, NY, USA.

Dierscha, H.-J. G., Perrochetb, P., 1999. On the primary variable switching technique for simulating unsaturated–saturated flows. Advances in Water Resources 23 (3), 271–301.

Domenico, P. A., Schwartz, F. W., 1998. Physical and Chemical Hydrogeology, 2nd Edition. John Wiley & Sons, Inc, New York, NY, USA.

EMRL, 2005. Groundwater Modeling System (GMS), Version 6.0. Environmental Modeling Research Laboratory, Brigham Young University, Provo, UT, USA.

Environment Canada, 2006. Canadian climate normals or averages 1971–2000. Website. http://climate.weatheroffice.ec.gc.ca/climate_normals/index_e.html

Environment Canada, 2002. Canadian Daily Climate Data on CD-ROM. Climate Products and Publications Division, Downsview, ON, CDCD 2002 — West. http://www.climate.weatheroffice.ec.gc.ca/prods_servs/cdcd_iso_e.html

Environment Canada, 2001. HYDAT CD-ROM user's manual. Water Survey of Canada, Downsview, ON, 2nd Edition.

ESRI, 2005. ArcGIS 9.1 software and documentation. Environmental Systems Research Institute, Redlands, CA, USA.

Eyles, N., Mullins, H.T., 1991. The seismic stratigraphy of Okanagan Lake, British Columbia: a record of rapid deglaciation in a deep 'fiord-lake' basin. Sedimentary Geology 73, 13–41.

Eyles, N., Mullins, H.T., Hine, A.C., 1990. Thick and fast: Sedimentation in a Pleistocene fiord lake of British Columbia, Canada. Geology 18, 1153–1157.

Fayer, M.J., 2000. UNSAT-H version 3.0: unsaturated soil water and heat flow model — theory, user manual, and examples. Tech. rep., Pacific Northwest National Laboratory.

Flerchinger, G.N., 2000. The Simultaneous Heat and Water (SHAW) model: technical documentation. Tech. rep., Northwest Watershed Research Center, USDA Agricultural Research Service, Boise, Idaho. ftp://ftp.nwrc.ars.usda.gov/download/shaw/ShawDocumentation.PDF

Flint, R.F., 1935. “white-silt” deposits in the Okanagan Valley, British Columbia. Royal Society of Canada, Transactions 29, 107–114.

Foley, J., Allard, R., Sacre, J., 2005. Initial phases in the development of a groundwater protection plan – Town of Oliver. Tech. Rep. 03-1440-057, Golder Associates, Ltd., Kelowna, BC.

Foweraker, J.C., 1969. Southern Okanagan Lands Irrigation District ARDA projects Nos. 10010 and 29041, construction and testing of domestic water supply test wells — Oliver area. Tech. rep., Groundwater Division, Water Investigations Branch, BC Ministry of Environment.

Fulton, R.J., 1965. Silt deposition in late-glacial lakes of southern British Columbia. American Journal of Science 263, 553–570.

Fulton, R.J., 1969. Glacial lake history, southern Interior Plateau, British Columbia. GSC Paper 69-37, Geological Survey of Canada.

Fulton, R.J., 1972. Stratigraphy of the unconsolidated fill and Quaternary development of north Okanagan Valley. GSC Paper 72-8, Part B, Geological Survey of Canada.

Fulton, R.J., 1991. A conceptual model for the growth and decay of the Cordilleran Ice Sheet. Géographie physique et Quaternaire 45 (3), 281–286.

Fulton, R.J., Smith, G.W., 1978. Late Pleistocene stratigraphy of south-central British Columbia. Canadian Journal of Earth Sciences 15, 971–980.

Grasby, S. E., Hutcheon, I., 2001. Controls on the distribution of thermal springs in the southern Canadian Cordillera. Canadian Journal of Earth Sciences 38 (3), 427–440.

Harbaugh, A.W., Banta, E.R., Hill, M.C., McDonald, M.G., 2000. MODFLOW-2000, the U.S. Geological Survey modular ground-water model — User guide to modularization concepts and the ground-water flow process. Open-File Report 00-92, U.S. Geological Survey, Reston, VA, USA.

Hodge, W.S., Lowen, D.A., 1980. Contract 71: Construction and testing of test production wells for the BC Fruit Grower’s Association — Oliver, BC. Tech. rep., Groundwater Section, Water Management Branch, BC Ministry of Environment, ecoCat 6433.

Hodge, W. S., 1978. A preliminary study on the possible effects of low river releases on groundwater levels — Okanagan River Valley. Tech. rep., Groundwater Section, Hydrology Division, BC Ministry of Environment.

Jyrkama, M.I., Sykes, J.F., 2005. Estimating groundwater recharge in response to potential future climate change: the importance of winter temperatures. In: American Geophysical Union, Fall Meeting 2005. Vol. 86. San Francisco, CA, USA, pp. B1+, h52B-01.

Kalyn, D.J., 1983. Construction of observation well no. 282 Meyers Flat area. Contract 73, BC Ministry of Environment, Water Management Branch, Victoria, BC.

Kenk, E., Sondheim, M.W., 1987. CAPAMP: Data entry and validation procedures for soil, agriculture capability, surficial geology and the all purpose entity. MOEP Manual 10, Surveys & Resource Mapping Branch, BC Ministry of Environment and Parks, Victoria, B.C.

Lesemann, J-E., Brennand, T.A., Shaw, J., 2005. A revised conceptual model for growth and decay of the Cordilleran Ice Sheet in British Columbia, Canada, unpublished.

MacAulay, H.A., Hobson, G.D., 1972. A seismic refraction survey of the north Okanagan and south Shuswap Valleys. GSC Paper 72-8, Part A, Geological Survey of Canada.

Mantua, N.J., Hare, S.R., 2002. The Pacific Decadal Oscillation. Journal of Oceanography 58, 35–44.

Massey, N.W.D, MacIntyre, D.G., Desjardins, P.J., Cooney, R.T., 2005. Digital geology map of British Columbia: whole province. Geofile 2005-1, Ministry of Energy and Mines.

McDonald, M. G., Harbaugh, A. W., Orr, B. R., Ackerman, D. J., 1991. A method of converting no-flow cells to variable-head cells for the U.S. Geological Survey modular finite-difference ground-water flow model. Open-File Report 91-536, U.S. Geological Survey, Reston, VA, USA.
http://pubs.er.usgs.gov/usgspubs/ofr/ofr91536

McNeely, R., Clague, J.J., 1996. Database of selected British Columbia radiocarbon dates. Open File 3259, Geological Survey of Canada.

MSC, 2004. Canadian daily climate data — western Canada. CD-ROM, 2002 CDCD WEST CD.

Mullins, H.T., Eyles, N., Hinchey, E.J., 1990. Seismic reflection investigation of Kalamalka Lake: a “fiord lake” on the Interior Plateau of southern British Columbia. Canadian Journal of Earth Sciences 27, 1225–1235.

Nasmith, H., 1962. Late glacial history and surficial deposits of the Okanagan Valley, British Columbia. Bulletin 46, BC Ministry of Energy, Mines and Petroleum Resources.

Natural Resources Canada, October 2005. Canadian digital elevation data, Level 1, product specifications. Edition 2.1, Natural Resources Canada, Centre for Topographic Information, Sherbrooke, QC, Canada.
http://www.geobase.ca

Neilsen, D., Koch, W., Smith, S., G., Frank, 2004. Crop water demand scenarios for the Okanagan Basin. In: Cohen, S., Neilsen, D., Welbourn, R. (Eds.), Expanding the Dialogue on Climate Change & Water Management in the Okanagan Basin, British Columbia. Environment Canada, Agriculture & AgriFood Canada and University of British Columbia, Ch. 8, pp. 89–119, Final Report.

Neilsen, D., Smith, C. A. S., Frank, G., Koch, W., Alila, Y., Merritt, W. S., Taylor, W. G., Barton, M., Hall, J. W., Cohen, S. J., 2006. Potential impacts of climate change on water availability for crops in the Okanagan Basin, British Columbia. Canadian Journal of Soil Science 86 (5), 921–935.

Nichols, R.W., 1993. A design brief on the floodplain mapping study, Okanagan River. Tech. rep., BC Ministry of Environment, Lands and Parks Water Management Division, Victoria, BC.

Niswonger, R. G., Prudic, D. E., 2005. Documentation of the Streamflow-Routing (SFR2) Package to include unsaturated flow beneath streams—a modification to SFR1 techniques. Techniques and Methods 6-A13, U.S. Geological Survey, Denver, CO, USA. http://pubs.usgs.gov/tm/2006/tm6A13/

Owen, S.J., Jones, N.L., Holland, J.P., 1996. A comprehensive modeling environment for the simulation of groundwater flow and transport. Engineering with Computers 12, 235–242.

Päivänen, J., 1973. Hydraulic conductivity and water retention in peat soils. Acta Forestalia Fennica 129, 1–70.

Pojar, J., Klimka, K., Meidinger, D.V., 1987. Biogeoclimatic ecosystem classification in British Columbia. Forest Ecology and Management 22, 119–154.

Prudic, D. E., 1989. Documentation of a computer program to simulate stream–aquifer relations using a modular, finite-difference, ground-water flow model. Open-File Report 88-729, U.S. Geological Survey, Carson City, NV, USA. http://pubs.er.usgs.gov/usgspubs/ofr/ofr88729

Rück, A., Walker, I.R., Hebda, R., 1998. A palaeolimnological study of Tugulnuit Lake, British Columbia, Canada, with special emphasis on river influence as recorded by chironomids in the lake's sediment. Journal of Paleolimnology 19, 63–75.

Scanlon, B.R., Christman, M., Reedy, R.C., Porro, I., Simunek, J., Flerchinger, G.N., 2002. Intercode comparisons for simulating water balance of surficial sediments in semiarid regions. Water Resources Research 38, 1323–1339.

Schaap, M.G., Leij, F.J., van Genuchten, M.Th., 2001. ROSETTA: a computer program for estimating soil hydraulic parameters with hierarchical pedotransfer functions. Journal of Hydrology 251, 163–176.

Schroeder, P.R., Dozier, T.S., Zappi, P.A., McEnroe, B.M., Sjostrom, J.W., Peyton, R.L., 1994. The Hydrologic Evaluation of Landfill Performance (HELP) model: engineering documentation for version 3. Tech. rep., U.S. Environmental Protection Agency Office of Research and Development, Washington, DC.

Scibek, J., 2005. Modelling the impacts of climate change on groundwater: A comparative study of two unconfined aquifers in southern British Columbia and northern Washington state. Master's thesis, Simon Fraser University, 8888 University Drive, Burnaby, BC.

Scibek, J., Allen, D.M., 2006a. Comparing modelled responses of two high-permeability, unconfined aquifers to predicted climate change. Global and Planetary Change 50 (1-2), 50–62.

Scibek, J., Allen, D.M., 2006b. Modeled impacts of predicted climate change on recharge and groundwater levels. Water Resources Research 42 (11), W11405.

Scibek, J., Allen, D.M., Cannon, A., Whitfield, P., 2006. Groundwater-surface water interaction under scenarios of climate change using a high-resolution transient groundwater model. Journal of Hydrology.

Scibek, J. and Allen, D.M. 2005. Numerical Groundwater Flow Model of the Abbotsford-Sumas Aquifer, Central Fraser Lowland of BC, Canada, and Washington State, US. Unpublished report prepared for Environment Canada, Vancouver, BC, 203pp.

Scibek J. and Allen, D.M. 2004. Groundwater Sensitivity to Climate Change (Part II): Analysis of Recharge for the Grand Forks Aquifer, Southern British Columbia. Report to BC Ministry of Water, Land and Air Protection, 166pp.

Scibek, J., Allen D.M., and Whitfield, P. 2004. Groundwater Sensitivity to Climate Change (Part III): Climate Change Modelling Results for the Grand Forks Aquifer, Southern British Columbia. Report to BC Ministry of Water, Land and Air Protection, 264pp.

Scibek J. and Allen, D.M. 2003. Groundwater Sensitivity to Climate Change (Part I): Analysis of Watershed Water Balance and River-Aquifer Interactions for the Grand Forks Aquifer, Southern British Columbia. Report to BC Ministry of Water, Land and Air Protection, 174 pp.

Schubert, B., 1983. Okanagan Flood Control System: plan, profile and cross-sections of Okanagan River 1980 survey. Survey Project No. 79-OBIP-2 (80), BC Ministry of Environment, Water Management Branch, Victoria, BC, Drawings A5221-1 to A5221-13.

Semenov, M.A., Barrow, E.M., 1997. Use of a stochastic weather generator in the development of climate change scenarios. Climate Change 35, 397–414.

Shabbar, A., Bonsal, B., Khandekar, M., 1997. Canadian precipitation patterns associated with the Southern Oscillation. Journal of Climate 10 (12), 3016–3027.

Shaw, J., 1977. Sedimentation in an alpine lake during deglaciation, Okanagan Valley, British Columbia, Canada. Geografiska Annaler 59A (3-4), 221–240.

Shaw, J., Muro-Stasiuk, M., Sawyer, B., Beaney, C., Lesemann, J.-E., Musacchio, A., Rains, B., Young, R.R., 1999. The Channeled Scabland: back to Bretz? Geology 27 (7), 605–608.

Sibson, R., 1981. A brief description of natural neighbor interpolation. In: Barnett, V. (Ed.), Interpreting Multivariate Data. John Wiley & Sons, New York, NY, USA, Ch. 2, pp. 21–36.

Silins, U., Rothwell, R.L., 1998. Forest peatland drainage and subsidence affect soil water retention and transport properties in an Alberta peatland. Soil Science Society of America Journal 62 (4), 1048–1056.

Tempelman-Kluit, D., Parkinson, D., 1986. Extension across the Eocene Okanagan crustal shear in southern British Columbia. Geology 14, 318–321.

Toews, M.W. 2007. Modelling the Effects of Climate Change on Groundwater in Oliver, British Columbia. Unpublished M.Sc. Thesis, Department of Earth Sciences, Simon Fraser University.

Trenberth, K.E., 1997. The definition of El Niño. Bulletin of the American Meteorological Society 78 (12), 2771–2777.

Tribe, S., 2005. Eocene paleo-physiography and drainage directions, southern Interior Plateau, British Columbia. Canadian Journal of Earth Sciences 42, 215–230.

USDA, 1986. Urban Hydrology for Small Watersheds, 2nd Edition. Technical Release 55. United States Department of Agriculture, Natural Resources Conservation Service, Conservation Engineering Division.

USGS, 1997. Standards for digital elevation models. Part 1 (General), U.S. Geological Survey, National Mapping Division. http://rockyweb.cr.usgs.gov/nmpstds/acrodocs/dem/1DEM0897.PDF

van Genuchten, M.Th., 1980. A closed-form equation for predicting the hydraulic conductivity of unsaturated soils. Soil Science Society of America Journal 44 (5), 892–898.

Vanderburgh, S., 1993. Basin architecture of the north Okanagan Valley fill, British Columbia. Ph.D. thesis, Simon Fraser University, Burnaby, BC, Canada.

Vanderburgh, S., Roberts, M.C., 1996. Depositional systems and seismic stratigraphy of a Quaternary basin: north Okanagan Valley, British Columbia. Canadian Journal of Earth Sciences 33, 917–927.

Wilson, J. D., Naff, R. L., 2004. MODFLOW-2000, The U.S. Geological Survey modular ground-water model — GMG linear equation solver package documentation. Open-File Report 2004-1261, U.S. Geological Survey, Denver, CO, USA. http://pubs.usgs.gov/of/2004/1261/

Wittneben, U., 1986. Soils of the Okanagan and Similkameen valleys. Report 52, British Columbia Soil Survey, BC Ministry of Environment, Victoria, BC, Canada.